Geochemistry and Origin of Granitoid Xenoliths From the Navajo Volcanic Field, Four Corners Area, SW United States

by

Natalie Latysh

A Thesis Submitted in Partial Fulfillment of the Requirements for

Master of Science in Geochemistry

October, 1997

New Mexico Institute of Mining and Technology

Socorro, New Mexico, USA

Abstract

Granitoid xenoliths from six diatremes in the Navajo Volcanic Field (NVF) fall into three main age populations, 1745 to 1720 Ma, 1700 to 1640 Ma, and 1452-1412 Ma, which are similar to ages of exposed Proterozoic granitoids in the Southwestern United States. All three age populations are similar in mineralogical and chemical composition, and deformation/alteration textures are pervasive. The xenoliths range in composition from diorite to granite, with granites greatly dominating, and most are metaluminous ($Al_2O_3/(CaO+Na_2O+K_2O) < 1$) I-types. In this respect, they are unlike most exposed Proterozoic plutons in the SW, where slightly peraluminous A-types dominate. There are no obvious correlations between granitoid age, diatreme composition, texture, geographic locality, xenolith chemical composition, or degree of alteration within the granitoid xenolith suite.

Based on trace element discriminant diagrams, NVF granitoids are arc types, and on primitive-mantle normalized plots, they show negative Ta-Nb, Th, P, and Ti anomalies. Chondrite-normalized REE patterns are enriched in LREE with Eu anomalies ranging from positive to negative. Geochemical modeling and Nd isotopic data indicate that parent granitoid magmas cannot be produced from partial melting of associated metasediment xenoliths. Most successful models for the granites involve vapor-absent melting of diorite/tonalite sources, similar in composition to some of the xenoliths. Negative Ta-Nb anomalies are inherited from arc sources and negative Th, P, and Ti anomalies may be produced by fractionation of monazite, apatite, and ilmenite, respectively. It would appear that granitoids of all three ages were derived from similar juvenile crustal sources.

Acknowledgments

Table of Contents

I. Major Element Modeling

List of Tables

List of Figures

CHAPTER 1: INTRODUCTION

1.1 Background

Most continental crustal sections are extremely heterogeneous, lithologically and chemically, both laterally and vertically (Condie, 1989). Due to lack of accessibility into the interior of the crust, the evolutionary history, composition, and structure of the deep crust is still not well understood. Crustal xenoliths, samples of the deep crust which are entrained and transported to the Earth's surface during eruption of volcanics and kimberlites, provide a means to sample a cross section of the crust. By determining their depth of origin (through thermobarometry), abundance of various lithologies (through field studies), and their ages, an evolutionary history of the crust may be constrained.

The Colorado Plateau has been a stable continental block since the Late Proterozoic (McGetchin *et al.*, 1977). Exposed uplifted sections of the crust are exiguous in the Southwest, and therefore crustal characteristics must be determined through drill core data and xenolith studies. Modern drilling technologies can be expensive and drilling to great depths is not easy, making xenoliths the ideal way to investigate the crust.

The Navajo Volcanic Field (NVF), located in central Colorado Plateau, hosts numerous crustal xenolith-bearing diatremes and was chosen as the site for this xenolith study. Forty-nine granitic rocks were collected from six diatremes which sample a 10,000 km^2 area. Three of these are kimberlites: Moses Rock, Red Mesa, Garnet Ridge and three minettes: Shiprock, Mitten Butte and Thumb (Figure 1.1).

1
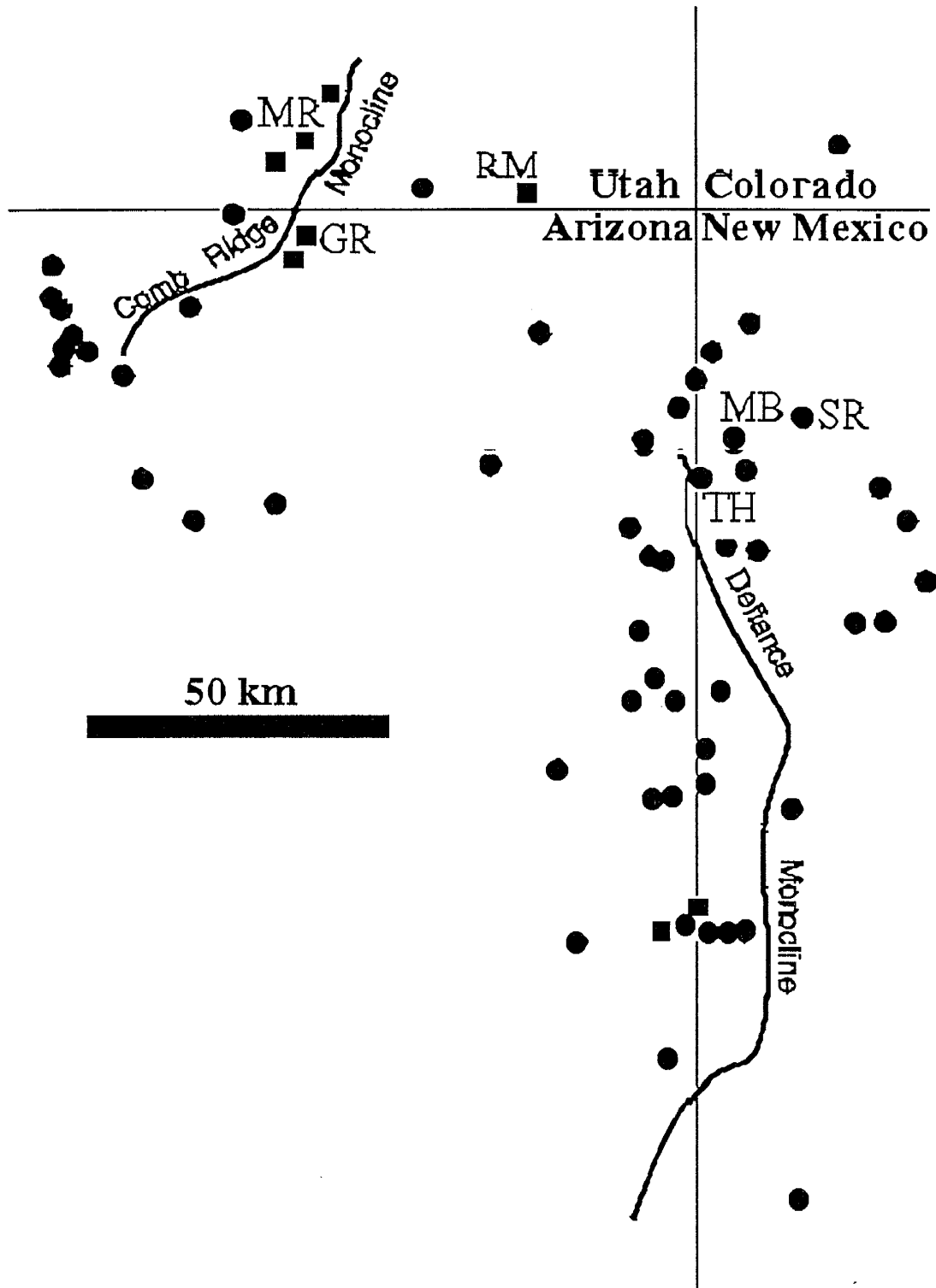
Figure 1.1. Map of kimberlites (squares) and minettes (circles) in the Navajo Volcanic Field. Granitoid xenoliths were sampled from minettes: SR-Shiprock, MB-Mitten Butte, TH-Thumb and kimberlites: MR-Moses Rock, RM-Red Mesa, GR-Garnet Ridge. Map from Mattie *et al.* (1997)

1.2 Crustal Composition

The average composition of the upper crust is similar to granodiorite (Condie, 1989),
determined by extensive sampling of Precambrian shields, sediments and exposed crustal
sections. The Colorado Plateau's upper crust varies in thickness from 10 to 20 km
(Condie, 1989) and consists of granitoids, gneisses, rhyolites, meta-basalts and non-
garnet-bearing schists and amphibolites (Wendlandt *et al.*, 1993).The lower crust of the
Colorado Plateau is probably composed of predominantly mafic, meta-igneous rocks
(Mattie *et al.*, 1997). The primary xenolith lithologies derived from depths of 20 km to the
seismic Moho (43 km) are garnet granulites, garnet amphibolites, and gabbros (Wendlandt
et al., 1993).

1.3 Purpose and Approach

The purpose of this study is to determine the composition and origin of granitoids in the
upper crust of the Colorado Plateau by identifying the different granitic xenolith
populations using petrographic and geochemical methods. This study focuses on the late
stages of magmatic evolution in the region's crustal development, including 1) the role of
juvenile material in granitic magma generation through partial melting and differentiation
processes; 2) geochemical implications of tectonic regimes involved in evolution of the
upper felsic crust; 3) establishing correlation between the 1400 and 1700 Ma plutonism,
which occurred throughout the Southwestern USA; 4) investigating possible relationships
with other granitoids in the Southwest. Major and trace element geochemical composition
of xenoliths were acquired by X-ray fluorescence and instrumental neutron activation
analysis. Xenoliths vary in chemical composition from mafic to highly siliceous, and the
protolith and restite material involved in granitoid petrogenesis may be represented in the
xenolith populations. Geochemical modeling was used to constrain the nature of the
protolith for the NVF granitoids. By combining the results of this study with information
collected from metasedimentary and mafic xenoliths collected from the same area, a more

3

comprehensive picture of the composition and evolution of the Colorado Plateau has been acquired. In addition, this study lends an increased understanding of how accretionary arcs evolve into felsic continental crust and subsequent lithospheric stabilization.

1.4 Previous Work

Numerous studies have been carried out on crustal xenoliths in the Colorado Plateau (Wendlandt *et al.*, 1993; Mattie *et al.*, 1997; Condie and Selverstone, 1997; Menzies *et al.*, 1987). Most of these studies have focused on lower crustal material to understand crustal formation and extraction from the heterogeneous mantle (Wendlandt *et al.*, 1993; DePaolo *et al.*, 1991; Bennett and DePaolo, 1987; Menzies *et al.*, 1987), to examine magmatic involvement in crustal underplating (Wendlandt *et al.*, 1993; Mattie *et al.*, 1997), and to evaluate geochemical modifications during different tectonic regimes which have affected the crust (Menzies *et al.*, 1987).

1.5 Geology of the Four Corners Region

The Four Corners region is located at the junction of Colorado, Utah, Arizona and New Mexico, in the east-central Colorado Plateau. The area consists of semi-arid grasslands, arid deserts and forested mountain ranges, with elevations ranging from 1,200 to 3,400 m (Semken, 1992). The Colorado Plateau is a geological province with an aerial extent of over 360,000 km^2 (Wendlandt *et al.*, 1993). The Plateau is bounded to the south and west by the Basin and Range Province, on the north and northeast by the Rocky Mountains and on the east by the Rio Grande rift (Figure 1.2). The Plateau is different from the bounding provinces by its smaller degree of deformation and igneous activity (McGetchin *et al.*, 1977).
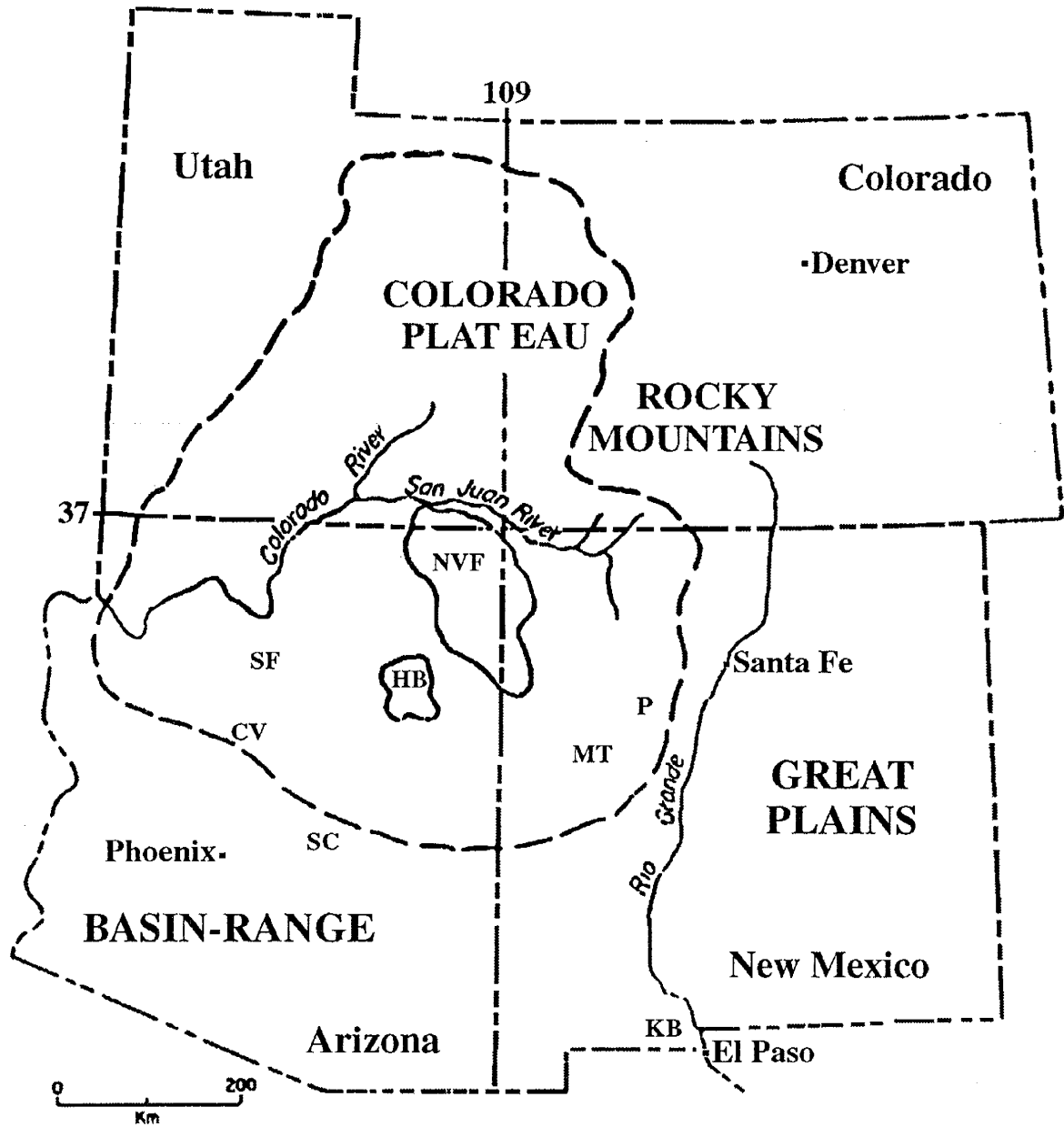
Figure 1.2. Location map of the Colorado Plateau and volcanic centers of the Southwestern United States. NVF-Navajo Volcanic Field; HB-Hopi Buttes; MT-Mount Taylor; P-Puerco Necks; KB-Kilbourne Hole; SC-San Carlos; CV-Chino Valley; SF-San Francisco Peaks. Map from McGetchin *et al.*, 1977.

The Colorado Plateau has been a stable continental block for the past 1.2 Ga. The Plateau was a shelf environment during the Paleozoic and Mesozoic Eras. Cenozoic sedimentary strata are missing in much of the central Colorado Plateau (McGetchin *et al.*, 1977).

5

Laramide tectonic activity is responsible for the folded anticlines and the north to northeast-trending (Laughlin and Charles, 1992), west-dipping monoclines (Semken *et al.*, 1992), which may be related to reverse faults at depth (Laughlin and Charles, 1992). The Plateau hosts many volcanic features including the San Francisco, Hopi Buttes, Chino Valley, Navajo and Mount Taylor Volcanic Fields (Figure 1.2) (McGetchin *et al.*, 1977). Uplift and erosion has exposed Cretaceous and Tertiary igneous rocks, which are scattered throughout the region.

Navajo Volcanic Field

The Navajo Volcanic Field (NVF) is located in the Four Corners area. It spans over 40,000 km^2, extending 200 km northeast from the Monument Upwarp to Mesa Verde and 300 km southeast to Zuni Bandera Volcanic Field, New Mexico (Vaniman *et al.*, 1985). The NVF hosts numerous kimberlite and minette diatremes (Figure 1.1), characterized by explosive volcanism and more passively emplaced potassic and ultrapotassic dikes and flows, respectively. Preserved lava flows are rare in the Navajo Volcanic Field unlike the nearby Hopi Buttes Volcanic Field (Williams, 1936). Kimberlites and minettes emplaced during the Mid-Tertiary are believed to have originated in the upper mantle, reflecting localized liberation of volatiles during partial melting in the mantle (McGetchin *et al.*, 1973). Much of the volcanism is associated with subduction along the western edge of the growing continent (Menzies *et al.*, 1987). The diatremes host a variety of crustal xenoliths entrained as magma ascended through the Precambrian crystalline basement and an overlying, gently folded, sedimentary sequence (Delaney and Pollard, 1981). Emplacement of these structures preferentially occurred along or near monoclines approximately 28 to 19 Ma (Laughlin and Aldrich, 1992). Few kimberlite dikes cluster at the edge of the Comb Ridge monocline, which defines the eastern boundary of the Monument uplift, a regional uplift (McGetchin *et al.*, 1973). The Colorado Plateau began acting as an independent geologic

6

province 28 Ma, unaffected by the ENE-WSW extension prominent in the Southwestern

United States (Laughlin and Aldrich, 1992).

1.6 Diatreme Characteristics

Minette

Volcanic necks are composed of minette, a massive, blocky, porphyritic lamprophyre

characterized by high K_2O/Na_2O ratios, compatible and highly incompatible trace element

and Mg abundances and LREE enrichment with respect to HREE (Semken et al., 1992;

Menzies et al., 1987). Minettes range in color from gray, due in part to abundance of K-

feldspar, to shades of black, green and brown (Williams, 1936). They are the dominant

volcanic rock type and are generated by melting of enriched mantle lithosphere (Roden,

1981). Alignment of mica occurs at margins of diatremes, providing a platy appearance

(Williams, 1936). The minettes are typically fine-grained, although larger volcanic necks

are composed of coarser material (Delaney and Pollard, 1981). Minette mineralogy consists

predominantly of alkali-feldspar (orthoclase, sanidine) (Williams, 1936), diopside and

phlogopite or biotite, with accessory phases olivine, apatite and calcite (Delaney and

Pollard, 1981). Compositional heterogeneities of minettes are attributed to extent of

fractional crystallization and contamination from the continental crust, entrained

sedimentary material and contributions from the lithospheric mantle (Menzies et al., 1987).

The Thumb

The Thumb is a cylindrical, minette-filled conduit (McGetchin et al., 1977), 100 m in

diameter (Menzies et al., 1987), located 18 km southwest of Shiprock (McGetchin et al.,

1977). The diatreme crops out in the Jurassic Morrison Formation. A thin rind of tuff-

breccia covers the Thumb's western side, however it is primarily composed of relatively

homogeneous, nonvesicular minette. The Thumb hosts numerous high pressure xenoliths

and the minette is notable for its enriched magnesian bulk composition, having a higher

mafic component than other minettes in the Navajo Volcanic Field (McGetchin et al.,

7

1977). Entrained metasedimentary and felsic crustal xenoliths range in size from 5 to 30 cm and compose approximately 10% of the outcrop (Menzies *et al.*, 1987).

Shiprock

Shiprock, a prominent volcanic neck, is located in northwestern New Mexico (Figure 1.3). The diatreme stands 500 m above the surrounding landscape (Semken *et al.*, 1992), with a basal diameter of approximately 400 m (Williams, 1936). The pipe is believed to have extended approximately 1,000 m above the present elevation. The diatreme crops out in Cretaceous Mancos Shale. Features in the vent indicate emplacement by a violent eruption (Semken *et al.*, 1992). Shiprock is composed of minette tuff-breccia, including plutonic and sedimentary fragments (Williams, 1936) and is locally dissected by veinlets of minette (Delaney and Pollard, 1981). The diatreme is surrounded by seven radiating dikes (Delaney and Pollard, 1981), arranged in echelon (Williams, 1936). The diatreme hosts abundant

Figure 1.3. Shiprock diatreme. Photograph taken facing north-east.

8

granitic xenoliths of various sizes (1-2 m being the largest) and textures. Small, mafic xenoliths are entrained in the minette matrix and there is a paucity of garnet-bearing samples.

Mitten Rock

Mitten Rock is a minette which is located approximately 13 km southwest of the Shiprock diatreme. It intrudes Cretaceous Mancos shale (Naeser, 1971) and is approximately 1200 m in length. The minette is rich in feldspar and mafic xenoliths dominate over granitoid and metasedimentary xenoliths (Williams, 1936).

Kimberlite

Kimberlites are often associated with carbonatites, lamprophyres and other alkalic rocks, often coinciding with epeirogenic uplift (McGetchin *et al.*, 1973). The Colorado Plateau hosts eight known kimberlite-bearing, breccia-filled diatremes (McGetchin and Silver, 1972), which are thought to have been emplaced contemporaneously with minettes (Roden, 1981). Granites and metabasalts comprise the largest xenoliths in most kimberlite pipes. Based on petrographic and geochemical data, kimberlites identified in the Four Corners area have been reclassified as serpentinized ultramafic breccia (SUM) and are unlike a true kimberlite (Roden, 1981). From ultramafic xenolith studies, these kimberlites appear to come from the upper mantle at depths of 50 to approximately 200 km (McGetchin and Silver, 1972). Kimberlites consist of pulverized upper mantle xenocrysts (olivine, diopside, orthopyroxene, spinel, pyrope) (McGetchin *et al.*, 1973) and crustal material (Semken *et al.*, 1992). Kimberlitic mineral constituents include garnet, spinel, olivine, pyroxene, phlogopite, serpentine, and chlorite. Kimberlite emplacement is believed to occur rapidly as fluidized solid particles and volatiles are driven to the surface by CO_2 and H_2O (McGetchin *et al.*, 1973).

Moses   Rock

Moses Rock is located 8 km southeast of Mexican Hat, Utah, and resides on Comb Ridge monocline (Naeser, 1971). Moses Rock is a 6 km long, curved, breccia-filled dike, which parallels the monocline. The dike crops out in the Permian Cutler Formation (McGetchin and Silver, 1972). The kimberlitic diatreme hosts a wide array of crustal xenoliths including gabbros, amphibolites, metasediments (including: biotite-garnet-quartz schist, sillimanite-quartz-feldspar schist and gneiss), granitoids, garnet amphibolites, garnet granulites and mantle xenoliths (Figure 1.4). Xenolith abundances vary with lithology along strike. Granitic xenoliths are subordinate to the mafic and metasedimentary xenoliths. Kimberlitic matrix constitutes roughly 1% of the dike and fills interstices between brecciated crustal and upper mantle fragments. The present surface of the dike is approximately 1 km below the original level of emplacement (McGetchin and Silver, 1972). Xenoliths range in size from fine grained particles to rounded boulders, over 2 m in diameter. Rhyolite and granitoid xenoliths are less abundant than metabasalt, gabbro and diorite samples. Roughly 75% of the clasts are igneous, 25% metamorphic and less than 1% are ultramafic (McGetchin and Silver, 1972). Carbonate (calcite) veins dissect the kimberlitic material throughout the dike (McGetchin *et al.*, 1973).

Figure 1.4. Picture of the ground covered with xenoliths at Moses Rock.

Garnet Ridge

Garnet Ridge diatreme is located 12 km southwest of Mexican Water, Arizona, again along Comb Ridge monocline (Figure 1.5). The kimberlite at Garnet Ridge consists of four pipes emplaced in the Jurassic Summerville Formation (O'Sullivan and Beikman, 1963). It hosts xenoliths of all lithologies listed at Moses Rock. The kimberlite is not exposed and

xenoliths are scattered at the surface. Granitoid xenoliths found in the area range in size, some are as large as 3 meters across (Figure 1.6). Granitoid xenoliths found in the area include biotite-granodiorite (which are most common), coarse grained granitoids, gneissic granitoids, some are migmatites, fine to medium-grained, pink granitoids, and leucogranites.

Red Mesa

Red Mesa diatreme is located approximately 4 km northwest of Red Mesa, on the Arizona-Utah border. The kimberlite crops out in the Jurassic Navajo Sandstone. Red Mesa diatreme has weathered into a low circular topographic depression, approximately 75 meters in diameter. Crustal xenoliths of many compositions are abundant (Semken *et al.*, 1992), including metasediments, granitoids, granulites, amphibolites, and quartzites (Mattie, 1996). The samples range in size, with some as large as 25 cm across.

Figure 1.5. Picture of Garnet Ridge cropping out in the Jurassic Summerville Formation.

Figure 1.6. Example of some of the larger granitoid xenoliths found at Garnet Ridge.

13

1.7 Xenolith Emplacement

Factors Influencing Entrainment

Sampling material in the crust via volcanism depends on many crucial factors, including relative abundance of rock types exposed in the vent walls, which is related to the structure of the particular rock formation in the vicinity of the vent; physical characteristics of the rocks, particularly, their resistance to entrainment and abrasion; the transporting material and its interaction with entrained crustal fragments; and the time interval between eruptions (McGetchin and Silver, 1972).

An inverse correlation exists between fragment size and depth of origin. Xenolith size is affected by the vertical distance the sample travels through the vent, and smaller samples are derived from greater depths (McGetchin and Silver, 1972). The upper crust is dominantly granitic in composition. Hence, larger crustal xenoliths (>1 m) are composed of granitoids and sediments. Plutonic xenoliths are less rounded than the deep-seated mafic xenoliths, reflecting further transport from the source.

Transit

Crustal xenolith transport is estimated to occur within several hours (McGetchin and Silver, 1972). The Four Corner granitoids probably originated within the top 10 km of the earth's crust (K. C. Condie, personal communication, 1996). Minimal chemical and physical changes most likely affect the xenoliths during transport to the surface. Some of the changes that may affect samples during the time of entrainment and transport to the time of collection include heating by transporting host material; mingling with the host; hydrothermal alteration by fluids derived from the transporting medium, which can mobilize the alkali earth elements; decompression-induced melting, which may result in development of microcracks and interstitial partial melting; mineral breakdown; and

14

weathering at the earth's surface (Rudnick, 1992). Garnet is especially susceptible to decompression-induced changes, often involving chlorite alteration (J. Selverstone, personal communication, 1997), and is observed in the garnetiferous samples (Figure 1.7). Hydrothermal alteration is especially prevalent in kimberlite-hosted xenoliths.
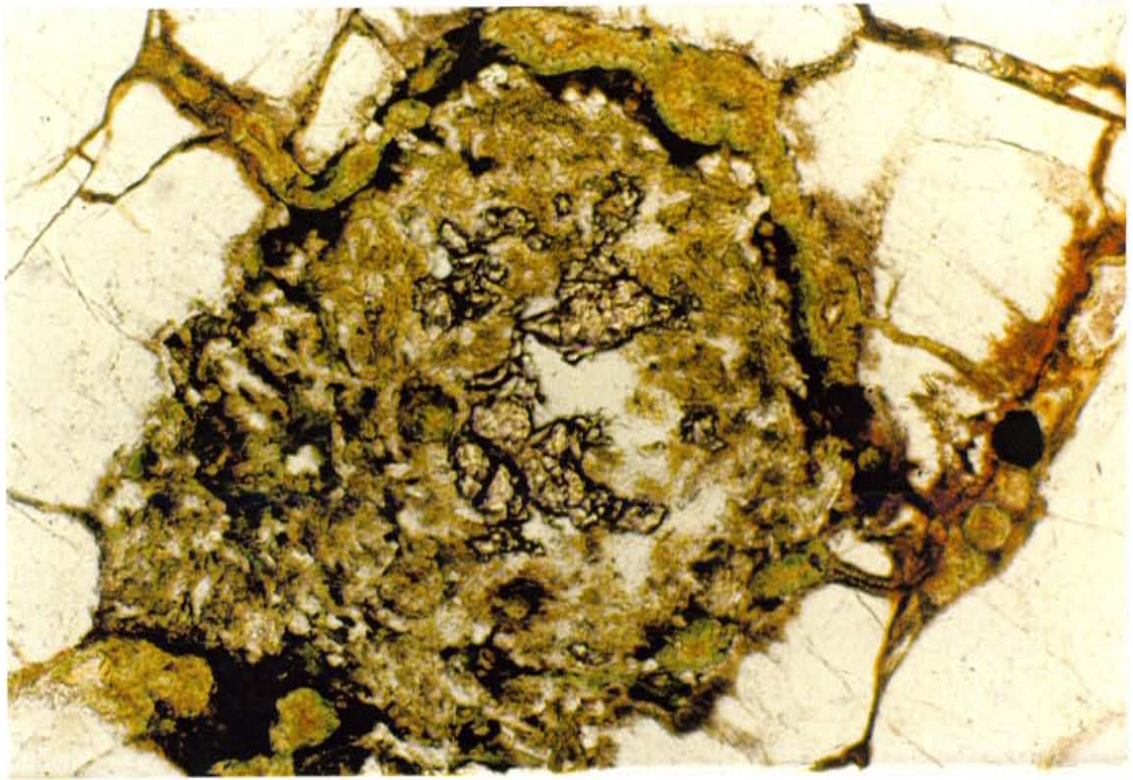
Figure 1.7. Thin section picture (GR-44) of chloritized garnet at 10x (scale=1 mm across). Top: plane polarized light; bottom: crossed polarized light.

CHAPTER 2: GRANITIC XENOLITH SUITE

2.1 Introduction

Over 250 samples were collected from the Navajo Volcanic Field and were sorted according to hand sample description, petrographic analysis, and geochemistry. The groups include metasediments, granitoids, and various mafic xenoliths. Forty-nine granitoid samples were selected for this study. All samples were analyzed by X-ray fluorescence for major and trace elements. Nine samples were selected for instrumental neutron activation analysis. The term 'granitoid' has been applied to members of the suite and describes intrusives ranging from tonalite-granodiorite to granite in mineral composition.

2.2 Granitoid Xenoliths

A SiO_2 content of 57% was arbitrarily chosen as the lower limit for this study's samples in order to isolate the granitoids from more mafic rock types. The NVF granitoids were classified according to collection locality (Table 2.1): Garnet Ridge, Moses Rock, Red Mesa, Mitten Butte, Shiprock (two populations) and Thumb.

Table 2.1. NVF Granitoid Xenoliths According to Site of Collection

Garnet Ridge	Mitten Rock	Moses Rock	Red Mesa	Shiprock A	Shiprock B	Thumb
n=5	n=2	n=8	n=13	n=4	n=3	n=14
GR-2	MT-6	MR-1A	RM-1	SR-1	SR-5	TH-2
GR-20	MT-7	MR-1B	RM-2	SR-3	SR-6	TH-3
GR-22		MR-2	RM-3	SR-4	SR-7	TH-4
GR-27		MR-5	RM-4	SR-8		TH-6
GR-44		MR-7	RM-7			TH-7
		MR-9	RM-8			TH-8
		MR-10	RM-9			TH-9
		MR-25	RM-10			TH-10A
			RM-11			TH-10B
			RM-12			TH-11
			RM-16			TH-12
			RM-17			TH-22
			RM-23			TH-24
						TH-27

n=number of samples

Distinct populations of granitoids were isolated according to hand sample characteristics, petrography, major and trace element geochemistry (discussed in Chapter 3). The granitoid xenoliths were first divided according to hand sample characteristics. Hand specimen groups include biotite granitoids, K-feldspar megacrystic granitoids, hornblende granitoids, granodiorites, leucogranites, high K-feldspar granites, and unclassified. Unclassified granitoids include samples which display peculiarities and do not qualify for the other populations. Hand specimen division depends on the following factors: mineralogy, degree of deformation and alteration, grain size, and color index.

The granitoid samples were also divided into several groups according to petrographic features (Table 2.2). The petrographic groups are based on modal mineralogy, texture, and extent of alteration and deformation. Only a few samples fall in similar petrographic and hand sample populations. This may in part be due to difficulty in identifying alteration and deformation in fine-grained hand samples, especially those lacking micaceous minerals, which can often expose the deformational fabric by intrinsic alignment. Recrystallization is prevalent among samples yet, it is inconspicuous except in thin section.

Table 2.2. Petrographic Groups of NVF Granitoid Xenoliths

Group	n	Sample	Characteristics
Garnet-rich	4	GR-44, TH-10B, RM-23, TH-27	garnet-rich samples which display moderate alteration, garnet is often altered to chlorite, garnet pseudomorphs range in size: 1-4 mm, calcite filled veins dissect minerals and fill interstices
Pristine	3	SR-1, GR-2, MR-5	samples are pristine, little to no alteration is observed, medium-grained, small amounts of biotite are present in few samples
Fine-grained	2	RM-11, MR-2, RM-4	samples are fine-grained, displaying minimal alteration, deformational fabric is common
Porphyritic	2	RM-2, SR-3, TH-10A, TH-12, RM-3	porphyritic textures dominate, biotite is locally aligned, recrystallized products often fill interstices between larger megacrysts
Recrystallized	3	MR-9, RM-12, SR-4	samples have largely been recrystallized, occasional megacrysts are surrounded and intruded by recrystallized veinlets, sericite alteration affects most plagioclase grains
Deformed	2	SR-5, SR-7	samples are biotite-rich, which is often aligned, reflecting induced deformational stress, recrystallized veinlets are scattered throughout samples
Altered	7	TH-6, TH-8, MT-6, MT-7, MR-1A, GR-20, MR-1B	samples are extremely altered, hydrothermal alteration is verified by the presence of secondary hornblende, muscovite, epidote and occasionally sphene

n=number of samples. Samples collected from minettes: SR-Shiprock, TH-Thumb, MT-Mitten Rock and from kimberlites: GR-Garnet Ridge, MR-Moses Rock, RM-Red Mesa.

The NVF granitoid xenoliths were grouped according to the degree of deformation observed during petrographic analysis. Deformation may aid element remobilization and its effects are qualitatively examined by segregating the xenoliths according to weakly, moderately and strongly deformed textural variations exhibited in thin section (Table 2.3). Samples characterized as strong deformation show 1) >35% recrystallization, exhibit veinlets of small, equant grains, filling interstices between larger megacrysts (Figure 2.1); 2) mineral alignment and elongation; 3) significant subgrain development (subgrains develop at edges of grains which have experienced deformational stress and have extinction angles less than 5 degrees from the stressed crystal); 4) presence of mechanical twins in plagioclase (Figure 2.2), few feldspar grains exhibit secondary myrmekitic textures parallel

to deformational fabric; 5) undulose extinction in quartz; 6) ubiquitous equant grains; and 7) metamorphic fabric. The moderately deformed population is characterized by similar features, but which are not as prominently developed. Some samples display mineral alignment; however, the crystals are euhedral and no significant recrystallization has occurred. A majority of the samples in the weakly deformed group display porphyritic textures. Larger grains are more stable and resistant to deformation than smaller grains (L. Goodwin, personal communication, 1997). Thin, recrystallized veins fill some interstices between the euhedral megacrysts in this group. With these exceptions, the weakly deformed group samples lack subgrain development and a deformational fabric.

Table 2.3. NVF Granitoid Classification According to Degree of Deformation

Strongly Deformed	Moderately Deformed	Weakly Deformed
>35% recrystallization, pervasive mineral alignment, significant subgrain development, prevalence of equant, elongate grains and lack of original grain shapes	10-35% recrystallization, some mineral alignment- mostly exhibited by biotite, preservation of original mineral shapes	<10% recrystallization, no mineral alignment, preservation of megacrysts and original habits, little to no subgrain development
n=11	n=8	n=7
RM-2 -~60% recrystallized -foliation **MT-6** -~60% recrystallized -foliated fabric **GR-2** -~70% recrystallized -foliated fabric **MR-2** -~90% recrystallized -extremely foliated **RM-23** -~95% recrystallized -no fabric **TH-8** -~50% recrystallized -strong fabric **TH-6** -~90% recrystallized -foliated fabric **TH-10A** -~80% recrystallized -foliated fabric **GR-20** -~60% recrystallized -foliated fabric **RM-4** -~85% recrystallized -slight fabric **MT-7** -~65% recrystallized -elongate minerals -slight fabric	**TH-27** -slight fabric -elongate minerals -no recrystallization **SR-1** -no fabric -elongate minerals **SR-4** -~30% recrystallized -elongate minerals **RM-12** -~30% recrystallized -elongate minerals **TH-10B** -~30% recrystallized -elongate minerals -very similar to TH-27 **GR-44** -~20% recrystallized -elongate minerals -minor fabric **MR-9** -~35% recrystallized -no fabric **TH-12** -~10% recrystallized -elongate minerals -minor fabric **RM-11** -elongate minerals -mineral alignment	**RM-3** -~10% recrystallized -no fabric **SR-5** -~10% recrystallized -localized fabric **MR-5** -no fabric -little recrystallization **SR-7** -~10% recrystallized -no fabric **SR-3** -~10% recrystallized -no fabric **MR-1A** -porphyritic -minor recrystallization **MR-1B** -porphyritic -minor recrystallization

n=number of samples. Samples collected from minettes: SR-Shiprock, TH-Thumb, MT-Mitten Rock and from kimberlites: GR-Garnet Ridge, MR-Moses Rock, RM-Red Mesa.

21
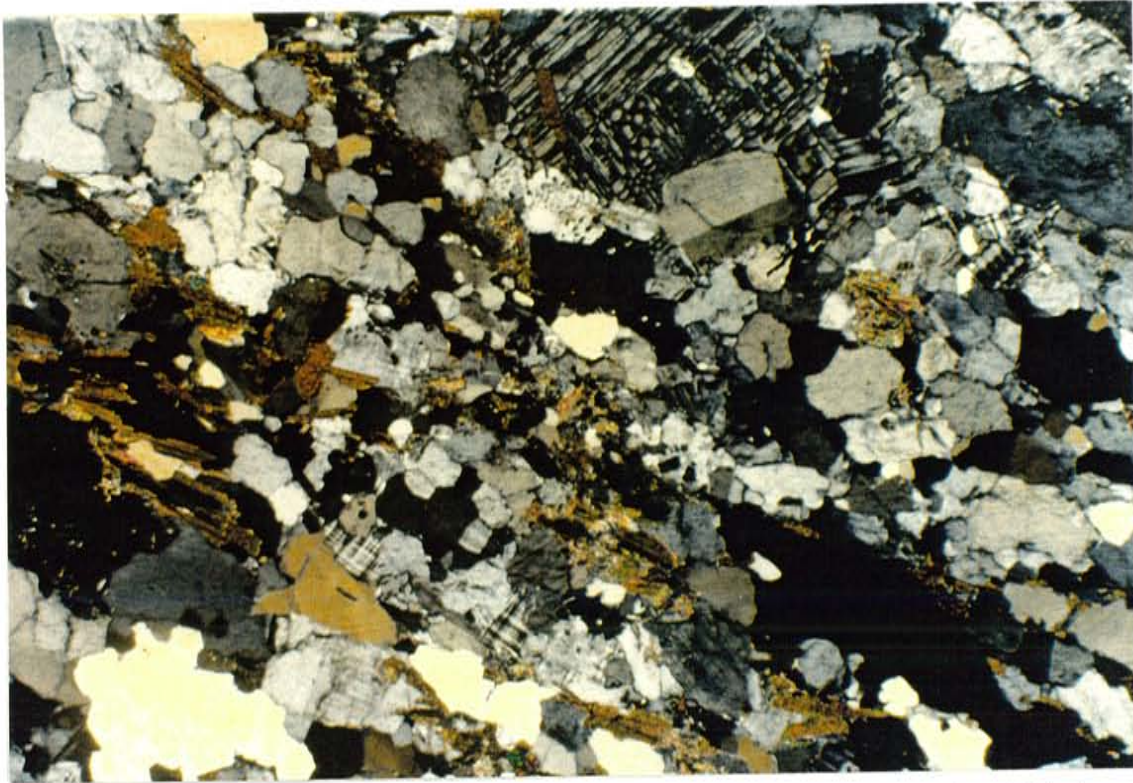
Figure 2.1. Thin section picture (RM-2) of recrystallization and deformational fabric at 2x (scale=5 mm across).
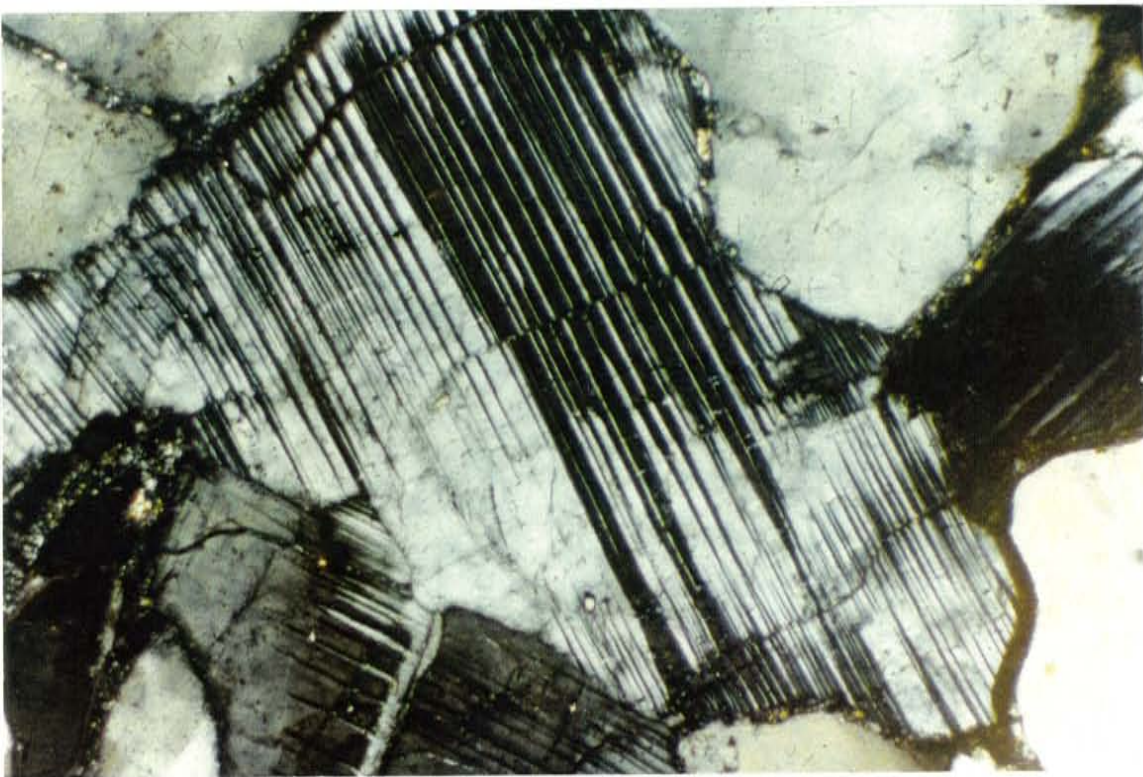
Figure 2.2. Thin section picture (SR-5) of mechanical twins in plagioclase and brittle deformation at 10x (scale=1 mm across).

2.3 Petrography

Introduction

Twenty-six of the least altered samples were picked for thin section analysis. Selection is based on the following: 1) choosing a representative distribution of the entire granitoid xenolith population, with at least one sample from each of the hand specimen groups; 2) geochemical features; and 3) selecting all samples analyzed by instrumental neutron activation analysis. In deformed rocks, samples are dissected perpendicular to deformational fabric for thin section analysis. Detailed petrographic descriptions for each sample are given in Appendix A.

Petrographic   Descriptions

Textural characteristics, mafic mineral abundances, and degree of deformation vary among the NVF granitoids, although they share many petrographic similarities. A representative sample consists of: K-feldspar (30-40%), quartz (25-35%), plagioclase (15-30%), biotite (2-10%), muscovite (1-3%), and opaques (<1%) (see Appendix A).

Granitoid textures vary from fine- to medium-grained, equigranular to coarse-grained, and most samples have feldspar-rich frameworks. All samples exhibit poikilitic textures with varying degrees of recrystallization. Recrystallized minerals, mostly K-feldspar and quartz, fill interstices and surround the larger megacrysts. Deformational fabrics are common and are characterized by mineral alignment and lack of intrinsic habit, stretched grains, ductile and brittle strain, often exhibited by plagioclase twins, convoluted biotite books, subgrain development (grains whose extinction angle differs less than 5° from the parent crystal) at edges of large crystals and recrystallization.

Hydrothermal alteration is ubiquitous and is represented by the presence of sericite, muscovite, epidote, chlorite, Fe-oxides, and calcite (Figure 2.3). Sericite is a common alteration product of plagioclase and coexists with large muscovite grains. Chlorite alteration occurs in garnetiferous samples and may be related to decompression. It is typically green, surrounds garnet crystals and radiates throughout the entire sample, filling interstices. Extensive calcite alteration affects several samples. Calcite often fills interstices and fractures, and occasionally replaces plagioclase grains.

Mineralogy

K-feldspar is often the most abundant mineral in the NVF granitoids. In most samples it is microcline, having a distinct cross-hatched pattern, although the orthoclase variety is prevalent in a few samples. Lack of twinning may be attributed to deformational stress. Myrmekitic and micrographic textures frequently occur at the edges of plagioclase and K-feldspar grains. Perthitic texture is especially common in coarse grained samples, whereas antiperthitic texture is rare. Exsolved albite globules in K-feldspar are frequently preferentially altered to sericite. K-feldspar appears to be the first mineral to begin to recrystallize and is often concentrated as small grains in interstices between the larger plagioclase and quartz particles.

Quartz grains have anhedral shapes and display undulatory extinction in all NVF granitoids. Quartz crystals are often elongated, stretched parallel to the deformational fabric. Subgrains form at edges of some quartz crystals due to deformational stress. Higher levels of stress result in cataclasis. Quartz crystals are commonly fractured into numerous grains of various sizes, which are rotated and have their own unique extinction angles.

Plagioclase grains are euhedral to subhedral, displaying polysynthetic albite twins. Pericline lamellae are less common. Occasionally crystals exhibit oscillatory zoning with a

24

sodic rim surrounding a calcic core. The grains are often turbid, due to sericite alteration generally concentrated in grain cores or along growth zones. The predominant plagioclase composition in most samples is oligoclase (An_{26}), as determined using the Michel-Levy method. Between samples, plagioclase ranges from An_{23} to An_{27}.

Biotite is a minor phase in equigranular samples, but comprises as much as 20% of the ductily deformed samples. Biotite grains are often euhedral to subhedral and are uniformly scattered throughout the samples or concentrated in deformational bands. Biotite is typically brown or brownish green, and is commonly altered in part to epidote. Subhedral biotite grains usually cluster with aggregates of limonite and secondary magnetite.

Muscovite is rarely magmatic and lacks the typical subhedral-euhedral habit. The small grains (<1 mm) are always found in association with plagioclase and biotite. Muscovite is usually scattered throughout sericitized regions in plagioclase grains, and it often replaces biotite at grain margins and occasionally replaces biotite completely.

Epidote usually surrounds or dissects biotite grains (Figure 2.4) and occasionally occurs in plagioclase, in the sericitized cores. It is rarely euhedral and often displays a 'moth-eaten' appearance. In these samples epidote is interpreted as secondary due to lack of euhedral shapes and its prevalent association with biotite. Due to its abundance in some NVF granitoids, epidote may be magmatic, however this is difficult to conclude solely based on criteria designated by Zen and Hammarstrom (1984). Zen and Hammarstrom (1984) have discussed textural characteristics indicative of magmatic epidote which include abundance of epidote in banded, mafic layers, euhedral shapes against other minerals, hornblende inclusions in epidote grains, and lack of alteration of other minerals. Minerals in NVF granitoids do not exhibit most of these characteristics. Epidote is one of numerous alteration products prevalent in the NVF granitoids. Epidote seldom displays a euhedral
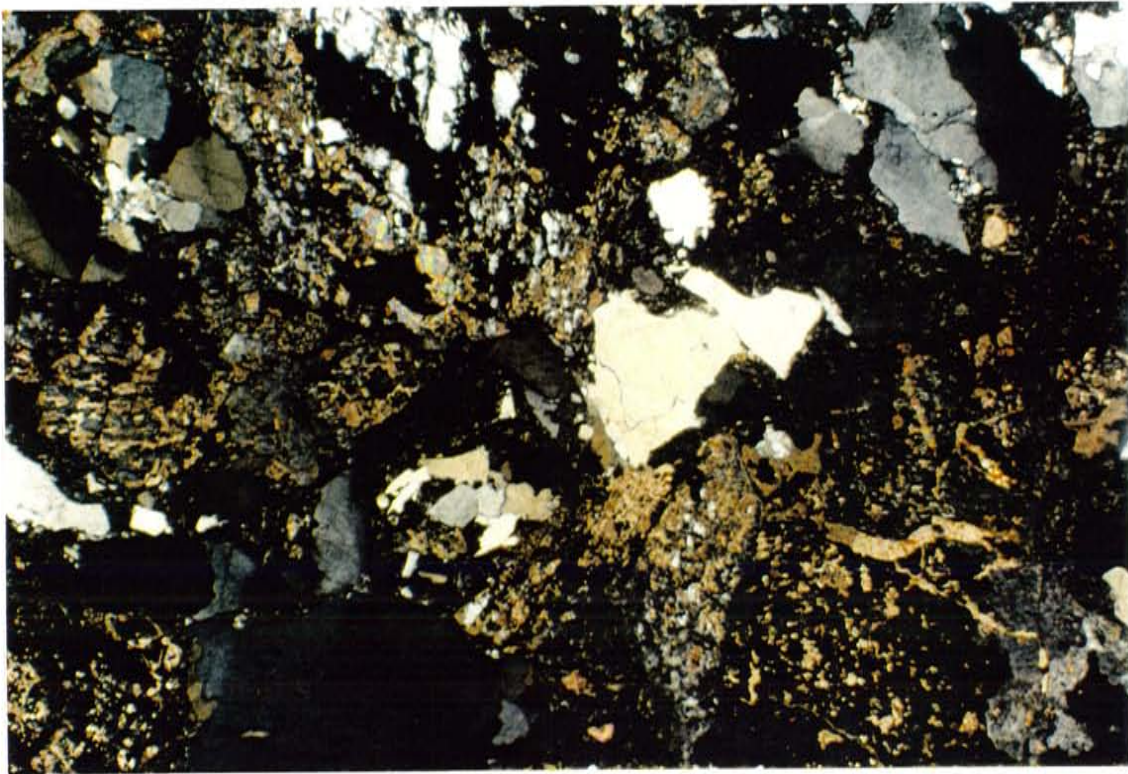
Figure 2.3. Thin section picture (TH-12) of calcite alteration at 2x (scale=5 mm across).
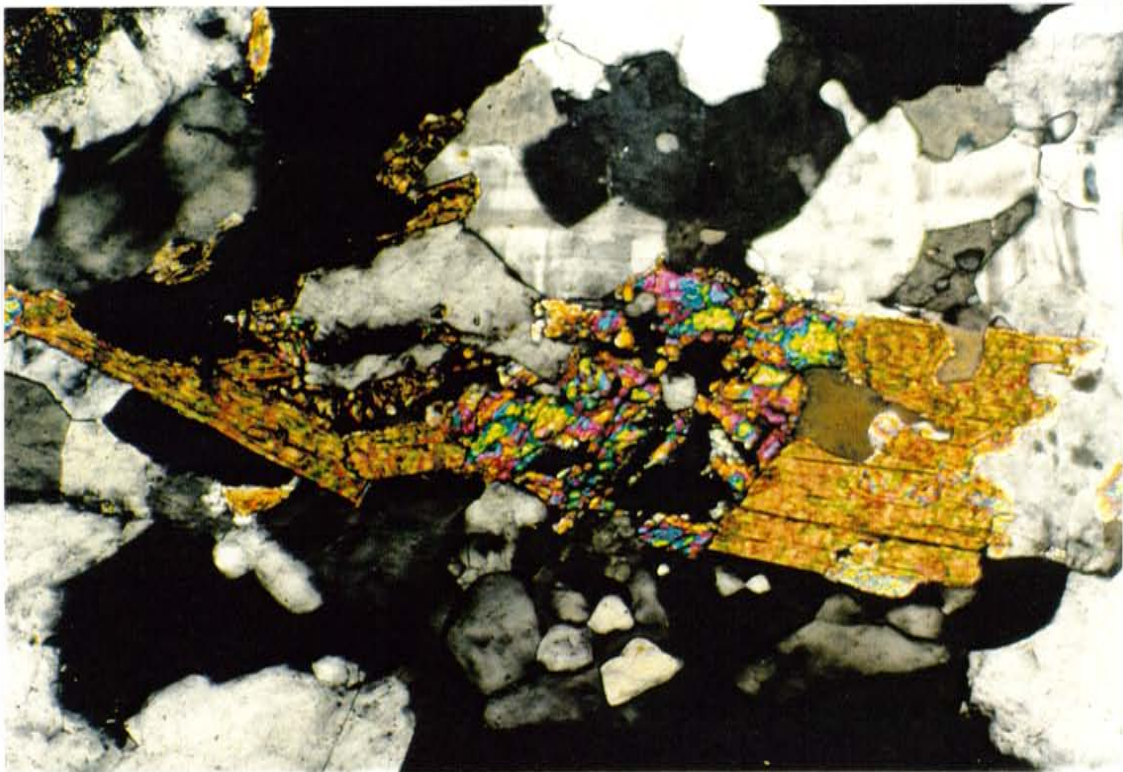
Figure 2.4. Thin section picture (SR-7) of biotite replacement by epidote at 10x (scale=1 mm across).

appearance and sometimes encloses altered biotite grains. Both biotite and epidote are concentrated in deformational bands in few samples. Epidote is always juxtapositioned against biotite, making the nature of association difficult to conclude.

Garnet is rarely preserved in the NVF granitoids. Small, disaggregated grains occasionally exist in cores of pseudomorphs which are filled with chlorite and Fe-oxides. Pseudomorphs are fairly large in most samples, ranging from 1 to 4 mm in diameter and are often oikocrysts for quartz and K-feldspar grains.

Accessory minerals include euhedral apatite, acicular rutile, secondary epidote, and scarce zircon and sphene. Opaques are subhedral to irregular and are often small, disseminated and equant, located in close proximity to biotite grains. Rutile, a lower temperature phase (L. Goodwin, personal communication, 1997), is scattered throughout quartz and K-feldspar as thin, needle-like grains and is rarely observed in plagioclase. Sphene is rare, present in only a few samples. It may be an alteration product of biotite, with which it is closely associated. Primary hornblende occurs in only a few samples and is most often secondary in the altered granitoids. Apatite crystals are ubiquitous, usually embedded within or between coarser grains. Zircon occurs as sporadic elongate blebs residing without preference in interstices and mineral interiors.

CHAPTER 3: GEOCHEMISTRY

3.1 Introduction

Forty-nine xenoliths were selected for chemical analysis from the Navajo Volcanic Field.

All samples were analyzed for major and trace element concentrations by X-ray

fluorescence (XRF) using a Philips PW 2400 spectrometer on whole rock fused disks and

pressed powder pellets. Ten of these samples, representing the range of textural variations

and geochemical compositions, were analyzed for additional trace elements by instrumental

neutron activation analysis (INAA). All data are tabulated in Appendix B, together with

CIPW norms. Sample preparation is described in Appendix C. The samples were analyzed

at the New Mexico Institute of Mining and Technology. Analytical procedures, precision

and accuracy for standards analyzed by XRF and INAA are summarized in Appendix D.

3.2 Results

Norm and Mode Classification

The CIPW norm is the most commonly used scheme for classifying granitoid rocks

(Rollinson, 1993). CIPW norms are calculated using IGPET2.1 computer program (Table

3, Appendix B) (Carr, 1994). The majority of the xenolith samples plot in the granodiorite

and granite fields on the Ab-An-Or classification diagram of O'Connor (1965) using CIPW

norms (Figure 3.1 a).
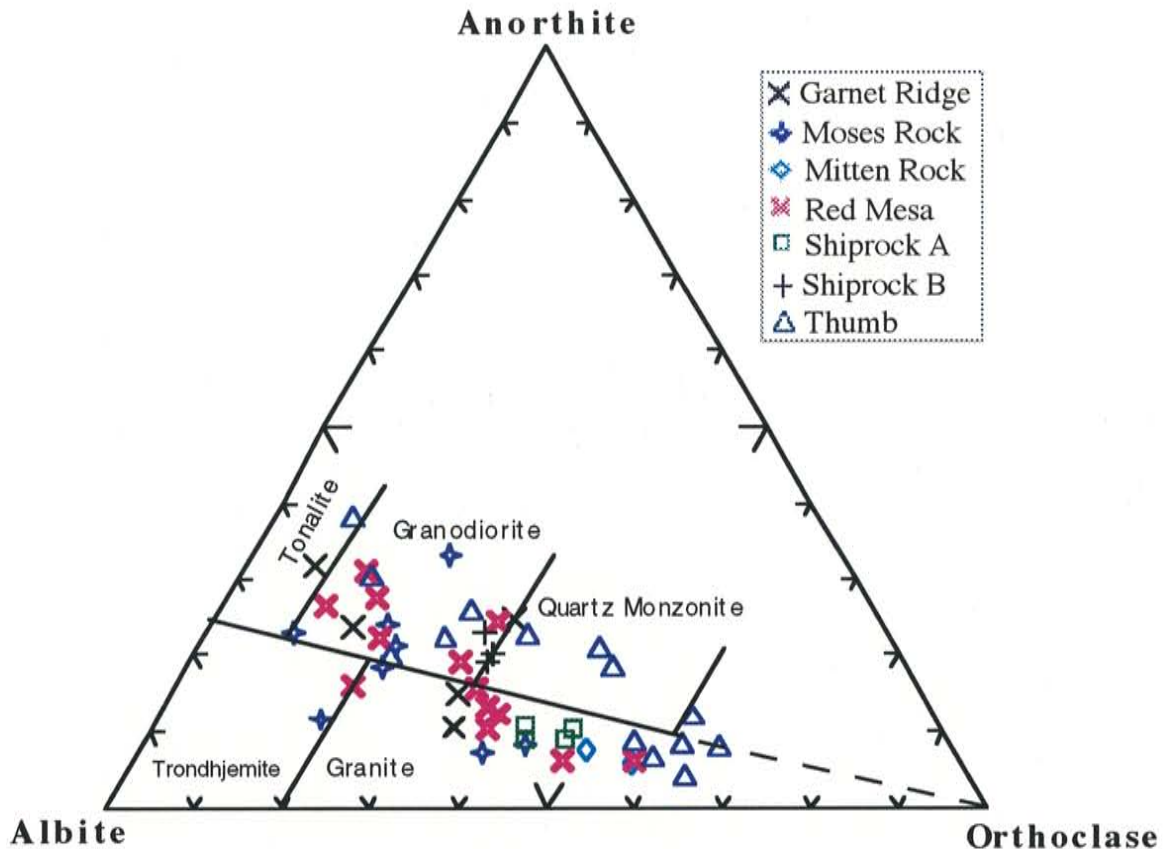
Figure 3.1 a. An-Ab-Or, CIPW normative mineral classification (after O'Connor, 1965) of the NVF granitoid xenoliths.

The NVF granitoids fall in the granite, granodiorite and tonalite fields on the modal IUGS granitoid classification diagram (Figure 3.1 b). One sample, MR-5, is composed of large megacrysts and plots in the quartz-syenite field. The few discrepancies between the two plots may be attributed to several factors. First, it is difficult to quantify modal feldspar percentages, especially when albite exsolution in K-feldspar is prevalent. This effect shifts samples toward the alkali feldspar corner on the IUGS plot. Samples that display calcic alteration may plot close to the anorthite corner on the CIPW normalized plot if CaO has been introduced. Also, CIPW calculations do not calculate normative hornblende and biotite, since the magma is assumed to be anhydrous, nor are other ferromagnesian minerals taken into account (Rollinson, 1993). This may lead to an overestimation of orthoclase in the samples, since biotite also incorporates K into its structure.
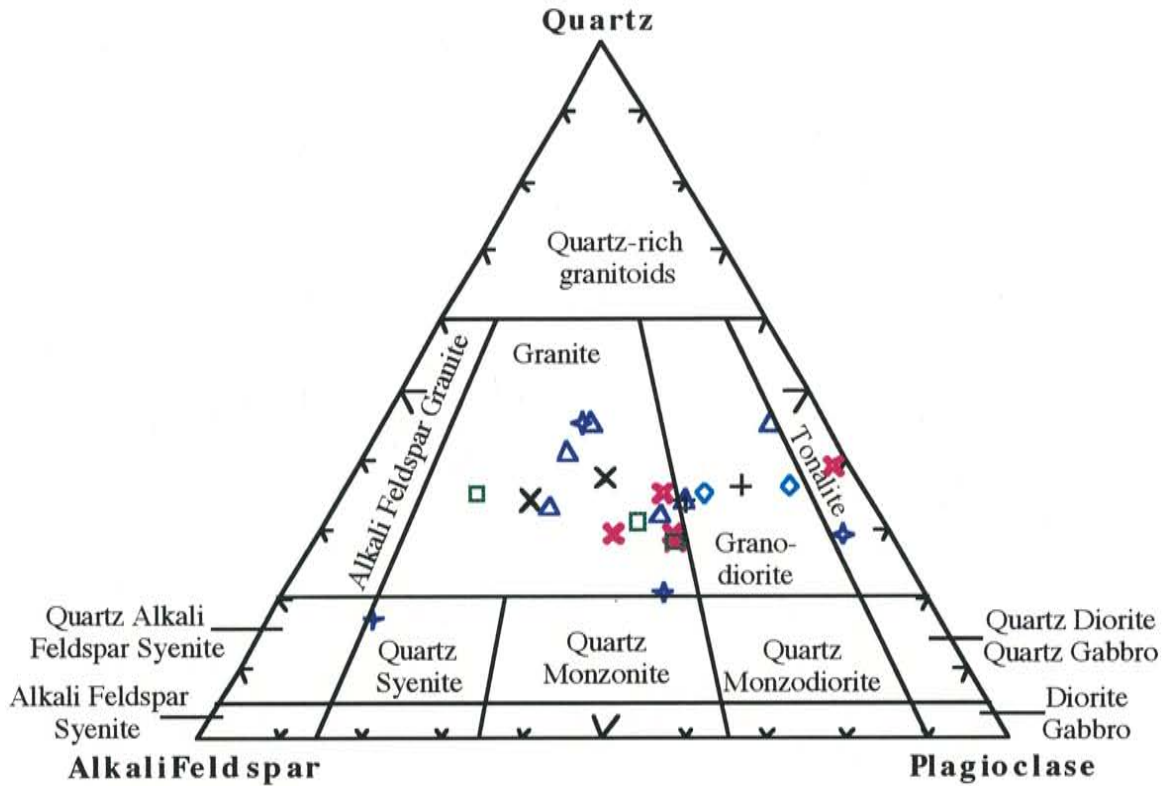
Figure 3.1 b. Modal IUGS classification of granitoids (after Streckeisen, 1976). Modal mineralogy was deduced from petrographic analysis for the NVF granitoid xenoliths.

Major Elements

Major element abundances for the NVF granitoid xenoliths are given in Table 1, Appendix B. The evolution of the NVF granitoids conforms to the calc-alkaline trend (Figure 3.2) even though the xenoliths probably come from different plutons (discussed in Chapter 4). With the exception of one sample, the granitoids range between 57 and 75% SiO_2. Sample MR-25, with SiO_2 content of 81.4%, has a more evolved composition and may have been silicified during an alteration episode.
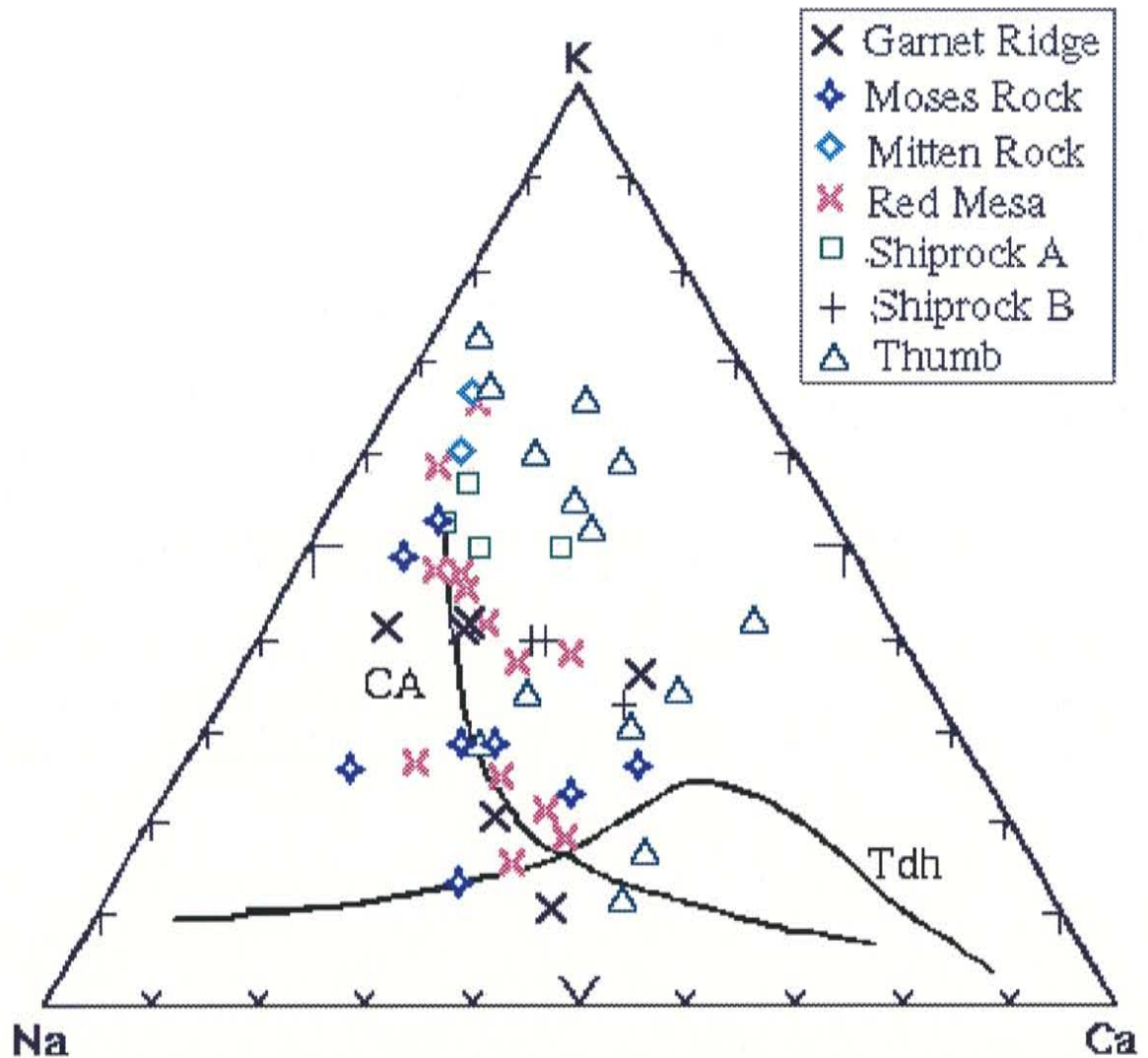
Figure 3.2. K-Na-Ca diagram from Barker and Arth (1976) illustrating the calc-alkaline evolution trends of plutons from which the Navajo Volcanic Field granitoid xenoliths were derived. Tdh=Trondhjemitic; CA=Calc-alkaline trend.

Major element bivariate plots (Harker diagrams) were constructed to show geochemical variation among samples and to identify petrologic trends (Figures 3.3 a-h). Seventeen U/Pb zircon ages, ranging from 1412 to 1799 Ma (see Chapter 4) are identified on some of the geochemical variation diagrams to establish possible geochemical correlations with age. With exception of K_2O, MnO and Na_2O, major element oxides show a weak negative correlation with SiO_2 due to the constant sum effect (Figures 3.3 a-h) (Leake, 1996). Decreasing Fe_2O_3, MgO and TiO_2 with increasing SiO_2 are paralleled by decreasing

abundances of ferromagnesian minerals, mainly biotite. The lowest silica (<60% SiO_2) samples from Moses Rock (MR-2, MR-7) exhibit some of the highest TiO_2 (up to 1.25%), MnO (up to 0.18%), MgO (up to 2.89%), Al_2O_3 (up to 18.21%) and Fe_2O_3 (T) (up to 7.94%) values. Both CaO and Fe_2O_3 (T) range between 0.5 and 8.0% and Al_2O_3 values range from 9 to 18% in the NVF granitoids. MnO, Na_2O and K_2O show no correlation with SiO_2, which may be due to element remobilization or differences in source characteristics. MgO and Na_2O vary from 0.16 to 2.89% and 1.85 to 5.0%, respectively, while K_2O displays notable variation from 0.75 to 7.1%. The highest and lowest K_2O (>6.0% and 0.75%) samples are from the Thumb.

The two xenolith groups from Shiprock are distinguished from the general population by their close geochemical proximity to each other in every plot (see Figures 3.3 a-h). Only two granitoid samples are analyzed from Mitten Rock. They are geochemically alike on all major element plots, possibly indicating a similar source. Several samples (GR-20, TH-27) plot in the oceanic plagiogranite field (K_2O<1.0%) (designated by Maniar and Piccoli, 1989) (see Figure 3.3 b). Petrographic investigation reveals that sample GR-20 (K_2O=0.92%) is almost completely sericitized and sample TH-27 contains garnet, which is extensively chloritized and calcite veins are ubiquitous throughout this sample. Their position in the plagiogranite field is most probably due to loss of K during alteration . The existence of plagiogranites in the Colorado Plateau is doubtful due to the volcanic arc nature of the host terrane.
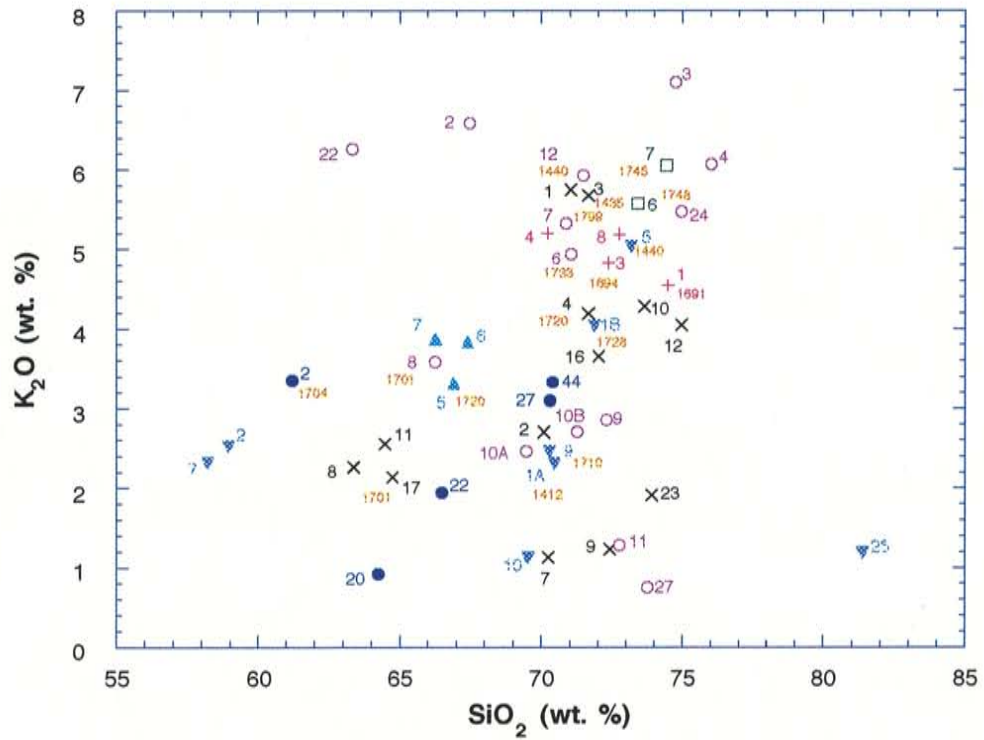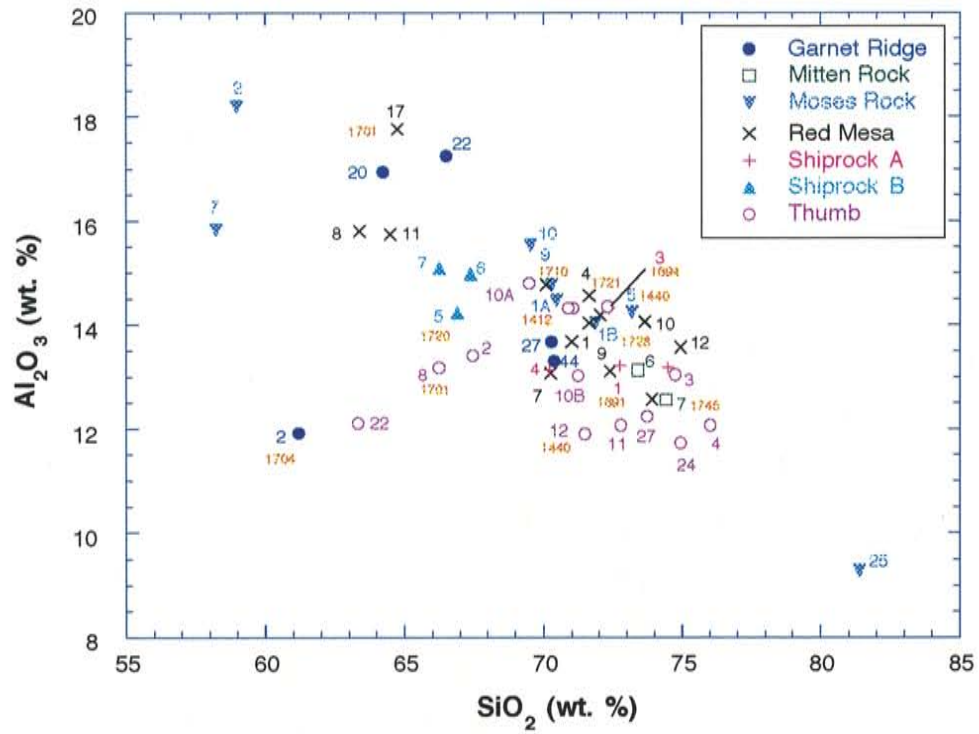
Figure 3.3 a, b. Major element oxides (in weight %) versus SiO_2 for granitoid xenoliths from the Navajo Volcanic Field. Numbers in orange represent U/Pb zircon ages.

33
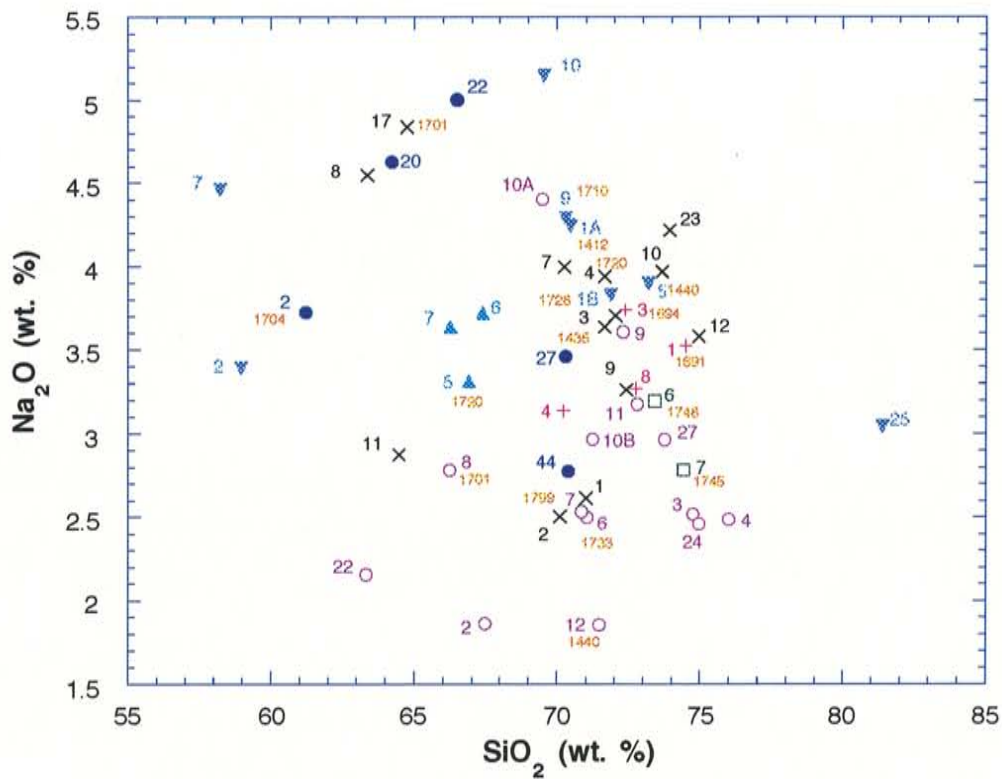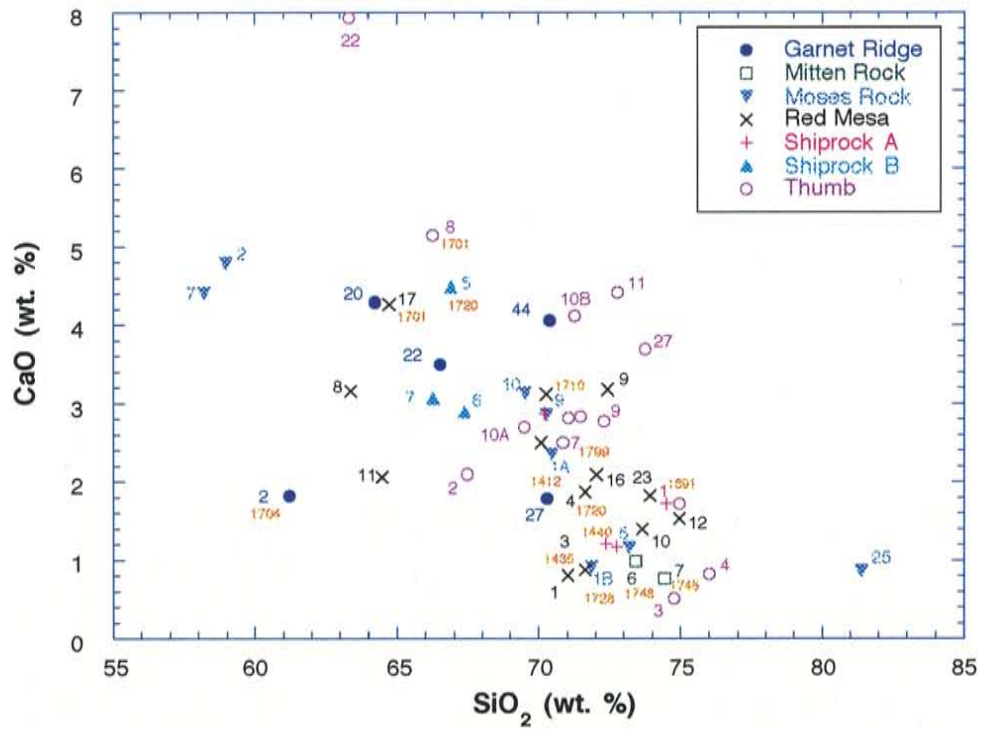
Figure 3.3 c, d. Major element oxides (in weight %) versus SiO_2 for granitoid xenoliths from the Navajo Volcanic Field. Numbers in orange represent U/Pb zircon ages.

34
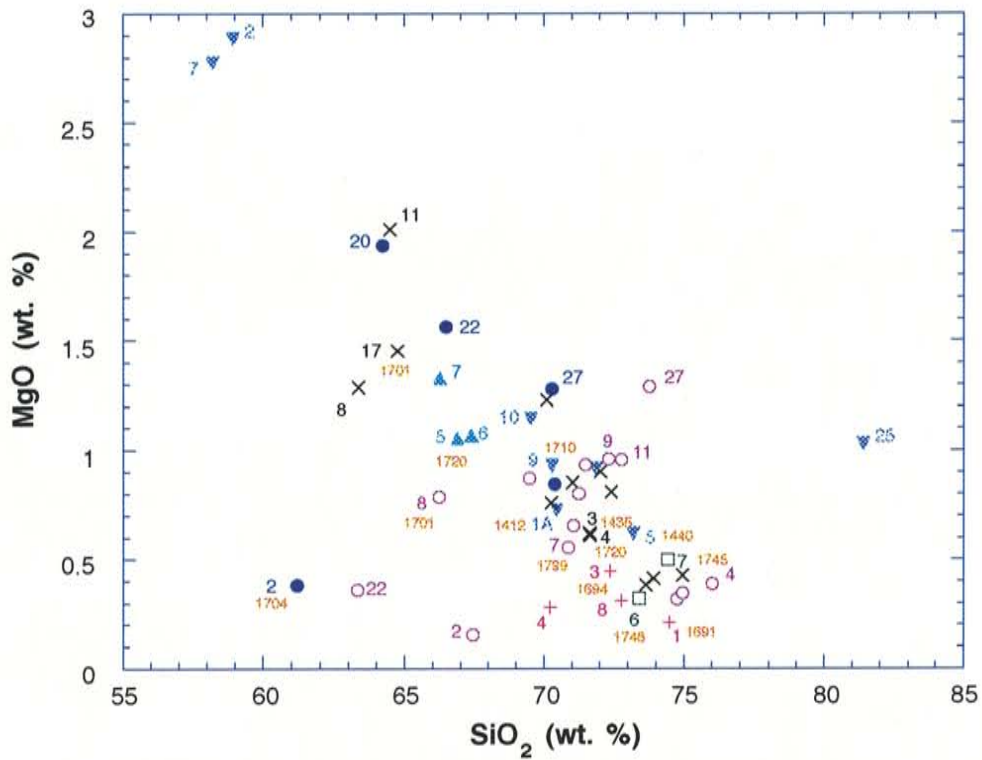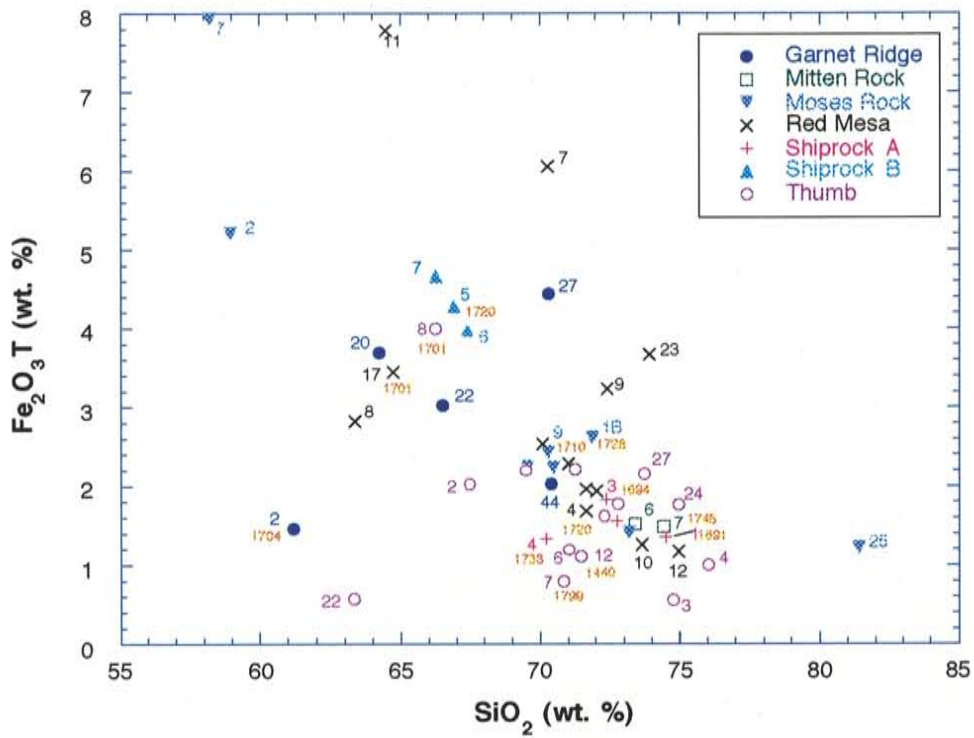
Figure 3.3 e, f. Major element oxides (in weight %) versus SiO_2 for granitoid xenoliths from the Navajo Volcanic Field. Numbers in orange represent U/Pb zircon ages.

35
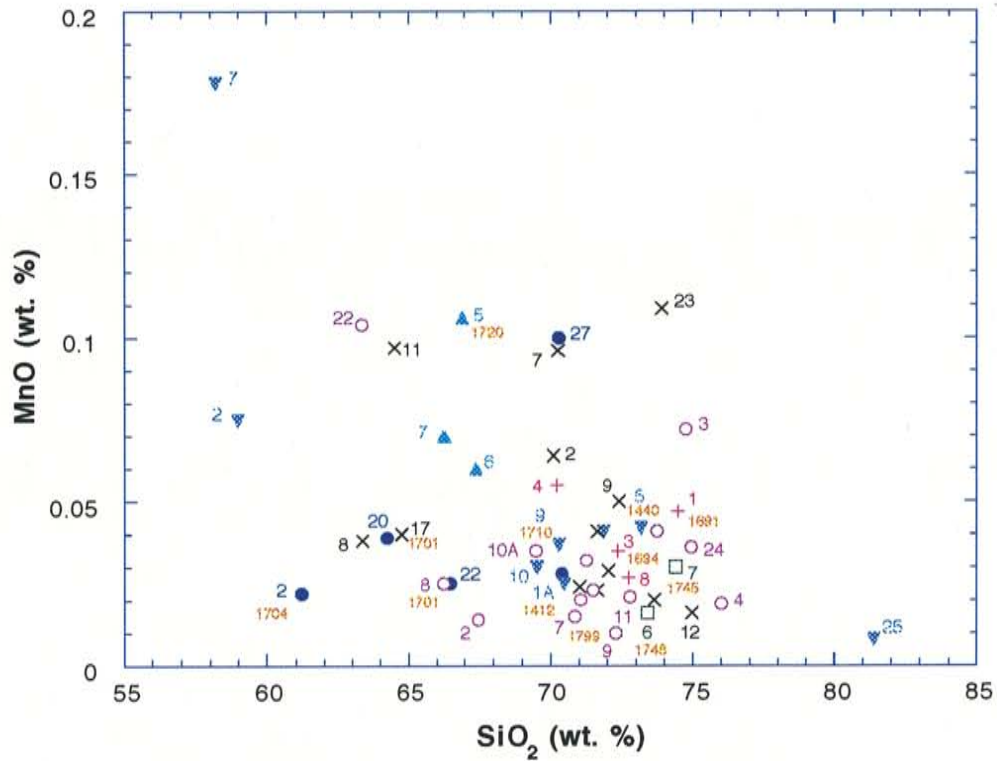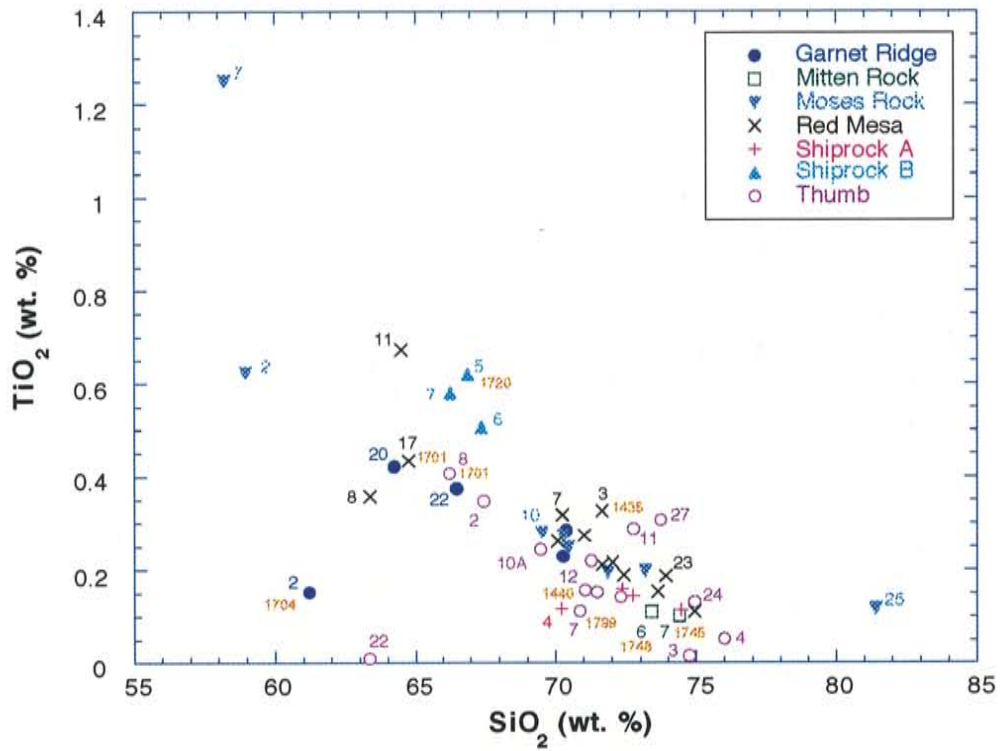
Figure 3.3 g, h. Major element oxides (in weight %) versus SiO₂ for granitoid xenoliths from the Navajo Volcanic Field. Numbers in orange represent U/Pb zircon ages.

36

Alteration

Element mobility is a significant concern in interpreting geochemical data. Many of the NVF granitoid samples have been ductily deformed prior to entrainment, which promotes diffusion leading to element mobility. Samples display varying degrees of alteration and carbonates commonly fill interstices and occasionally replace minerals. It is difficult to constrain the timing of alteration, which probably affected the samples before and after entrainment. The least altered specimens were picked for the granitoid population and were chemically analyzed. However, it was only after petrographic analysis was completed that the full extent of alteration was deduced. Alteration can sometimes systematically affect mobile elements (such as K, Rb, Ba, Sr) making geochemical trends difficult to quantify. CaO and Al_2O_3 show slight declining trends with increasing silica content (Figures 3.3 a, c). However, K_2O and Na_2O display no correlation (Figures 3.3 b, d), which may be attributed to different source characteristics or more likely to secondary modifications of the rocks. There is no apparent correlation between the amount and type (chloritization, sericitization) of alteration and concentration of any element.

Data Assessment

To evaluate the geochemical results, bivariate, trivariate, and normalized incompatible element plots were constructed for the granitoid xenoliths. Major and trace element diagrams are used to identify correlations between different samples and to identify geochemical trends. Some diagrams are used to compare results with experimental data and to evaluate magma production.

From the U/Pb zircon ages and variability in trace element data between samples, it is apparent that numerous plutons exist in the basement of the Four Corners region. Geochemical differences between the xenoliths may be due to alteration, variability in magma sources and generation processes. Factors that may contribute include mixing

between sources, varying degrees of partial melting, degree of assimilation, mobilization of elements by volatile fluxing, differing fractionation trends during crystallization, varying degrees of restite involvement, and/or different rates of cooling. Crystallization of minor phases such as zircon, apatite, allanite, and garnet, which have an affinity for specific trace elements (e.g. REE, Hf, Zr, Nb, Ta), make chemical interpretation difficult (Pearce *et al.*, 1984), since they are usually heterogeneously scattered throughout the plutons (Hassanen, 1997). Sample size may also be a factor contributing to geochemical heterogeneities. A standard representative sample size used for geochemical analysis is approximately 5 kg (P. Kyle, personal communication, 1997). A few xenoliths contributed only 3-4 kg of material for analysis. Lack of appropriate sample size is a concern for large grained samples since complete homogenization may not be acquired.

Slight declining trends with increasing SiO_2 concentration are observed for some of the elements on the Harker diagrams (Figures 3.3 a-h). The meaning of these trends, however, is not entirely clear. The constant sum effect introduces negative bias into the correlations and could lead to deceptive correlations (Rollinson, 1993). There is also an apparent reduction in scatter of values with increasing SiO_2 content (Figures 3.3 a-h). Since SiO_2 comprises more than half of the composition the other variables make up the proportion of the remainder. Therefore, a forced association exists between them. It is well known that summing of analytical data to 100% introduces a correlation between the samples (Rollinson, 1993).

Geochemical   Correlation

The petrographic groups outlined in Table 2.2 are plotted on bivariate geochemical plots to examine correlations between the groups (Figure 3.4 a, b). There is no apparent correlation between any of the petrographic groups and modal mineralogy or geochemistry.

The three deformational groups outlined in Table 2.3 are plotted on bivariate geochemical plots to examine relationships between the samples (Figure 3.5 a, b). There is no apparent correlation between any of the deformational groups and modal mineralogy or geochemistry.

An attempt was also made to classify the NVF granitoid xenoliths using major and trace element distributions. Few samples consistently display similar geochemical behavior. The samples from different diatremes overlap and there is no geochemical correlation between them, except perhaps for two populations at Shiprock, which are designated as Shiprock A and Shiprock B populations (Table 2.1). The samples in these two groups also have petrographic similarities.
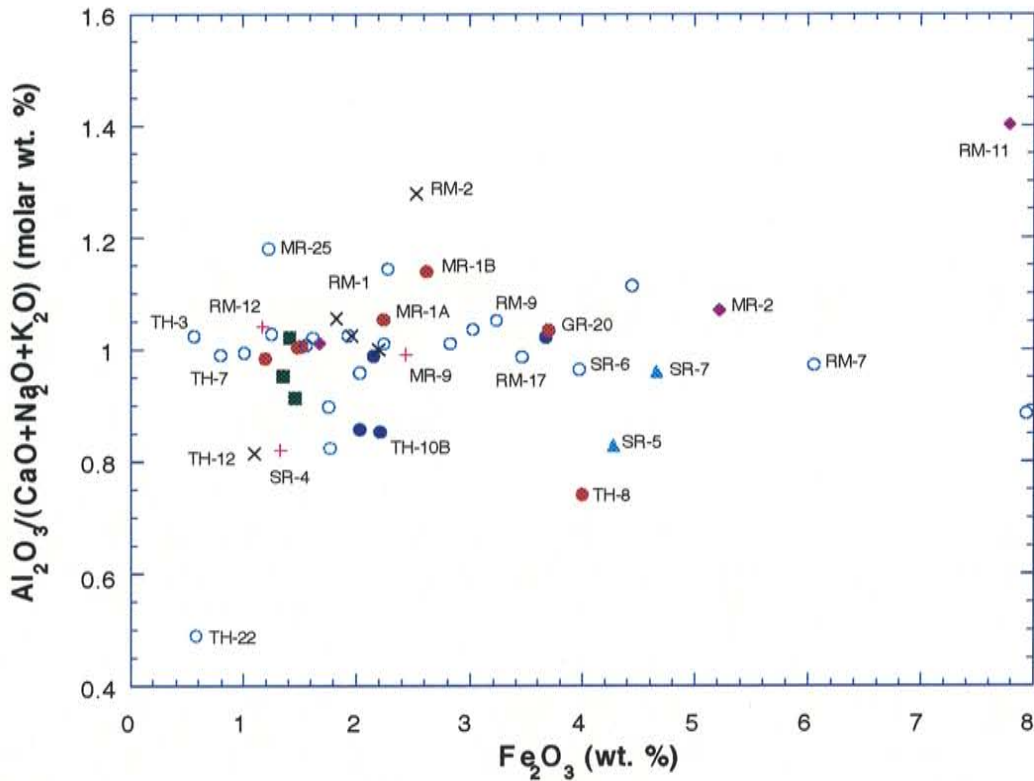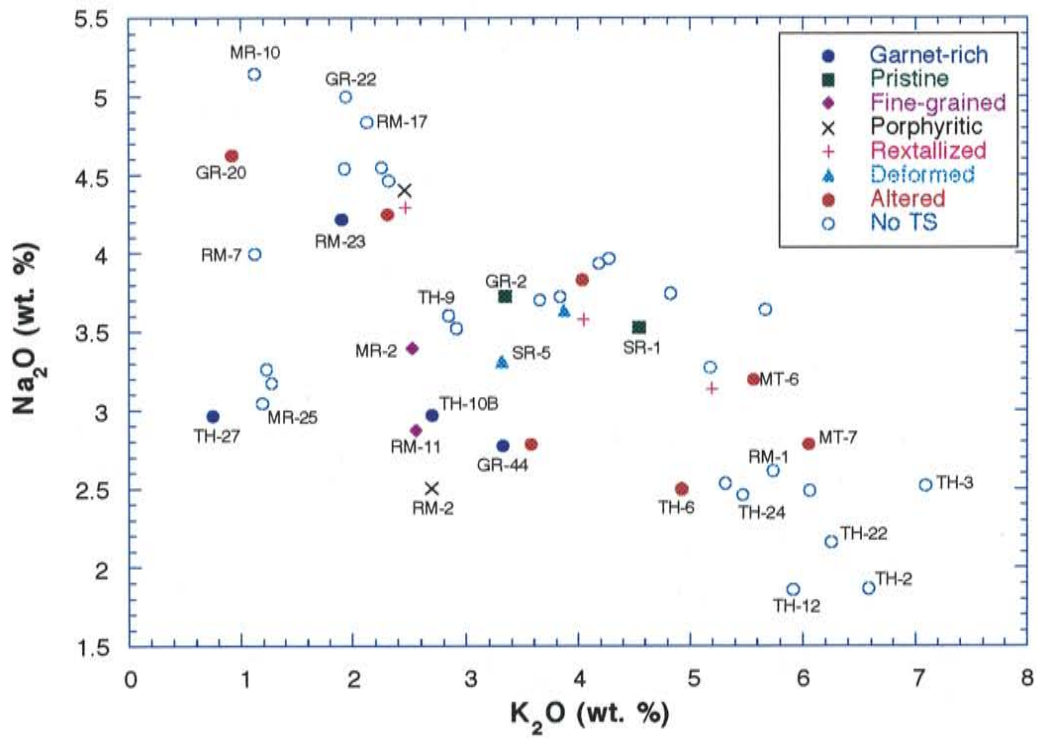
Figure 3.4 a, b. Selected major element variation diagrams for NVF xenoliths. Samples are divided into populations according to petrographic characteristics (Table 2.2). Xenoliths were collected from minettes: SR-Shiprock, MT-Mitten Rock, TH-Thumb and kimberlites: GR-Garnet Ridge, RM-Red Mesa, MR-Moses Rock.
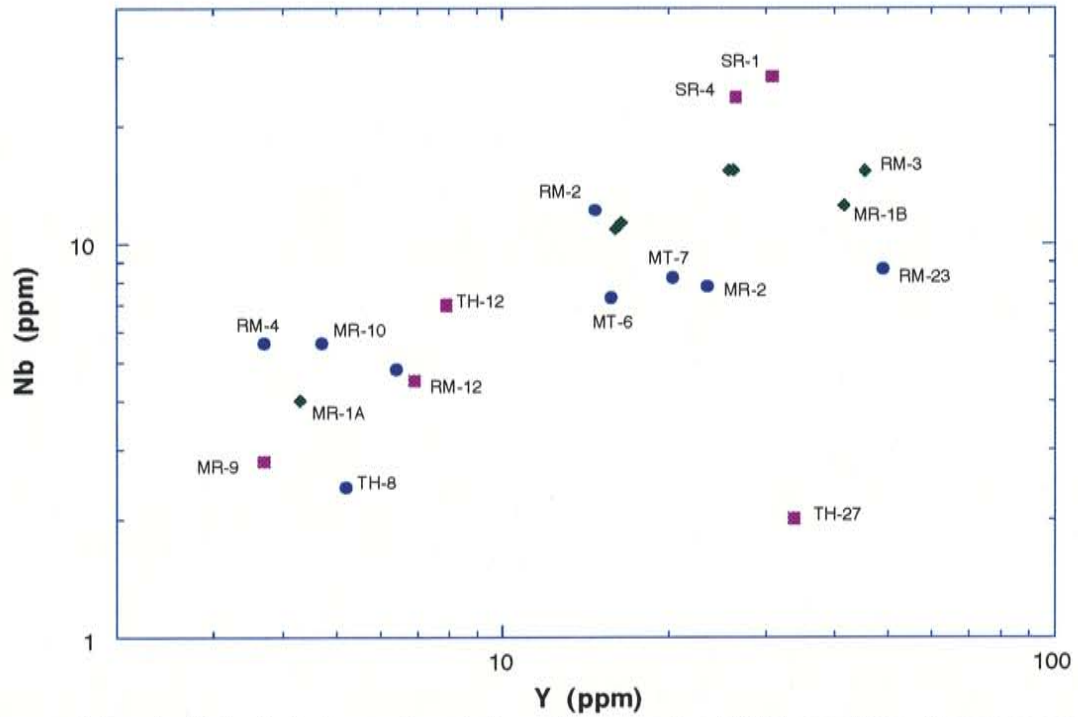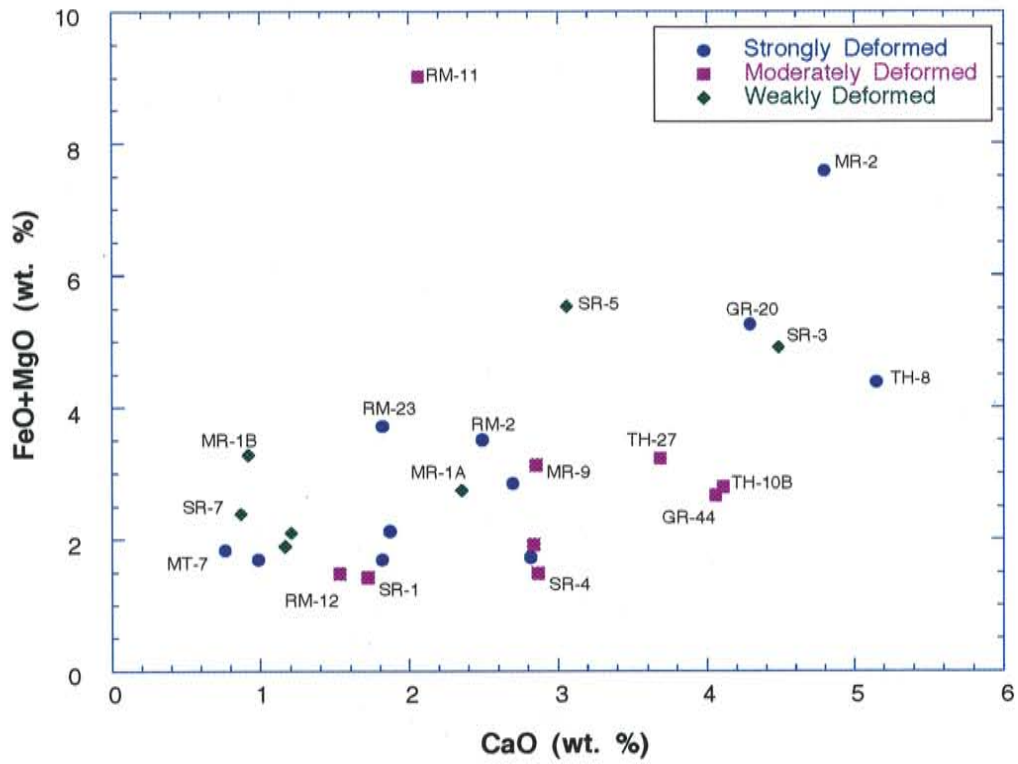
Figure 3.5 a, b. Selected element variation diagrams for NVF xenoliths. Samples are divided into populations according to degree of deformation (Table 2.3). Xenoliths were collected from minettes: SR-Shiprock, MT-Mitten Rock, TH-Thumb and kimberlites: GR-Garnet Ridge, RM-Red Mesa, MR-Moses Rock.

The xenolith groups based on hand sample, petrographical characteristics or deformation show little correlation with geochemistry. Using petrography, major and trace element concentrations, and hand sample analysis for genetic relationships is not feasible, due to possible element remobilization during alteration and deformation, derivation of granitoids from different sources and heterogeneities within individual plutons.

Trace Elements

Trace chemical analyses are given in Table 2, Appendix B and selected trace element distributions are illustrated in Figures 3.6 a-f. High field strength elements such as Ti, Zr, Y, Nb and P are immobile in aqueous fluids (Rollinson, 1993) and are concentrated in residual phases (Harris et $al.$, 1986). However, little is known about the melting and crystallization behavior of these phases.

Trace elements display a great deal of variation with SiO_2 content. The slight negative trend of V with SiO_2 (Figure 3.6 d) indicates incompatible behavior of V. There is no apparent elemental behavior illustrating fractional crystallization in the other trace element plots. A wide range of Nb and Y values exists, ranging from 2 to 27 ppm and 2 to 82 ppm, respectively. Variable fractionation of apatite, sphene, and biotite during segregation
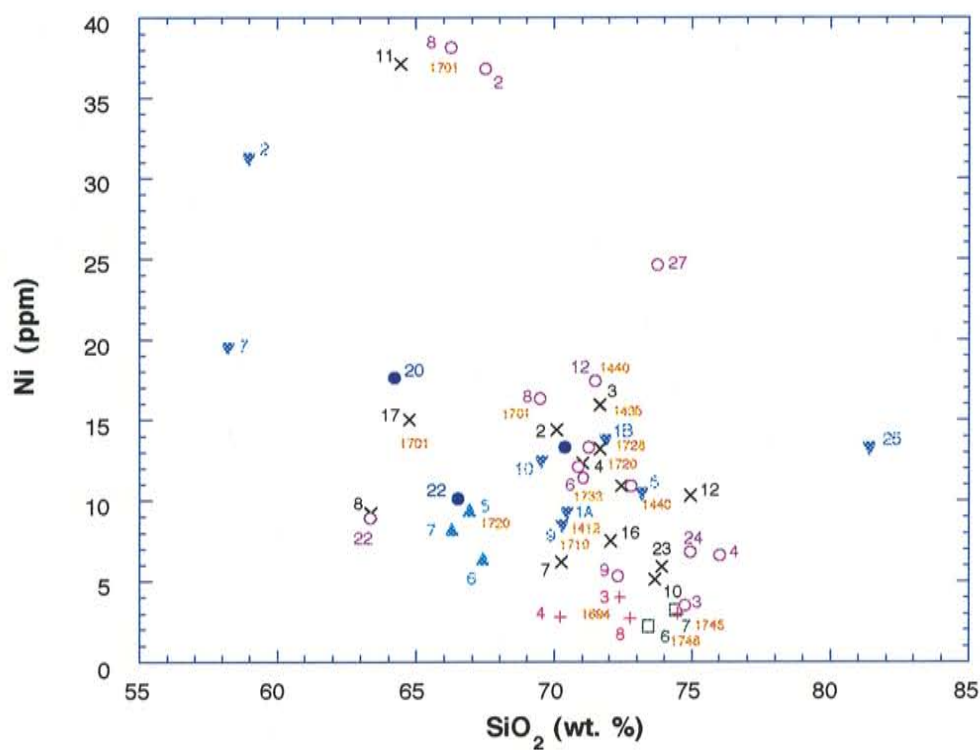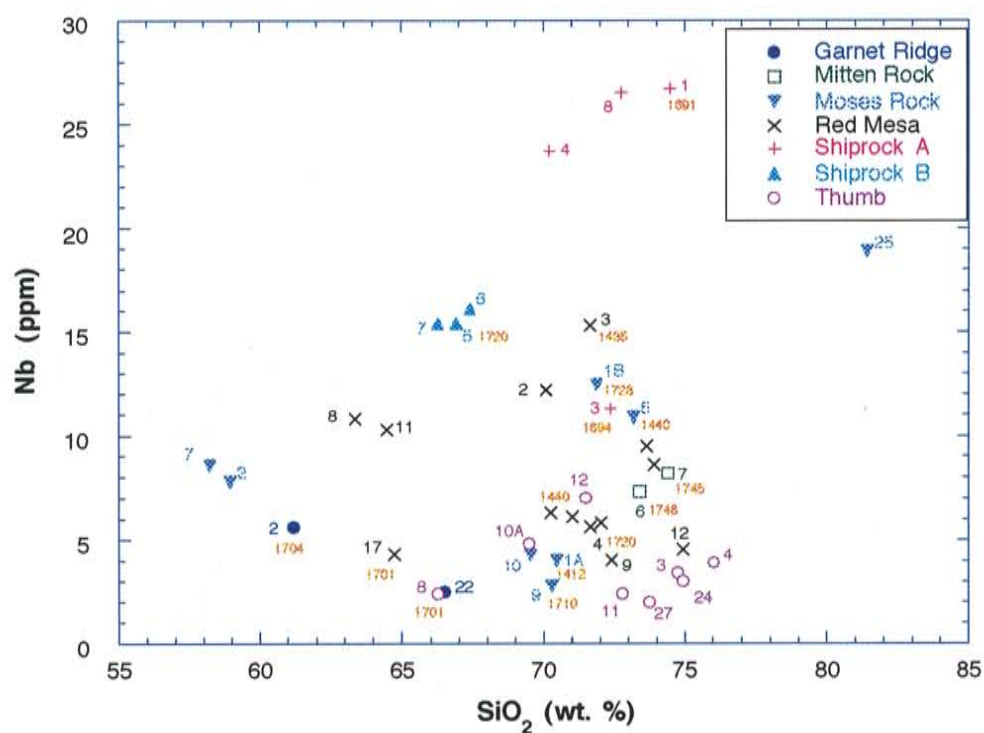
Figure 3.6 a, b. Nb- and Ni-SiO$_2$ variation diagrams for granitoid xenoliths from the Navajo Volcanic Field. Numbers in orange represent U/Pb zircon ages.

43
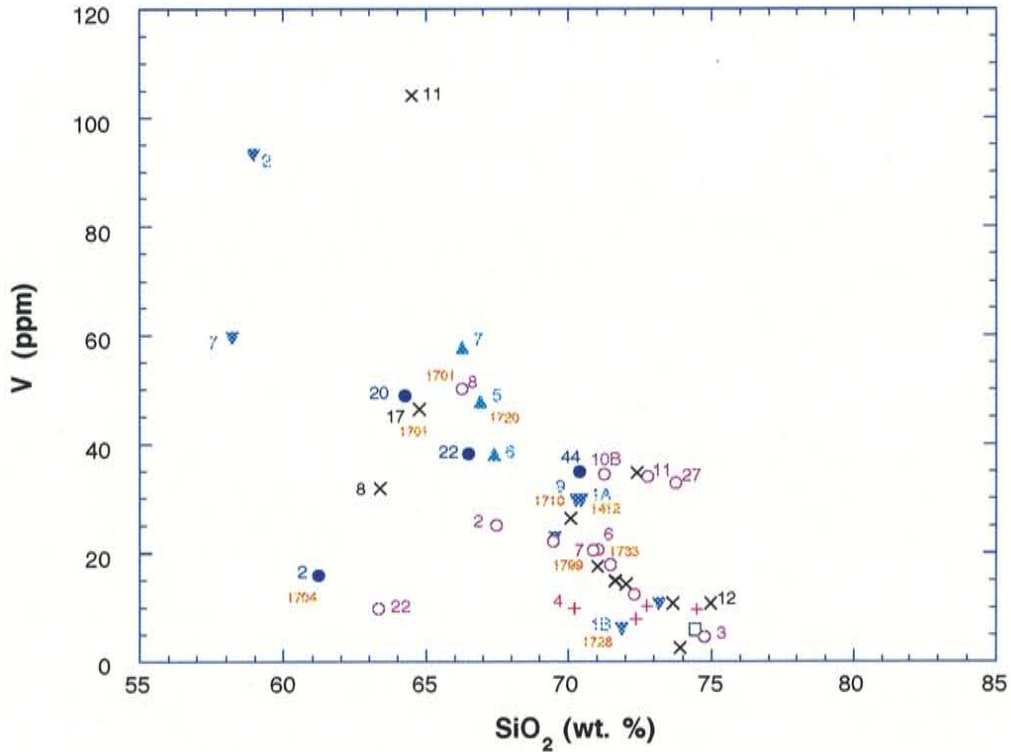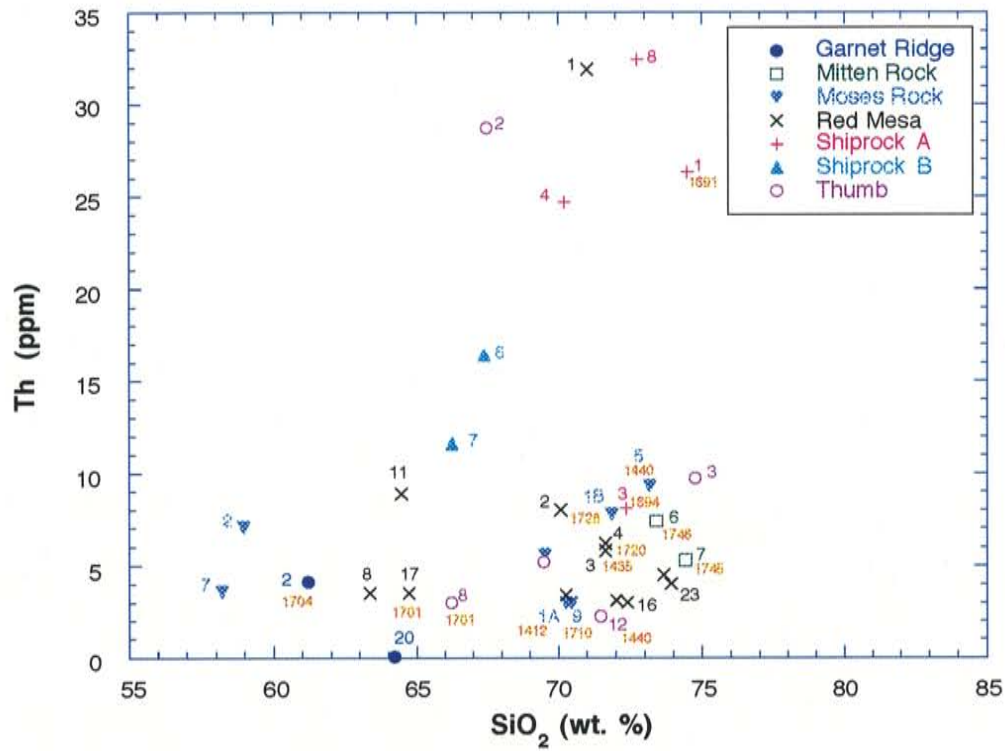
Figure 3.6 c, d. Th- and V-SiO$_2$ variation diagrams for granitoid xenoliths from the Navajo Volcanic Field. Numbers in orange represent U/Pb zircon ages.

44
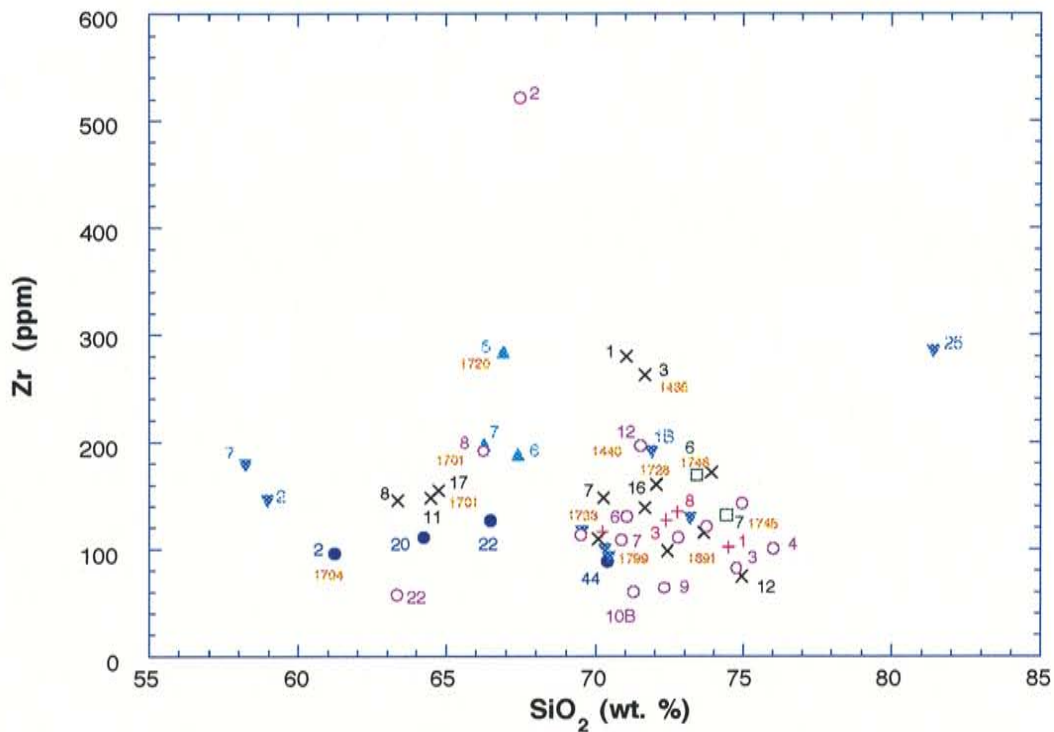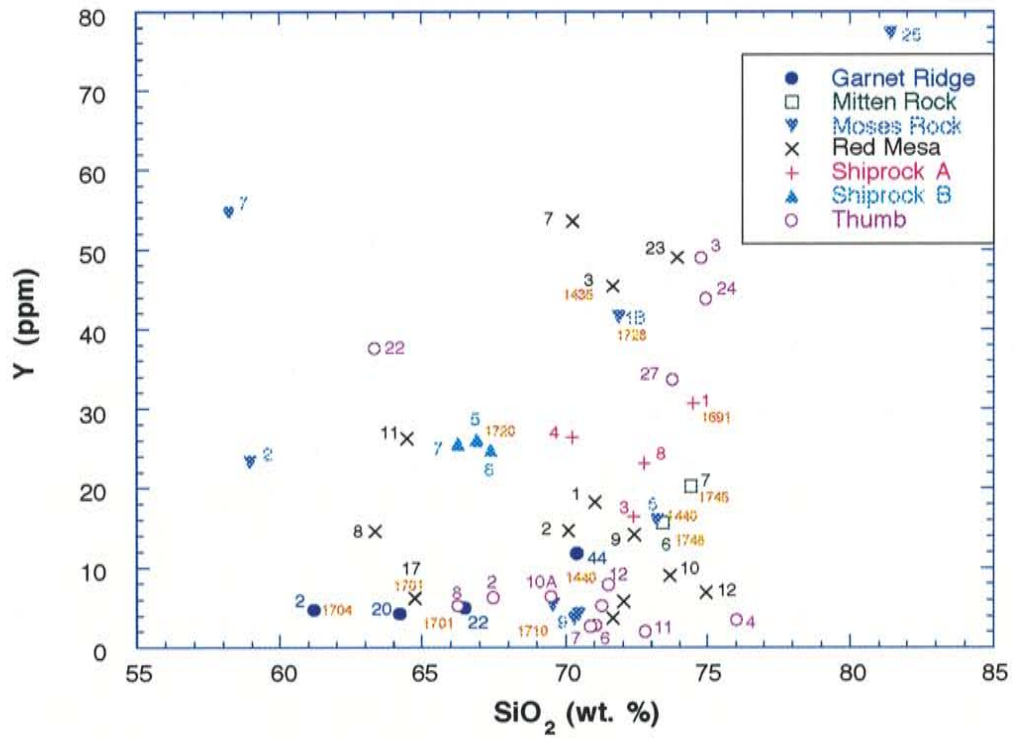
Figure 3.6 e, f. Y- and Zr-SiO$_2$ variation diagrams for granitoid xenoliths from the Navajo Volcanic Field. Numbers in orange represent U/Pb zircon ages.

45

of melt from the restite, may be responsible for some of the chemical diversity among samples, although different source characteristics may also be important. Three out of the four samples from Shiprock A group display anomalously high Nb values (23-27 ppm), while the majority of samples range between 2 and 15 ppm. Petrographic investigation does not reveal the presence of sphene in the Shiprock A group to account for the exceptionally high Nb concentrations. However, recrystallization and other secondary modifications, which are prevalent in this group may mask its presence. These samples also have high Th concentrations and may reflect zircon or allanite content. Allanite is not observed in the Shiprock A samples. Zr concentration in the Shiprock A samples is not exceptionally different from the rest of the granitoid population indicating that zircon is not responsible for the high Th values. Zr concentrations are quite variable among the granitoids. The majority of the samples have Zr contents of 57 to 284 ppm, although TH-2 has an anomalous concentration of 521 ppm.

Aluminum Saturation Index

The NVF granitoid samples show a broad range in molecular $Al_2O_3/(Na_2O+K_2O+CaO)$ values, the aluminum saturation index (ASI) (Zen, 1986). Most of the samples have A/CNK values close to 1 however, they display a wide range in values of 0.48 to 1.30. Forty percent of the granitoids are peraluminous (A/CNK>1), 53% are metaluminous (A/CNK<1) and 7% plot on the boundary between the two fields (Figure 3.7 a). There are no peralkaline (A/NK<1) granitoids among the NVF samples. No apparent relationships exist between the degree of alumina saturation and SiO_2 concentration (Figure 3.7 b), therefore fractional crystallization is an unlikely process responsible for the observed trends. Element mobilization, perhaps during alteration is a more likely explanation.
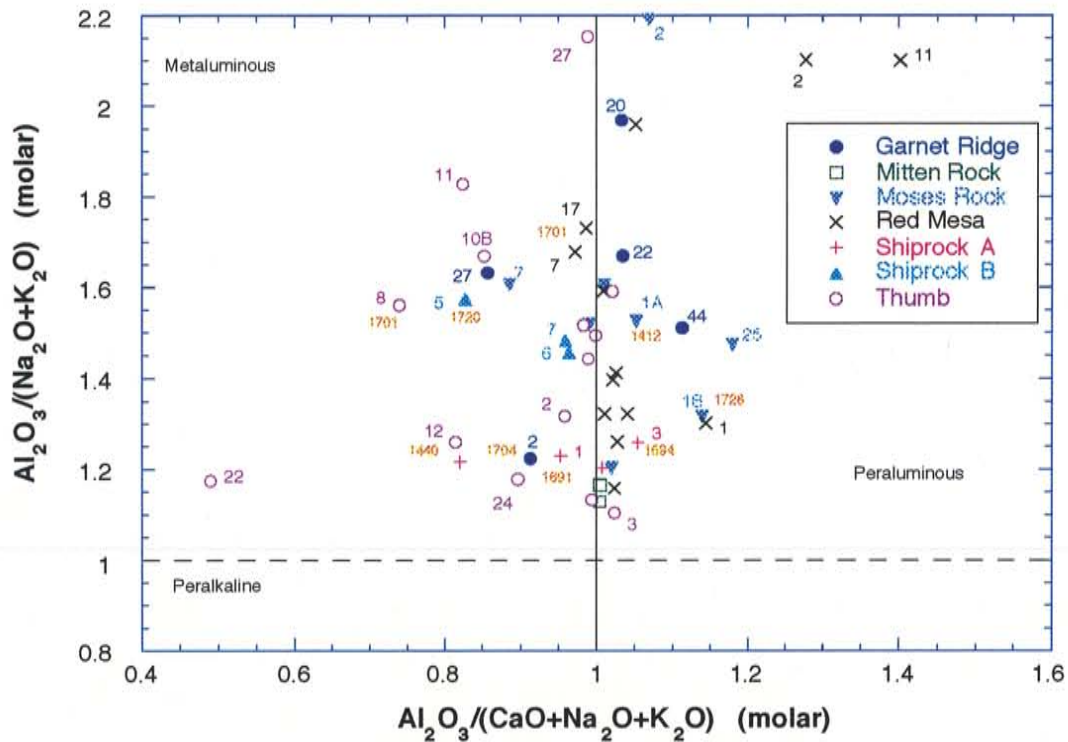
Figure 3.7 a. NVF granitoid xenoliths plotted according to Shand's ASI index (Shand, 1951). Peraluminous: A/CNK>1.0; metaluminous: A/NK>1.0, A/CNK<1.0; peralkaline: A/NK<1.0.

Alumina undersaturation may be due to the presence of amphiboles in the source (Chappell and White, 1992). Also, hydrothermal alteration can result in feldspar alteration and mobilization of Na, K and Ca affecting the ASI values. Granitoids generated at lower temperatures, approximately 600° C in presence of excess water at midcrustal depths (Hall, 1971), can also acquire slightly peraluminous compositions (Chappell and White, 1992). The peraluminous component in the source of the NVF granitoids does not represent material that has previously been subducted and incorporated into the melt because these are I-type granitoids (Chappell and Stephens, 1988). Nd isotopes also support this conclusion (discussed in Chapter 4). Therefore, source characteristics and magmatic conditions are more likely explanations for the differences in ASI values.

47
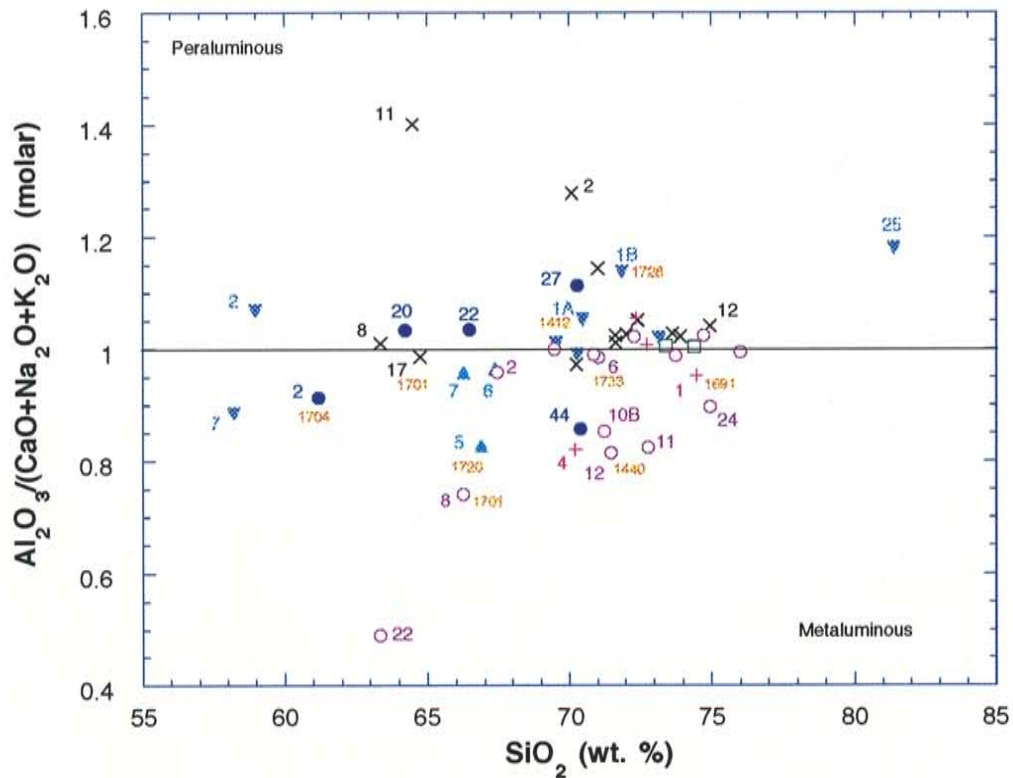
Figure 3.7 b. SiO$_2$-A/CNK discrimination diagram for the NVF granitoids.

Large Ion Lithophile Elements

Figure 3.8 displays the behavior of Rb, Sr, Ba with silica concentration for the NVF granitoids. Sr concentration appears to slightly decrease with increasing silica content. Scatter of values is more prevalent for samples with lower silica concentrations. MR-2 has a distinctively high Sr content (1593 ppm), which most likely reflects greater plagioclase accumulation during fractional crystallization; however, derivation from a different source, or heterogeneities within a single pluton may also be accountable. There is no apparent correlation of Ba with SiO$_2$. Sample TH-8 has an unusually high Ba content (3300 ppm), perhaps reflecting K-feldspar and/or biotite accumulation. Rb shows a slight positive correlation with silica concentration. Three of the four Shiprock A samples have notably
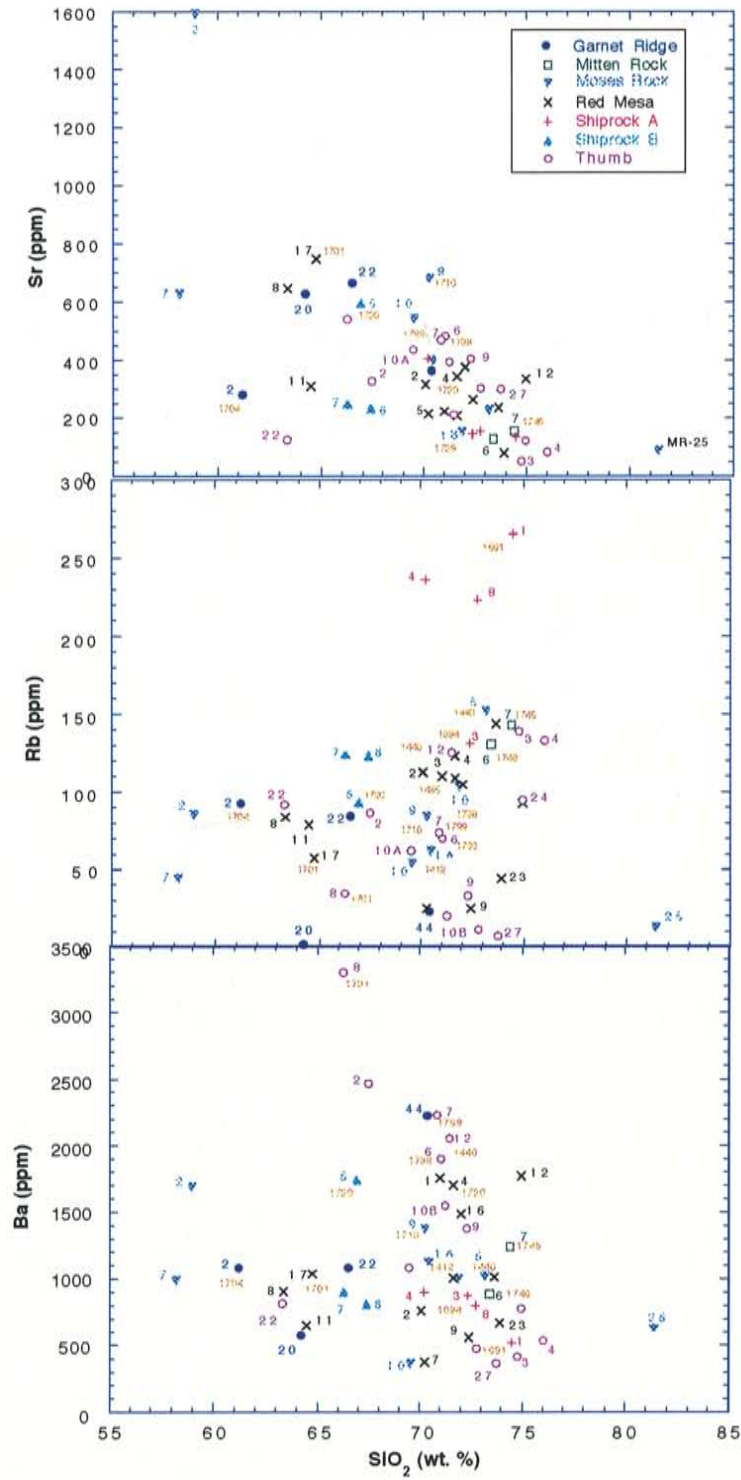
Figure 3.8. Sr, Rb, Ba-SiO₂ variation diagrams for granitoid xenoliths from the Navajo Volcanic Field. Numbers in orange represent U/Pb zircon ages.

49
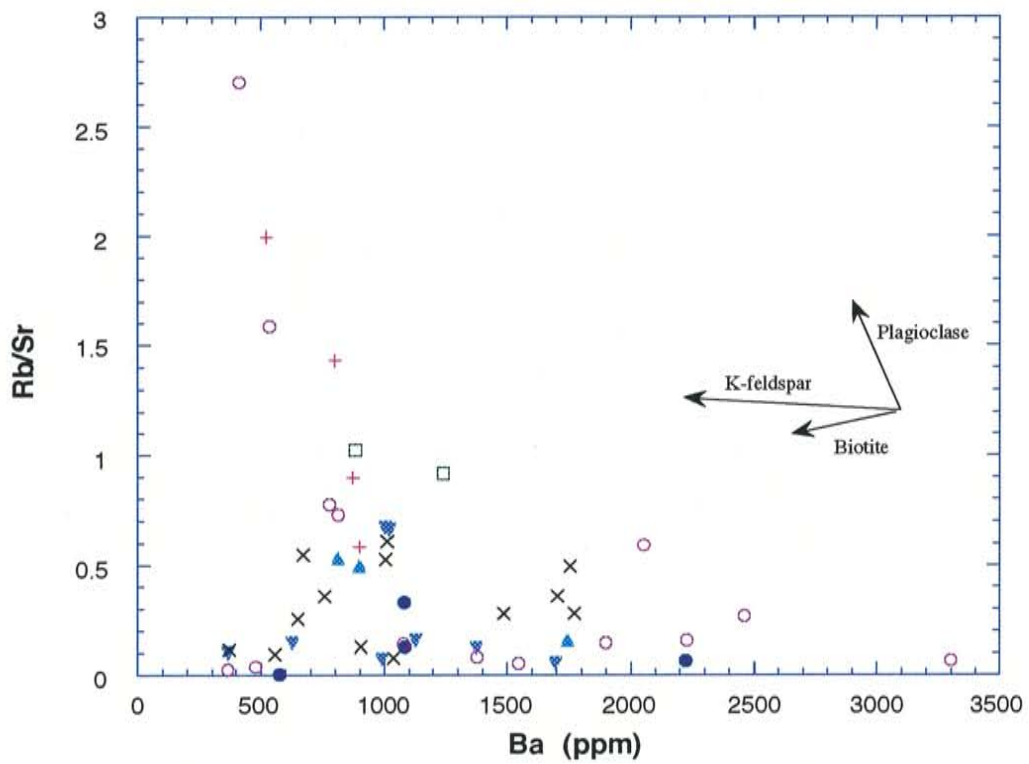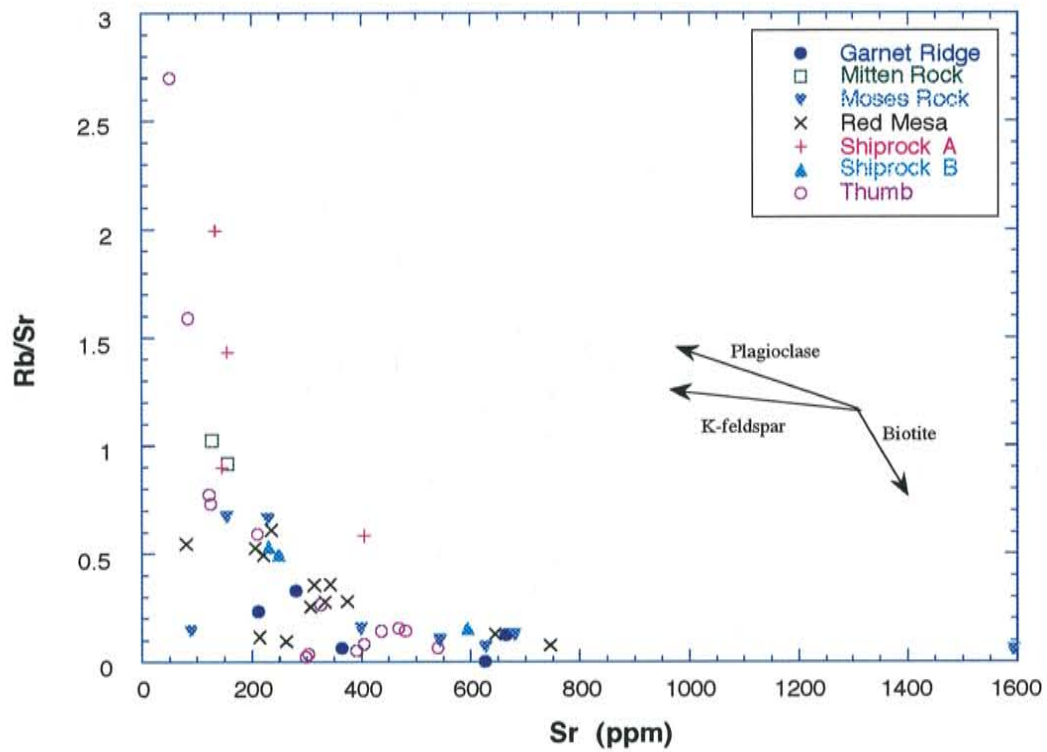
Figure 3.9 a, b. Rb/Sr versus Sr and Rb/Sr versus Ba for granitoid xenoliths from the Navajo Volcanic Field. Arrows are fractional crystallization vectors for plagioclase, biotite and K-feldspar.

high Rb values and are isolated from the general population. These samples contain 7-8% biotite, which is slightly greater than that of an average NVF granitoid.

Rb/Sr ratio varies from 0.02 to 2.7 and the Ba/Sr ratio ranges from 0.67 to 9.72 (Figure 3.9 a, b). A majority of the samples define a fairly shallow trend, indicating that Rb/Sr ratio changes at approximately the same rate as Sr and Ba. This is ascribed to fractional crystallization of feldspars and biotite (McDermott *et al.*, 1996). Elevated Rb/Sr and lower Sr and Ba values are attributed to variable sources and magma dynamics such as partial melting (McDermott *et al.*, 1996) and restite involvement, and to alteration.

Rare Earth Elements

Rare earth elements (REE) are useful for interpreting petrogenesis of igneous rocks. They are the least soluble elements and are not easily mobilized during low-grade metamorphism and weathering. However, alteration may have some affect on their concentrations (Rollinson, 1993). REE are concentrated in accessory phases, such as monazite, allanite, xenotime, zircon, apatite and sphene (Condie, 1978; Mittlefehldt and Miller, 1983).

Chondrite-normalized whole-rock REE abundances of the NVF granitoids are shown in Figure 3.10, using normalizing values of Haskin *et al.* (1968) (listed in Appendix E). Chondritic meteorites are thought to be unfractionated material in the solar system and serve as a reference standard for REE concentrations. Normalizing REE values eliminates abundance variations between odd and even atomic number elements. It also provides a way of identifying fractionation of REE relative to chondritic meteorites (Rollinson, 1993). Normalized values are denoted by the subscript letter n.

REE abundances vary over a wide range for the NVF xenoliths and may be controlled by differences in source and by crystal-melt equilibria (Rollinson, 1993). The samples display variable Eu anomalies, moderate LREE enrichment and with the exception of sample RM-

51

23, HREE depletion. Differences in REE distributions also do not correlate with geographic locality, mode of emplacement, extent of alteration, or deformation.

HREE deficiency may be ascribed to the presence of garnet and to a lesser degree to zircon or hornblende in the source (Rollinson, 1993). RM-23 is the only sample which exhibits HREE enrichment. Its modal mineralogy includes garnet (approximately 2%), which may be responsible for HREE fractionation. A plot of Yb_n versus La/Yb_n (Figure 3.11) illustrates the degree of REE fractionation with REE content. La/Yb_n values range from 2.3 to 39 and most of the samples have similar La/Yb_n ratios. There is a slight negative trend exhibited by an increase in the Yb_n content with decreasing La/Yb_n ratio. Again, sample RM-23 is enriched in HREE relative to LREE accounting for the low La/Yb_n ratio. Sample RM-4 is especially depleted in the HREE and has the highest La/Yb_n ratio.

Eu anomalies for the samples analyzed by INAA method have been calculated and are represented by Eu/Eu*. Eu is the measured value obtained by INAA. Eu* is derived by extrapolating between the normalized values of Sm and Gd. A Eu/Eu* value greater than one represents a positive anomaly, whilst a value of less than one denotes a negative anomaly. Large positive Eu anomalies correspond to feldspar accumulation in a cooling magma, which in turn is partly controlled by magma characteristics (viscosity, degree of partial melting, temperature).
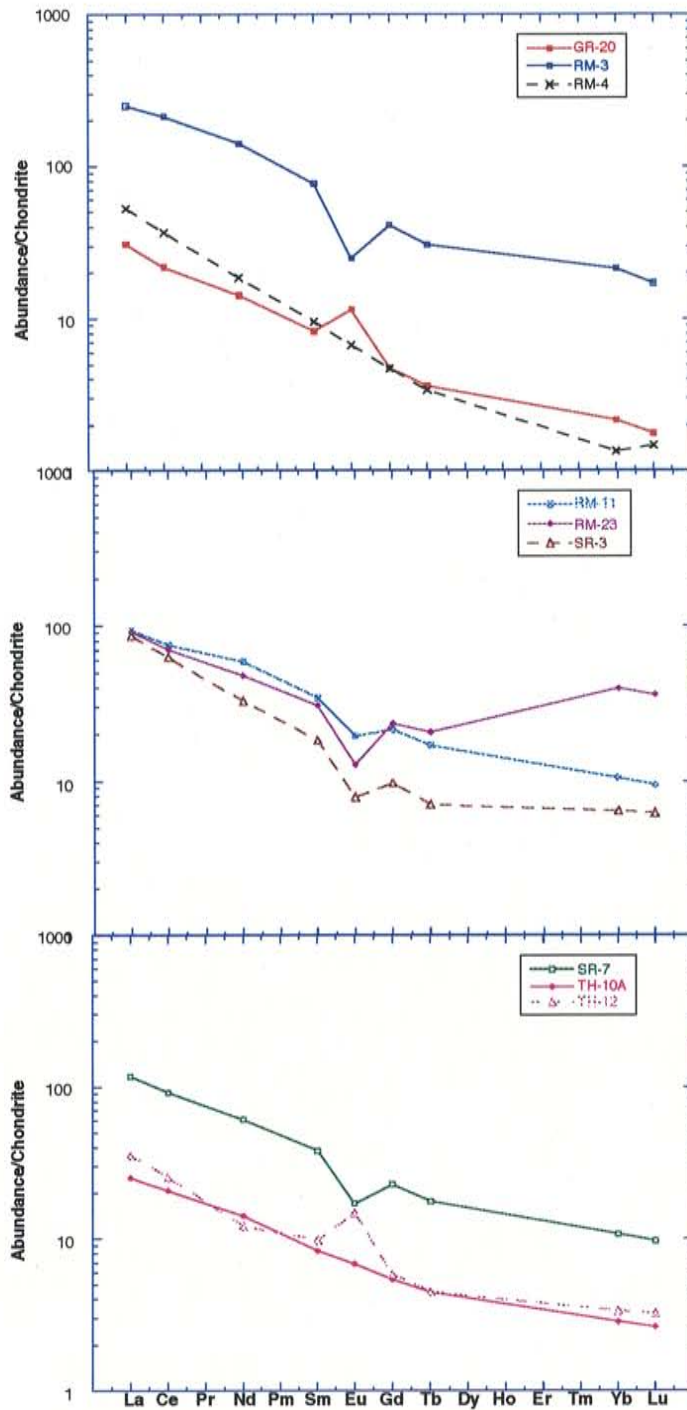
Figure 3.10. Chondrite normalized REE profiles for granitoid xenoliths from the Navajo Volcanic Field. Chondrite normalizing values after Haskin *et al.*, 1968.

53
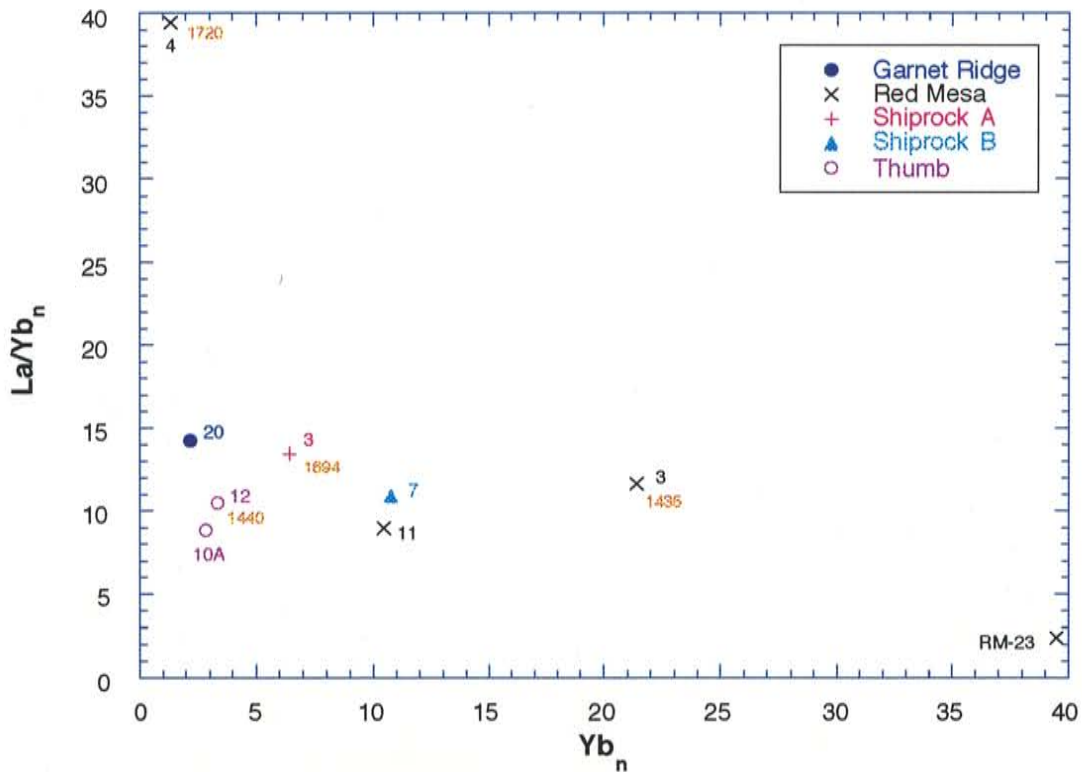
Figure 3.11. Chondrite normalized Yb_n vs. La/Yb_n diagram. Normalizing values for Yb and La/Yb after Haskin *et al.*, 1968.

There is no apparent relationship between La/Yb_n and Eu anomalies (Figure 3.12). The highest and lowest Eu/Eu* ratios occur in the same range of La/Yb_n values (10.5-11.6). This indicates that incorporation of residual material such as garnet has no correlation with feldspar content. However, this interpretation is complicated by the observation that REE equilibration between garnet and siliceous melts is extremely slow at low temperatures (<800° C) (McDermott *et al.*, 1996).

Middle REE are generally controlled by sphene and apatite and to a lesser extent by hornblende. Sphene and hornblende do not appear to play a large role in the NVF granitoids since both are rarely observed in petrographic investigation. Apatite is common in all NVF granitoids with an average concentration of 0.3%. The concentrations of middle

54
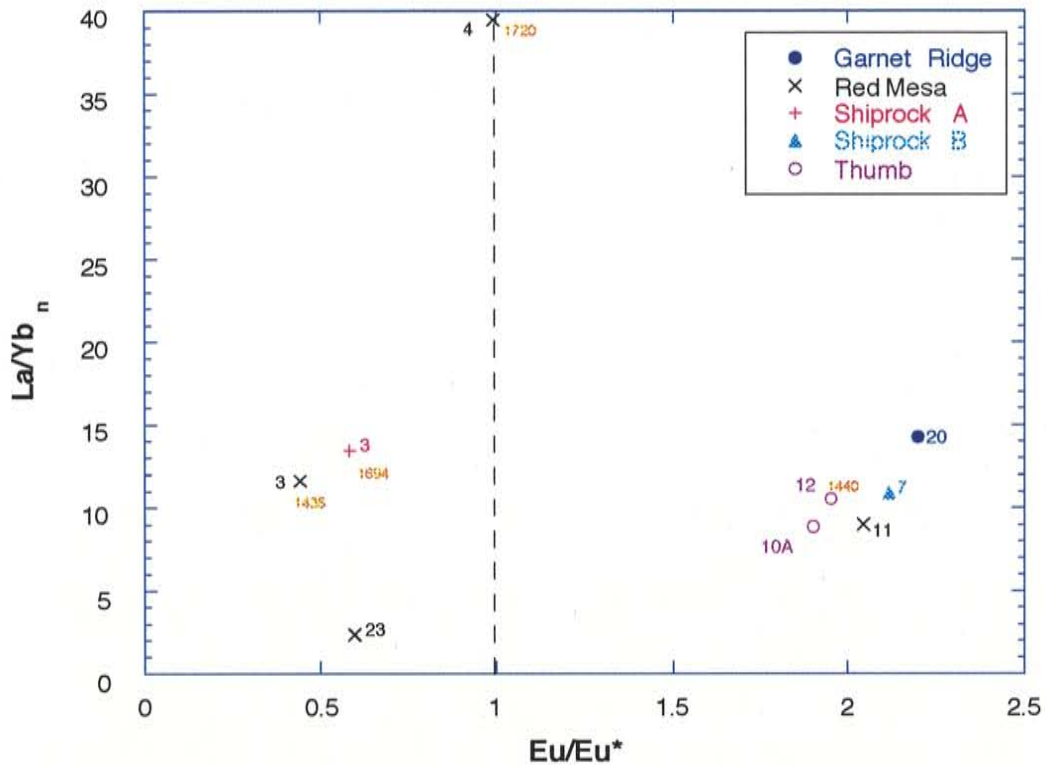
Figure 3.12. Eu/Eu* versus La/Yb$_n$ diagram for the NVF granitoid xenoliths. Eu is a measured value, while Eu* is obtained by extrapolation between normalized values of Sm and Gd. Chondrite normalizing values for La/Yb after Haskin *et al.*, 1968.

REE are consistent with the general declining trend from the LREE to HREE, indicating that apatite is not enriched or depleted in the NVF granitoids. Monazite and allanite may be responsible for depleting the LREE in felsic magmas (Rollinson, 1993) however, their effect in the NVF samples is minimal since LREE depletion is not observed.

Figure 3.13 is a plot of Eu/Eu* versus Sr. Sr and Eu are preferentially incorporated by the feldspars and this figure illustrates feldspar involvement in controlling these two elements. A slight positive correlation is apparent for the NVF data. Deviation from a linear behavior may be attributed to derivation from different sources and may be in part due to mobilization of Sr. Petrographic analysis indicates that plagioclase displays intense secondary alteration. Sample, GR-20, exhibits the highest Eu/Eu* and Sr content. This
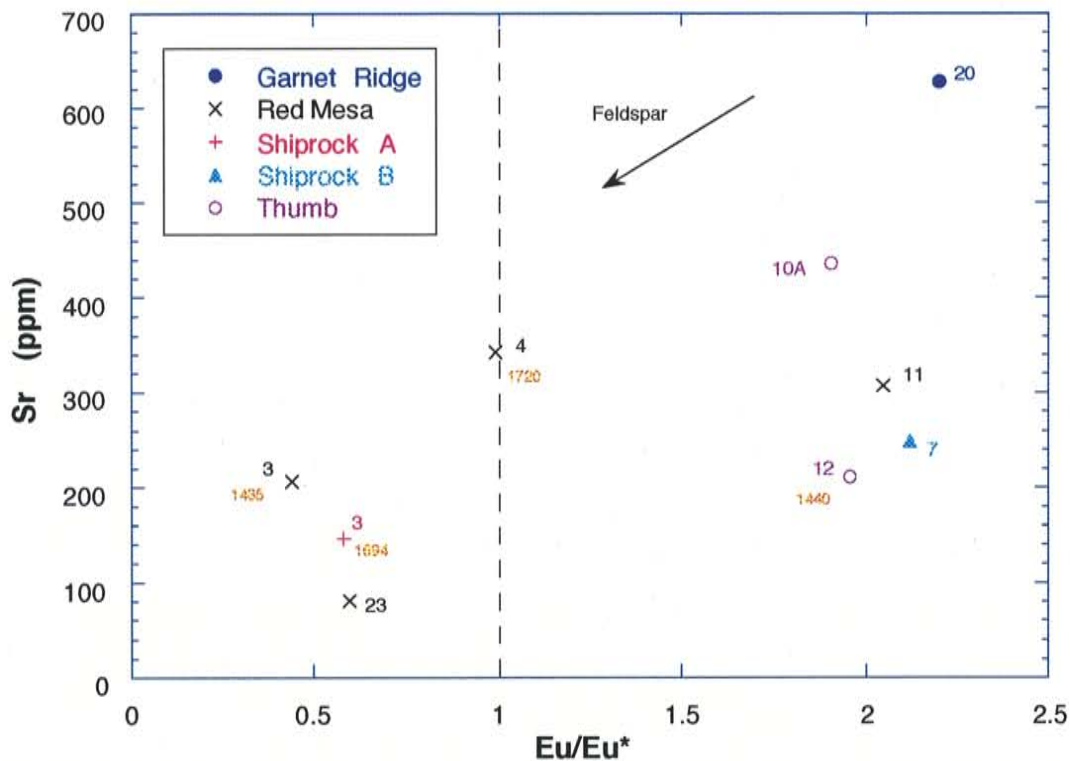
Figure 3.13. Variation in Sr concentration as a function of Eu anomaly (Eu/Eu*). The slight positive correlation is ascribed to preferential incorporation Sr and Eu in feldspars. Arrow represents evolving chemical composition of a melt during feldspar fractionation.

sample is extremely sericitized and contains hornblende, which may be responsible for the high Eu anomaly and Sr content. Samples from Red Mesa and Shiprock are scattered across the plot, verifying that there is no apparent correlation between geochemistry and locality. Also, results suggest the absence of a relationship between age and either geochemistry or location.

Incompatible Elements

Primitive mantle (PM) normalized spidergrams for the Four Corner granitoids are shown in Figures 4.6 a-c. Primitive mantle values are from Sun and McDonough (1989) and are listed in Appendix E. Element concentrations plotted on the diagrams (Chapter 4) are averaged for thirty-five of the least altered NVF granitoid samples. Although, in detail, the

trends are erratic and oscillatory, as expected an overall decrease in concentration from Rb to Y is apparent. Ta and Nb are depleted in the NVF granitoids (Figures 4.6 a-c). Negative deviation of Ta and Nb from the general trend reflects a subduction component, which was probably inherited from the volcanic arc source (see Chapter 4). While Ta concentration ranges from 0.03 to 1.17, Nb displays a great deal of variation with concentrations ranging from 2.0 to 26.7. Th is depleted in the NVF granitoids, which may indicate granulite metamorphism of the source, since Th is generally immobile during alteration and subduction processes may selectively enrich Th (Brown *et al.*, 1984). The average Rb, Ba and K abundances are in a similar range, with no major variation. Sr is depleted in the NVF granitoids. Sr depletion may be due to loss during alteration of plagioclase or by its retention in the restite component. P and Ti are depleted in the NVF granitoids. Depletion in P and Ti may be due to fractionation of apatite (P) and hornblende or sphene (Ti).

CHAPTER 4: DISCUSSION

4.1 Geochronology

U-Pb zircon ages of seventeen NVF granitoid samples were determined at the Geochronology Laboratory at the University of Kansas by W.R. Van Schmus and M. Kozuch (results are given in Appendix F). Numerous zircon grains are used in deriving the age for an individual sample. Large associated errors with calculated ages reflects deviations of U/Pb ratios measured on zircons used in deriving a sample's age. Figure 4.1 shows the distribution of ages in the NVF diatremes and is useful in deducing possible relationships between rocks which may have been derived from the same pluton. It is apparent that plutons in the NVF vicinity were generated during two magmatic pulses, 1400 Ma and 1700 Ma. There may be two plutons represented in the 1400 Ma magmatic pulse. The possible age span of MR-1A does not coincide with that of MR-5 and TH-12, although it overlaps with RM-3. At least two plutons exist beneath Moses Rock. There is an overlap in ages of RM-3, MR-5 and TH-12, however if they share a similar plutonic source, it is a very large body.

Rocks generated during the 1700 Ma event show a great deal of overlap in age and some samples have large errors. The Shiprock samples have similar ages and show a great deal of overlap. However, SR-5 belongs in Shiprock B group and has different geochemical characteristics than SR-1 and SR-3, which belong in Shiprock A group. These samples were generated contemporaneously possibly from similar sources, and have experienced different degrees of fractional crystallization and assimilation. TH-7 is slightly older than other samples. Its age overlaps with only a few samples, coinciding with TH-6, SR-5, MT-6, MR-1B. It does not overlap with TH-8, possibly indicating that there are at least two plutons in the crust beneath the Thumb. The age of GR-2 does not coincide with MT-6 and the ages of TH-8 and MR-9 do not coincide with those of MT-6, RM-17 and TH-8.

GR-Garnet Ridge
MR-Moses Rock
MT-Mitten Rock
SR-Shiprock
RM-Red Mesa
TH-Thumb

├—◆—┤ GR-2

├—◆—┤ MR-1A

├◆┤ MR-5

├————◆————┤ MR-1B

├◆┤ MR-9

├———◆———┤ MT-6

├◆┤ MT-7

├—◆—┤ RM-3

├———◆———┤ RM-4

├◆┤ RM-17

├————◆————┤ SR-1

├———◆———┤ SR-3

├—————◆—————┤ SR-5

├————◆————┤ TH-6

├———◆———┤ TH-7

├——◆——┤ TH-8

├◆┤ TH-12

```
1400        1500        1600        1700        1800
                        (Ma)
```
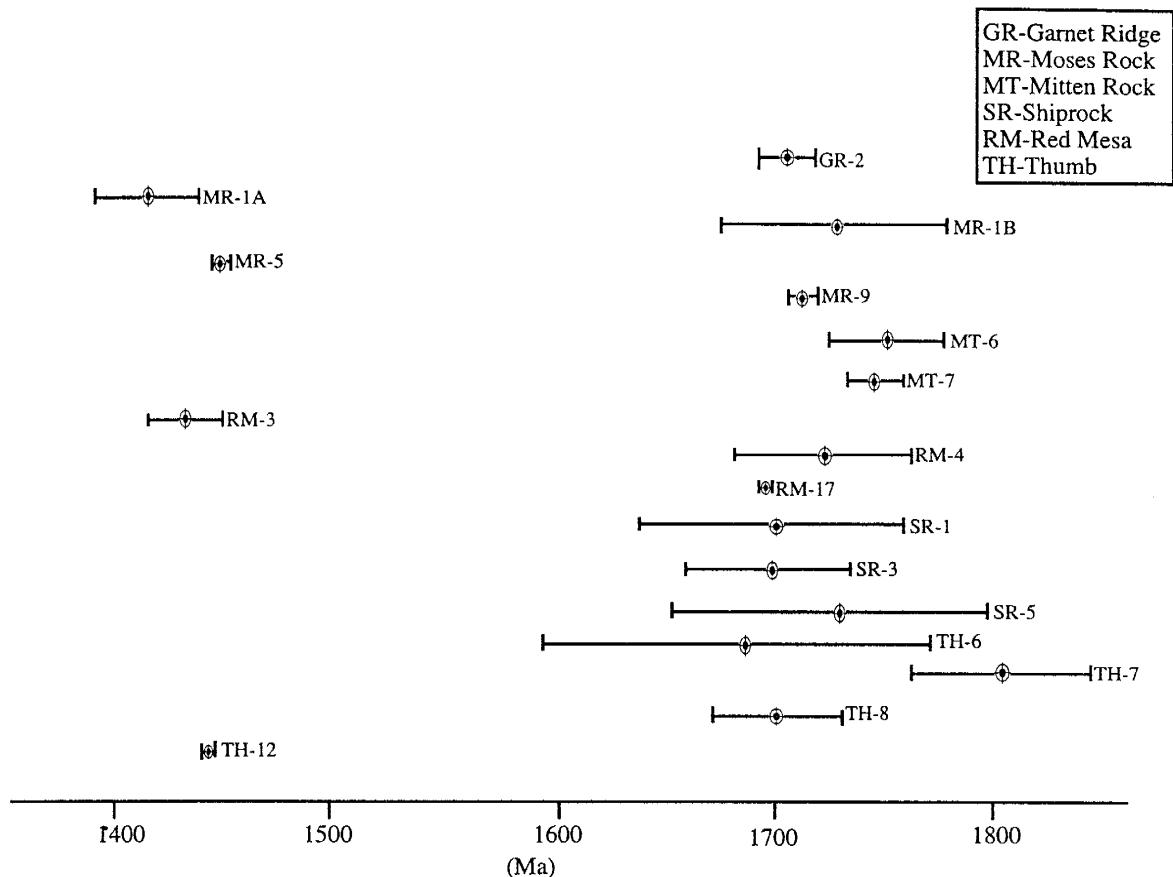
Figure 4.1. A schematic illustration of crystallization ages for the NVF granitic xenoliths. Representative bars account for dating error. Ages were obtained by U/Pb zircon dating at the University of Kansas (see Appendix F).

The wide age distribution among the samples suggests there are numerous plutons of different ages in the upper crust of the Navajo Volcanic Field. There are at least four 1700-Ma plutons. At least two 1700-Ma plutons occur at depth in the Shiprock vicinity (indicated by geochemical variation among the populations), and at least three plutons beneath the Thumb diatreme, two of which were generated during the 1700-Ma event. A 1400-Ma and a 1700-Ma pluton exist in the crust beneath Red Mesa. The samples derived from Mitten Rock are probably from the same pluton since they share similar geochemical characteristics and are of approximately the same age. There are at least three plutons beneath Moses Rock, two of which were generated during the 1400 Ma event. Only one age is available from Garnet Ridge; however samples from this locality display wide geochemical variations, probably indicative of different plutonic bodies in the area.

59

4.2 Nd Isotopic Considerations

The Colorado Plateau is composed of several Early Proterozoic crustal segments which were derived from the mantle and accreted to the southern margin of the Archean Wyoming Province (Wendlandt *et al.*, 1993). Evolution of this region can be constrained with Nd isotopes. Epsilon Nd values can serve as a valuable tool in understanding the various components and their degree of interaction in the sources of the NVF granitoids, and also in constraining the nature and timing of secondary processes.

Sm-Nd Isotopic Systematics

^{147}Sm decays to ^{143}Nd by alpha decay. The Sm/Nd ratio increases in residual materials left behind after partial melts have been extracted during crustal forming events. Nd^{3+} has a larger radius, lower ionic potential, forms weaker bonds and is therefore more incompatible than Sm. It is enriched in the liquid phase, relative to Sm thus, the Sm/Nd ratio is lower in the melt than in the residual material. As the fraction of melt increases Sm and Nd are depleted and the Sm/Nd ratio in the residue increases. Magmatic processes can produce different reservoirs with distinct Sm/Nd ratios, from a single initial reservoir. These reservoirs develop different $^{143}Nd/^{144}Nd$ ratios with time. Source regions, with distinct ratios may be identified and the extent of their involvement in a mixing process may be constrained using Nd isotopic ratios (Rollinson, 1993). The Sm/Nd isotopic system is resistant to metamorphism and is useful in seeing through crustal modification events (DePaolo, 1988).

Epsilon notation (ε) is useful in expressing the $^{143}Nd/^{144}Nd$ deviation of samples from uniform reservoirs and to dispel interlaboratory differences (by normalizing radiogenic isotope values), simplifying comparative techniques. CHUR (Chondritic Uniform

60

Reservoir) is the common reference value to which $^{143}Nd/^{144}Nd$ ratios are compared. Epsilon values are calculated from the following general expression:

$$\varepsilon_{nd}=[(^{143}Nd/^{144}Nd_{sample,t}/^{143}Nd/^{144}Nd_{CHUR,\,t})-1)]x10^4$$

The composition of CHUR at time t is calculated using the following expression:

$$(^{143}Nd/^{144}Nd)_{CHUR,\,t}=(^{143}Nd/^{144}Nd)_{CHUR,\,today}-(^{147}Sm/^{144}Nd)_{CHUR,\,today}(e^{\lambda t}-1)$$

The time, t, may be derived from isochrons or implementation of other geochronological techniques. $\lambda=6.54x10^{-12}$ yr^{-1}, is the decay constant for ^{147}Sm (Rollinson, 1993). The $^{143}Nd/^{144}Nd$ ratio of CHUR, today is 0.511847 (Wasserburg et $al.$, 1981) and the $^{147}Sm/^{144}Nd$ ratio is equal to 0.1967 (Jacobsen and Wasserburg, 1980). Initial ε_{nd} values are useful, because they display the nature of the source from which igneous rocks are derived. Positive ε_{nd} values represent depleted sources, having elevated initial Sm/Nd ratios. A negative ε_{nd} value indicates an enriched source, such as the crust, which has a low Sm/Nd ratio and therefore develops a lower $^{143}Nd/^{144}Nd$ ratio with time in comparison to CHUR. ε_{nd} values may be plotted relative to CHUR to gain an understanding of the origin of a sample and contributions from various sources (DePaolo, 1988).

Nd isotopes have been determined for a selective group of the NVF granitoid xenoliths and associated metasediment xenoliths by W.C. Van Schmus and M. Kozuch at the University of Kansas (results are given in Appendix G). Initial ε_{nd} isotopic values of the NVF granitoids display minor variation from +1.88 to +4.31. The metasediment ε_{nd} isotopic values range from 0.50 to 4.20. The samples are plotted on an age vs. ε_{nd} diagram (Figure 4.2) to determine possible genetic associations between the metasediments and granitoids and the extent of crustal involvement in their production. Crustal material is ultimately

derived from the mantle which is represented by the depleted mantle Nd isotopic evolution line (from DePaolo *et al.*, 1991),

$$\varepsilon_{nd}(T)=8.6-1.91T$$
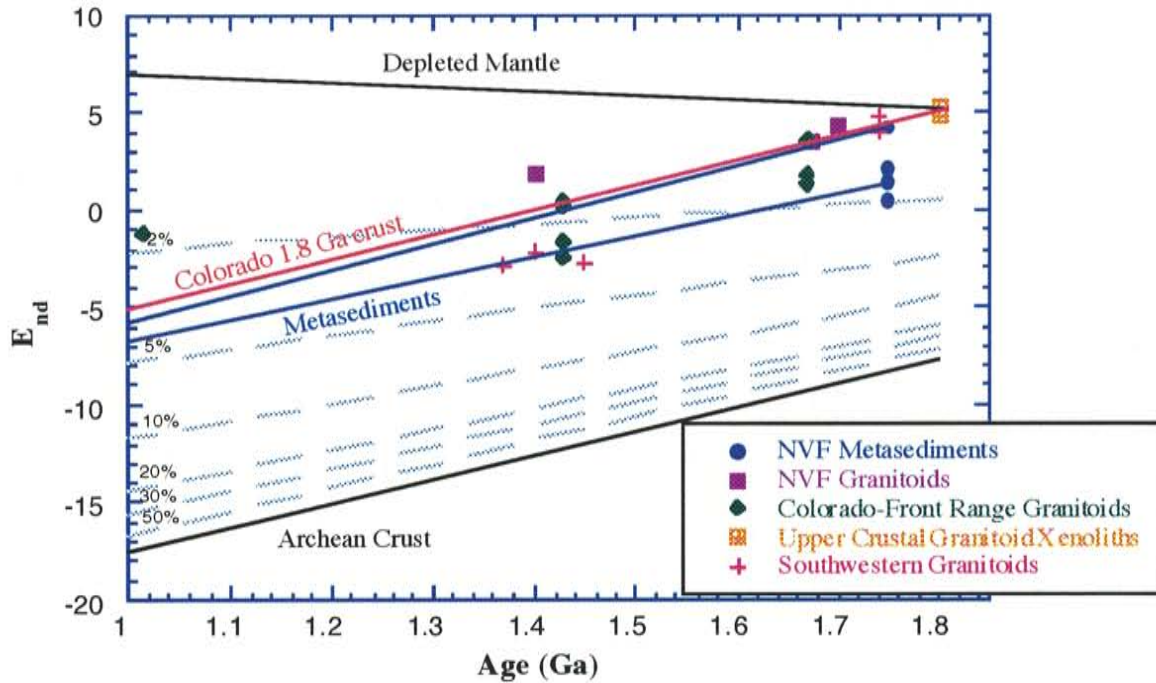
Figure 4.2. Age versus ε_{nd} diagram illustrating the degree of crustal involvement in production of NVF and other southwestern granitoids. NVF Metasediment data from W. R. Van Schmus and M. Kozuch (1997). Colorado Front Range data from DePaolo (1981), includes: Boulder Creek Intrusives granodiorite (1.67 Ga), Sherman Intrusives granite (1.43 Ga), Silver Plume Intrusives granite (1.415 Ga) and Pikes Peak Batholith granite (1.015 Ga). Upper Crustal Granitoid Xenolith data were obtained from Tertiary minettes in the Colorado Plateau from Wendlandt (1993). Southwestern Granitoids are from Government Canyon (1.74 Ga), Bagdad (1.74 Ga) and Hualapai Mountains (1.37 Ga) of Arizona; Whipple Mountains (1.4 Ga) of California; and Newberry Mountains (1.45 Ga) of Nevada, from Bennett and DePaolo (1987). Red line represents ε_{nd} evolution of typical 1.8 Ga Colorado crust (after DePaolo, 1981). Blue lines represent two ε_{nd} evolution trends for NVF metasediments. Depleted Mantle trajectory after DePaolo *et al.* (1991). 2.7 Ga Archean crust evolutionary trajectory after DePaolo (1988) and its contribution to crustal melts is represented by dashed percentage lines [ε_{nd} (1.8 Ga)=-7.67 (DePaolo, 1988), Nd=29.1 ppm (Condie, personal communication, 1996)], mixed with depleted mantle [ε_{nd} (1.8 Ga)=5.20 (DePaolo *et al.*, 1991), Nd=0.992 ppm (McCulloch and Bennett, 1994)] to produce observed ε_{nd} values.

The 1.8-Ga crustal growth line represents Nd isotopic evolution of a typical Colorado crust extracted from the mantle (Figure 4.2). The Archean crustal line represents Nd isotopic evolution of crust generated at 2.7 Ga. Also shown are mixing lines, which exhibit the percentage of Archean crustal contribution to a juvenile source. The following equation (Faure, 1986) was used to determine the evolutionary paths of the Archean mixing lines:

$$\varepsilon_{nd} = R_a X_a f + R_b X_b (1-f)/X_a f + X_b (1-f)$$

Table 4.1. Abbreviations Used in Determining Paths of Archean Mixing Lines (Figure 4.2)

a=crustal component endmember
b=depleted mantle component endmember
R=epsilon value
X=Nd concentration [X_a=29.1 ppm]
X_b=0.992 ppm (McCulloch and Bennett, 1994]
f=ratio of crustal involvement (a/a+b)

From Figure 4.2, it is apparent that most of the metasediments cannot be protoliths for the NVF granitoids since the metasediment ε_{nd} growth lines fall below that of the granitoids, which approximately coincide with the 1.8-Ga crustal growth line. However, metasediments may have contributed minor amounts of material to the generation of the NVF granitoids. Initial ε_{nd} values of NVF granitoids are characteristic of a depleted source that has had little contribution from crustal material. The 1700-Ma granitoids plot close to the mantle evolutionary trend, while the ε_{nd} values for 1400-Ma samples suggest some Archean crustal contamination. The 1.4 Ga and 1.7 Ga granitoids were derived by melting and differentiating the 1.75-1.8 Ga crust and acquired their ε_{nd} values at the time of crystallization from the evolving crustal source. The 1.4 Ga granitoids coincide with an episode of anorogenic granitic magmatism which occurred throughout the Southwestern United States, an event which may have contributed minor amounts of mantle-derived, juvenile material to the crust (Wendlandt *et al.*, 1993).

63

Most of the southwestern granitoids and NVF metasediments plot below the 1.8 Ga crustal evolution line indicating that they have interacted with an Archean crustal component or have acquired lower ε_{nd} values from subduction related sediments with recycled older components (all data is tabulated in Appendix G). The Navajo Volcanic Field lies near the inferred junction of two crustal provinces: Yavapai and Mazatzal, formed by continuous addition of island-arc material, whose Nd ages range from 1.7 to 2.0 Ga (Bennett and DePaolo, 1987). Younger crust, extending south from the Archean province, incorporated less Archean material and it is doubtful that a significant amount of the older crust was involved in formation of the NVF granitoids. Subduction related sediments, derived from accreted terranes and incorporated into the crustal sections, are more likely sources contributing to granitic generation and lowering their ε_{nd} values.

4.3 Tectonic Discrimination Diagrams

Granitoids may be classified according to their tectonic setting by considering incompatible trace element geochemical characteristics (Pearce *et al.*, 1984). Geochemical and petrological criteria may be used to constrain the environment of origin. Many granitoid geochemical characteristics are inherited from their sources (Pearce *et al.*, 1984) and may shed light not only on the generation of granitoid magmas, but provide valuable input in studying crustal evolution.

The trivariate plot, Hf-Rb/30-Tax3 of Harris *et al.* (1986) (Figure 4.3 a), suggests that all of the NVF granitoids were produced in a volcanic arc setting. This is further supported by the (Y+Nb) versus Rb plot (Pearce *et al.*, 1984) (Figure 4.3 b), where 84% of the xenoliths plot in the volcanic arc field. Only a few samples plot in the WPG, syn-COLG and ORG fields near the boundary of the arc field. Island arcs are favorable tectonic settings for generation of granitoid magmas due to abundance of fertile material derived

from the enriched mantle wedge overlying the subducting oceanic crust (Vielzeuf and Montel, 1994).
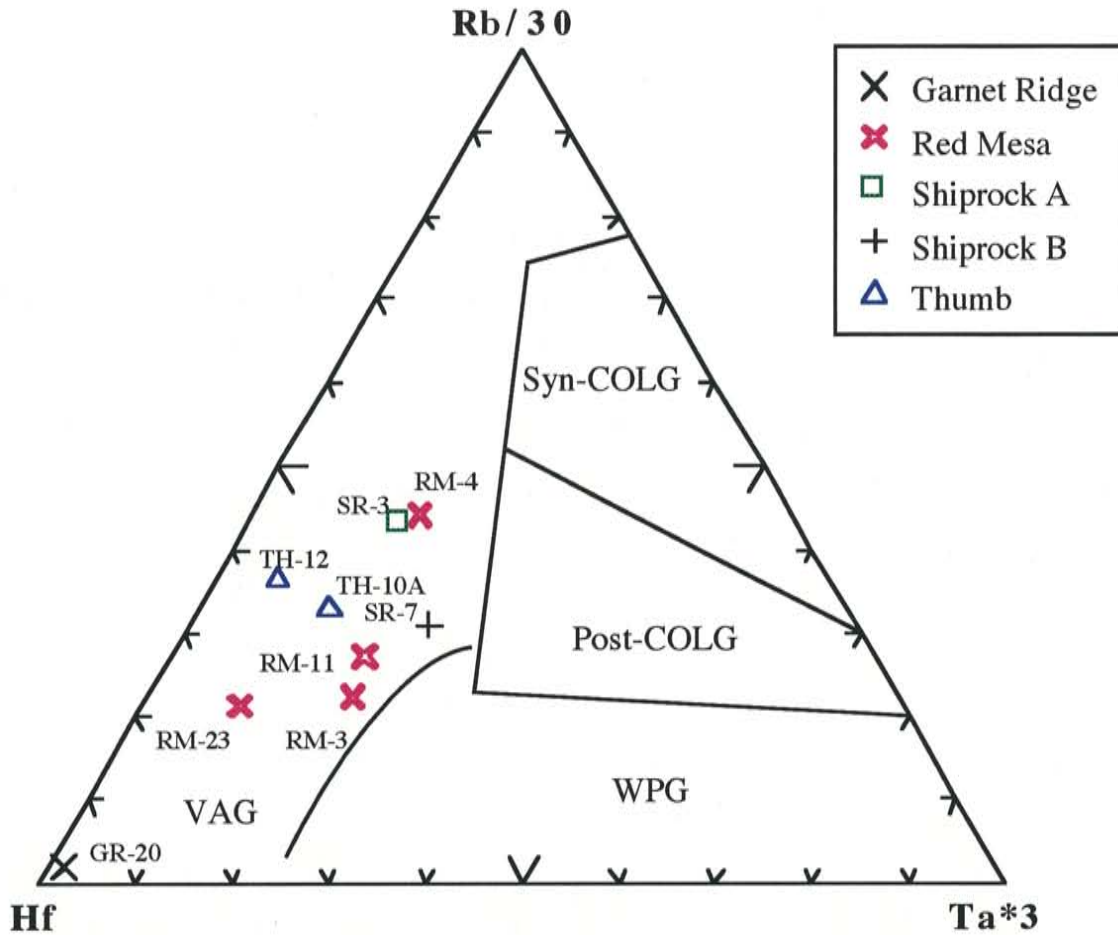
Figure 4.3 a. The Hf-Rb/30-Tax3 discrimination diagram for NVF granitoids (after Harris *et al.*, 1986), exhibiting fields for volcanic arc granites (VAG), within plate granites (WPG), syn-collisional (syn-COLG) and late and post collisional granites (post-COLG).

Volcanic arcs develop in both oceanic and continental environments. Granitoids derived from such settings can exhibit variable geochemical characteristics from tholeiitic through calc-alkaline to shoshonitic affinities (Peccerillo and Taylor, 1976). A majority of the NVF granitoid xenoliths plot in the 'Granite' field of the Streckeisen diagram (Figure 3.1 b) (Streckeisen, 1976), suggesting that they were derived from calc-alkaline or shoshonitic series in an active continental margin. This interpretation is further supported by the calc-

alkaline trend shown by the NVF granitoids (Figure 3.2), by biotite being the dominant

ferromagnesianmineral
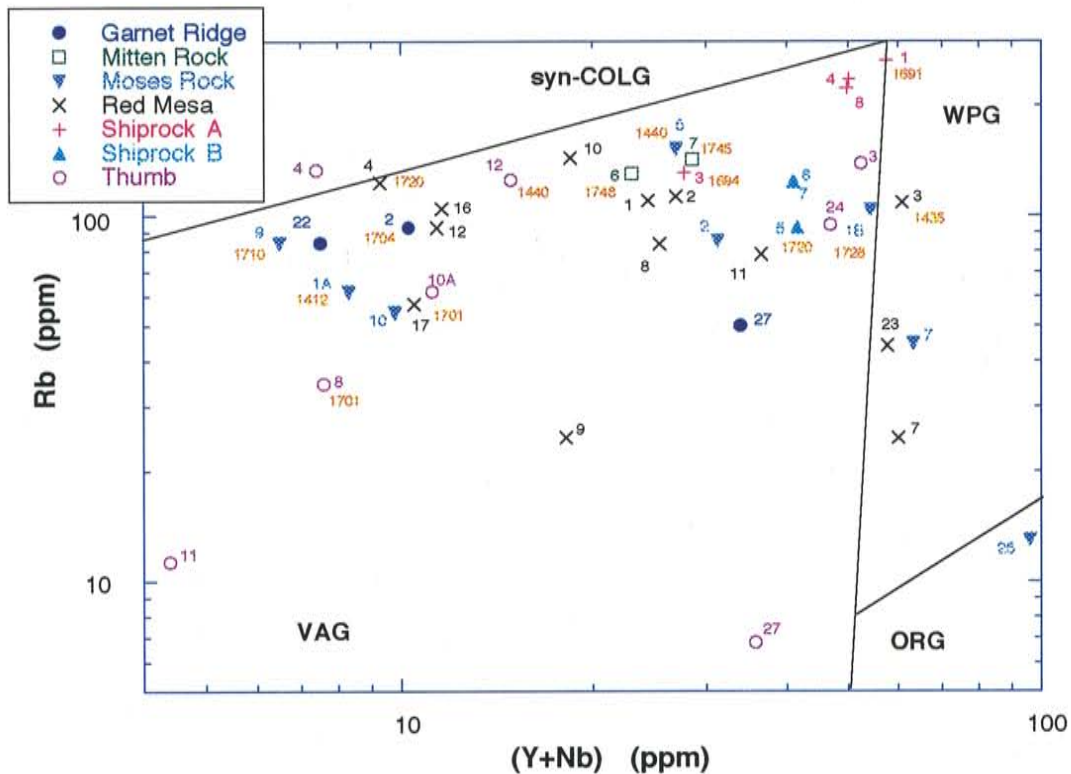
Figure 4.3 b. (Y+Nb) vs. Rb discriminant diagram for the NVF granitoids. The fields correspond to within plate granites (WPG), syn-collision granites (syn-COLG), volcanic arc granites (VAG), and ocean ridge granites (ORG). Coordinates of boundaries between different tectonic fields are: syn-COLG/VAG=(2,80) to (55,300); syn COLG/WPG=(55,300) to (400,2000); VAG/WPG=(55,300) to (51.5,8); VAG/ORG=(51.5,8) to (50,1); ORG/WPG=(51.8,8) to (2000,400) (from Pearce *et al.*, 1984).

(Pearce *et al.*, 1984), and by the selective LILE enrichment (Rb, Ba, K) and Ta, Nb

depletion, which are thought to be indicative of a subduction zone component (Pearce *et al.*, 1984).

4.4 Arc Maturity

A Nb-Rb/Zr plot may be used to gage arc maturity of the host terrane in which the NVF

granitoids reside. Rb is compatible in biotite and is enriched in the volatile phase during

subduction of sediments. Elevation in Rb may also reflect fractional crystallization of minerals with which it is incompatible such as plagioclase, pyroxene, K-feldspar and amphibole (Table 4.2). Zr may be in part be retained in residual zircon in the subducting slab and Zr may slightly decrease with increasing arc maturity through fractional crystallization of zircon. Therefore, Nb concentration at a given Rb/Zr value may reflect contribution from a within-plate source. Variation in Nb concentration is due to different degrees of fractional crystallization. Nb concentration increases with arc maturity because it is incompatible in major and most early crystallizing minor minerals. Increasing Nb at given Rb/Zr reflects greater arc maturity and more involvement from a within-plate source (which is rich in Nb) . Brown *et al.* (1984) have argued that in mature arcs, magma generation will occur further from an active trench and attain within-plate geochemical characteristics. With time, magmatic production changes from an enriched mantle subduction regime to a within plate magma source, reflected by evolving geochemical signatures. Shiprock A samples plot at elevated Rb/Zr and Nb values (Figure 4.4) and could reflect a within plate component (Figure 4.3 b). The differences between the NVF granitoids on the Rb/Zr-Nb diagram may be attributed to different mantle sources and/or greater contribution from a within plate component.
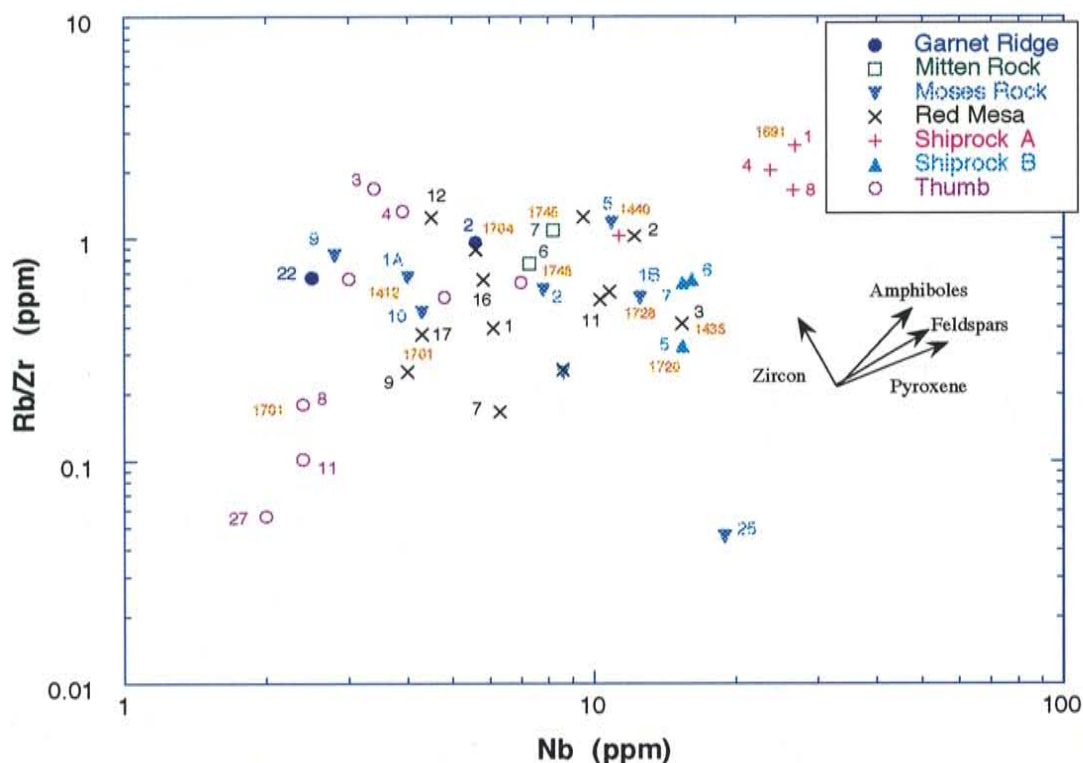
Figure 4.4. Nb versus Rb/Zr diagram for NVF granitoid xenoliths. Arrows are crystallization vectors of the liquid for pyroxene, feldspars, amphiboles and zircon. Progressive fractional crystallization of plagioclase, pyroxene, amphiboles and alkali feldspar leads to an increase in Rb concentration, while fractional crystallization of zircon will decrease Zr and increase Rb/Zr ratio in the liquid. Increasing arc maturity results in elevated Nb and Rb/Zr concentrations (Brown *et al.*, 1984).

4.5 Alphabet Classification of the NVF Granitoids

The A-, I-, M-, and S-type granite classification scheme conveys genetic information about the sources and tectonic regimes in which granitoids are generated (Raymond, 1995). However, it is often ambiguous due to lack of unequivocal boundaries between granitoids generated in different environments. Magmatic traits vary with temperature, pressure, and composition in the source region. Also, fractional crystallization and subsolidus alteration can modify granitoid composition, and some granitoids have hybrid sources (Chappell and White, 1992).

68

I-type granitoids are calc-alkaline to alkali-calcic, metaluminous to peraluminous suites, which consist of diorite, tonalite, granodiorite, monzogranite, granite and syenogranite. These granitoids become more alkali-calcic, silicic and peraluminous with increasing distance from the active subduction margin (Brown *et al.*, 1984). I-type granites are produced either by partial melting or fractional crystallization of mantle-derived source material. The source material may be basaltic to andesitic to tonalitic in composition (Chappell and White, 1992). I-type granitoids are higher in Na, Ca and Sr relative to S-type, which lose these elements when feldspars transform to clay minerals (Chappell, 1984).

Geochemical variation of the NVF granitoids on the 10,000xGa/Al vs. FeO/MgO plot (Figure 4.5 a) indicates that these granitoids are I-types, unlike many 1.4 Ga Proterozoic granitoids of the Southwest, which are A-types (Anderson and Bender, 1989). The NVF granitoids almost exclusively plot in the I- and S-type field. The NVF granitoids also do not fall in the A-type field in all of discriminant graphs of Whalen *et al.* (1987). On a ZNCY vs. A/CNK diagram (Figure 4.5 b), all but two of the NVF granitoids fall in the I-type field and are equally divided between the peraluminous and metaluminous fields. RM-3 plots in the A-type field and has anomalously elevated Zr, Ce, Y concentrations, which may be attributed to incorporation of accessory phases such as zircon and allanite. RM-3 does not plot in the A-type field on any of the Whalen *et al.*, 1987 plots and probably does not belong in that category.
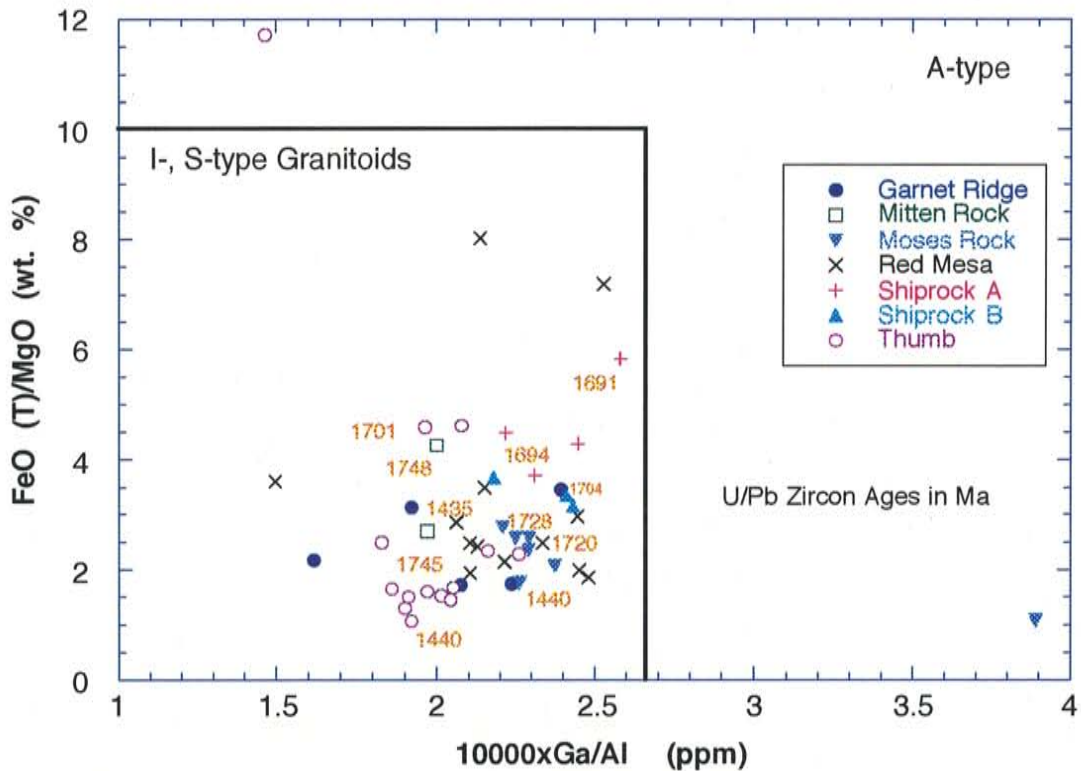
Figure 4.5 a. 10,000xGa/Al versus FeO/MgO diagram for NVF granitoid xenoliths. Xenoliths do not exhibit A-type characteristics. Rectangular box represents I-, S- and M-type granitoid field, whose coordinates are: X=2.6, Y=10. Plot after Whalen *et al.* (1987).

NVF granitoids do not exhibit S-type characteristics. The lack of biotite-rich samples, Ta-Nb depletion on chondrite normalized incompatible plots, LREE enrichment, variable Eu anomalies, and absence of Al-rich phases (sillimanite, cordierite, primary muscovite) is characteristic of I-type granitoids. This is further supported by isotopic properties. Crustal contamination by older crust has had little influence on Nd isotopes (Figure 4.2).
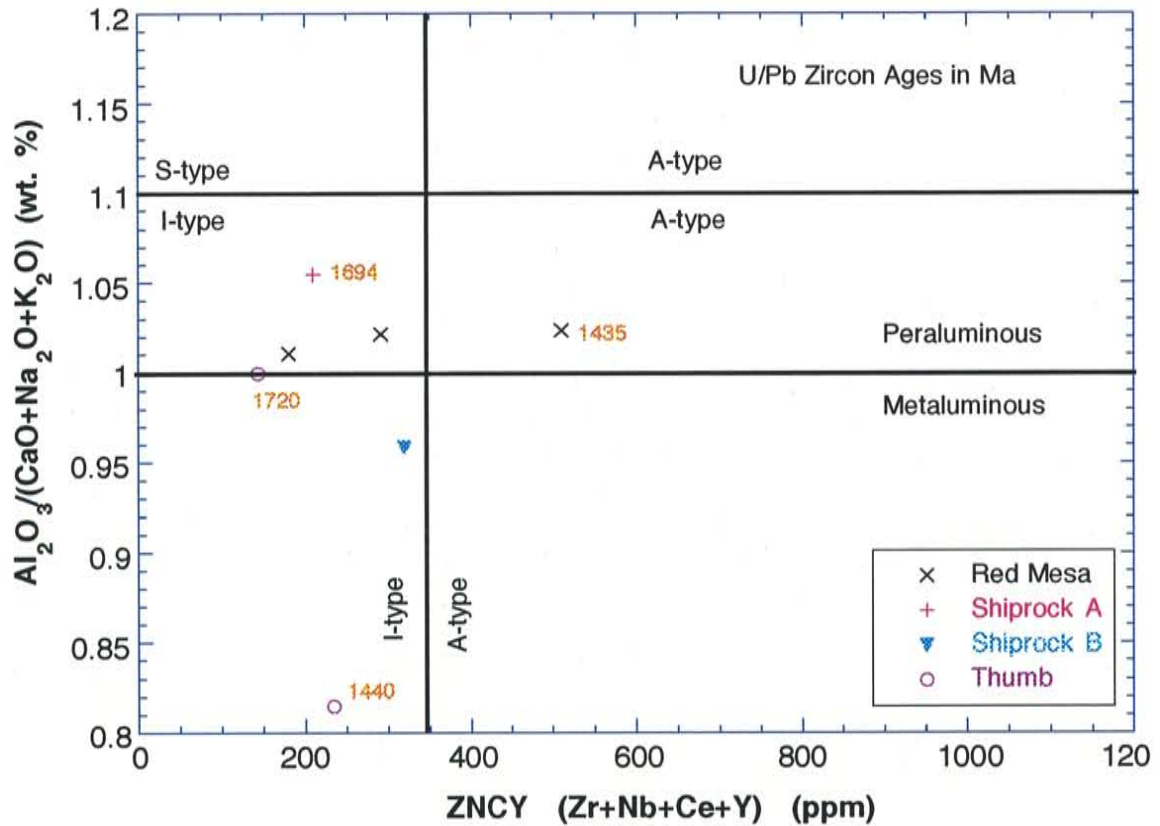
Figure 4.5 b. (Zr+Nb+Ce+Y) versus $Al_2O_3/(CaO+Na_2O+K_2O)$ (molar values) for NVF granitoid xenoliths. All but one of the samples display I-type affinities and are equally distributed between peraluminous and metaluminous fields. Diagram after Condie (1991).

4.6 Granitoid Comparisons

Incompatible Elements

To deduce the significance of the NVF spidergram patterns, results are compared with granitoids from other regions (all data are tabulated in Appendix H) (Figures 4.6 a-c). The Peru Coastal Batholith is dominantly I-type and was derived from heterogeneous sources (Figure 4.6 a) (Boily *et al.,* 1989). The element distributions in the NVF granitoids resemble those of the Peru Batholith, although Peruvian granitoids have a slight negative Ba anomaly and higher Ta and Ti values. NVF granitoids also resemble average granodiorite, although NVF absolute concentrations are generally smaller (Figure 4.6 a).

71

The granodiorite also has a negative Ba anomaly not found in the NVF granitoids. The NVF granitoids share similar incompatible element trends with the Peninsular Batholith rocks, which, however have significant Ta, Hf and Yb anomalies.
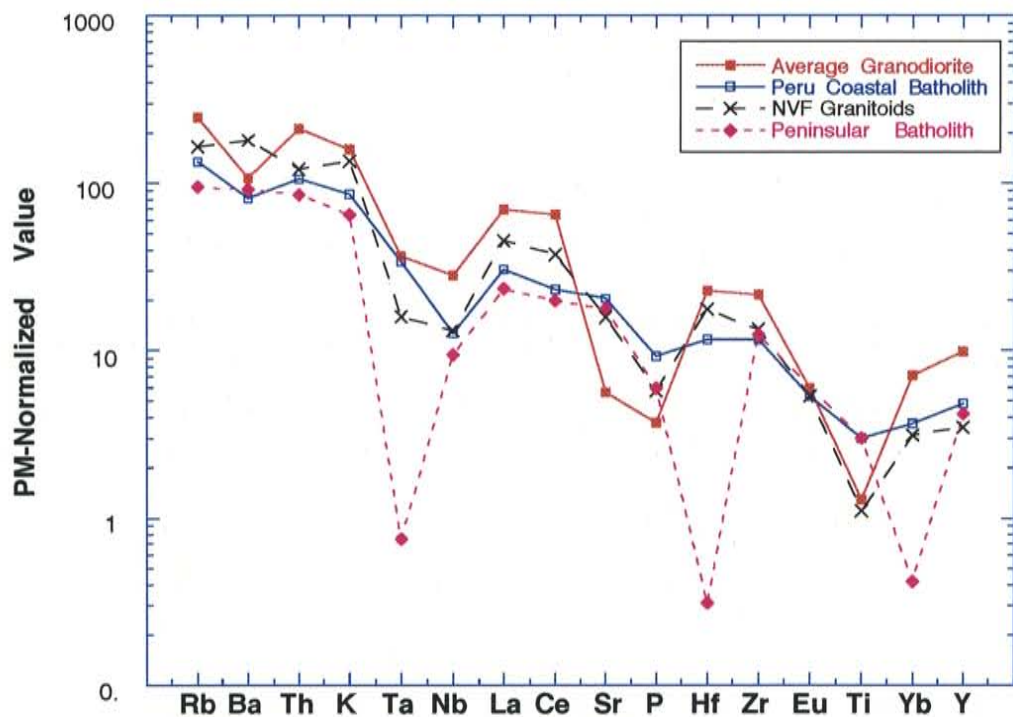
Figure 4.6 a. Primitive-mantle normalized incompatible element distribution diagram for granitoid xenoliths from the Navajo Volcanic Field and granitoids from various sources, gathered for comparative analysis. Average granodiorite data from Condie (1992). Peru Coastal Batholith values from Boily *et al.* (1989). Peninsular Batholith data from (Silver and Chappell, 1988). Primitive values after Sun and McDonough (1989).

In Figure 4.6 b, the NVF granitoids are compared to Anderson and Bender's (1989) 1.4-1.5 Ga A-type granites, which are abundant in the Southwest. The A-type granitoids share similar geochemical trends with the NVF xenoliths; however, there are some differences in overall abundances and in particular element concentrations. The A-type granites exhibit a great deal of variation among themselves. Dells granite is significantly depleted in Ba, La, Sr, Ti and slightly enriched in Ta and Nb, unlike the other granitoids. Dells granite's geochemical signature is notably different from the NVF granitoids. The geochemical trend

72

of NVF granitoids is fairly similar to the Gold Butte, Hualapai, and Lawler Peak granites.

Hualapai
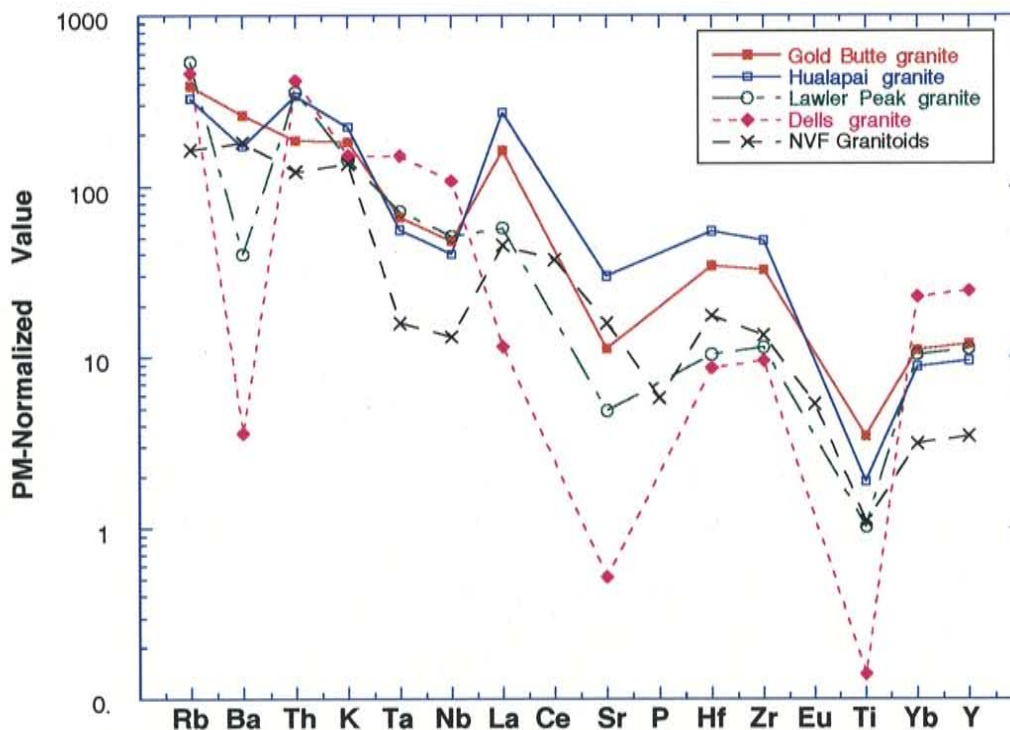
Figure 4.6 b. Primitive-mantle normalized incompatible element distribution diagram for granitoid xenoliths from the Navajo Volcanic Field and Proterozoic A-type granites of southwestern USA. A-type granite data from Anderson (1989). Primitive values after Sun and McDonough (1989).

and Gold Butte granites have greater overall abundances of Ta, Nb, La, Hf and Zr than the NVF granitoids. While the NVF granitoids are slightly enriched in Ba with respect to adjacent elements, other A-type granitoids are slightly (Gold Butte, Hualapai) to greatly (Lawler Peak, Dells) depleted in Ba.

Anderson (1983) has suggested that the A-type granitoids of the Southwest were derived by partially melting crustal rocks of quartz, diorite, tonalite and granodiorite compositions, while I-type granites are produced by partially melting basaltic to tonalitic sources (Chappell and Stephens, 1988). A-type granitoids may be derived from different sources

73

and are produced under different thermal conditions than those required for generation of I-type granitoids (Creaser *et al.*, 1991). Sources for A-type granitoids have lower water contents, either free or available from breakdown of hydrous minerals (Creaser *et al.*, 1991), than I-type precursors (Chappell and White, 1992) and require higher temperatures to initiate melt. A-type granitoids of the Southwest share many similarities with the NVF
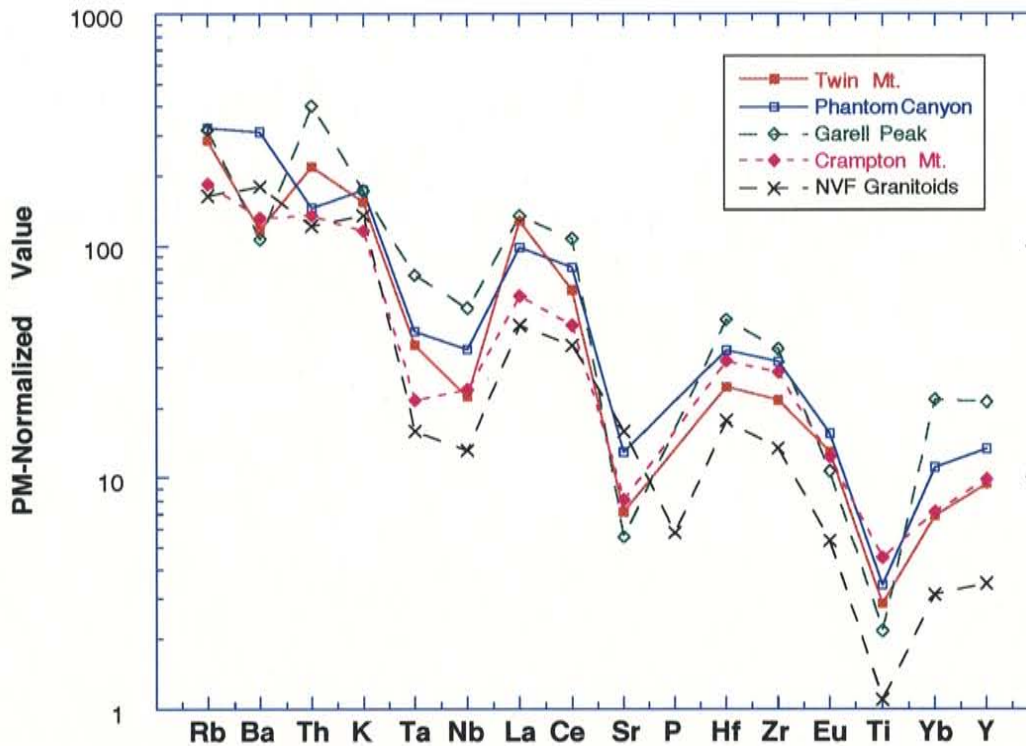
Figure 4.6 c. Primitive-mantle normalized incompatible element distribution diagram for granitoid xenoliths from the Navajo Volcanic Field and Early Proterozoic granitoids from the northern Wet Mountains of south-central Colorado. Colorado granitoid data from Hallett (1990). Primitive values after Sun and McDonough (1989).

granitoids in their incompatible element trends and were generated from sources which may have been geochemically alike.

Figure 4.6 c compares Early Proterozoic granitoids from the northern Wet Mountains in south-central Colorado (data from Hallett, 1990) with the NVF granitoids. Element

distributions of the NVF xenoliths are remarkably similar to the Colorado granitoids with few variations. Garell Peak and Twin Mountain are enriched in Th, while other granitoids are slightly depleted. Phantom Canyon and NVF granitoids are enriched in Ba with respect to Twin Mountain, Garell Peak and Crampton Mountain. The NVF granitoids exhibit marginally smaller overall element concentrations than the Colorado values. The protolith for the Four Corner granitoids may be geochemically similar to the source for the Twin Mountain, Phantom Canyon, Garell Peak and Crampton Mountain plutons.

Comparison with other Southwestern Proterozoic Granitoids

The NVF granitoids are compared with other Proterozoic granitoids from the Southwest. Most plutons from the Southwestern United States have ASI values near one, varying from slightly peraluminous to metaluminous, and they are both I and A types.
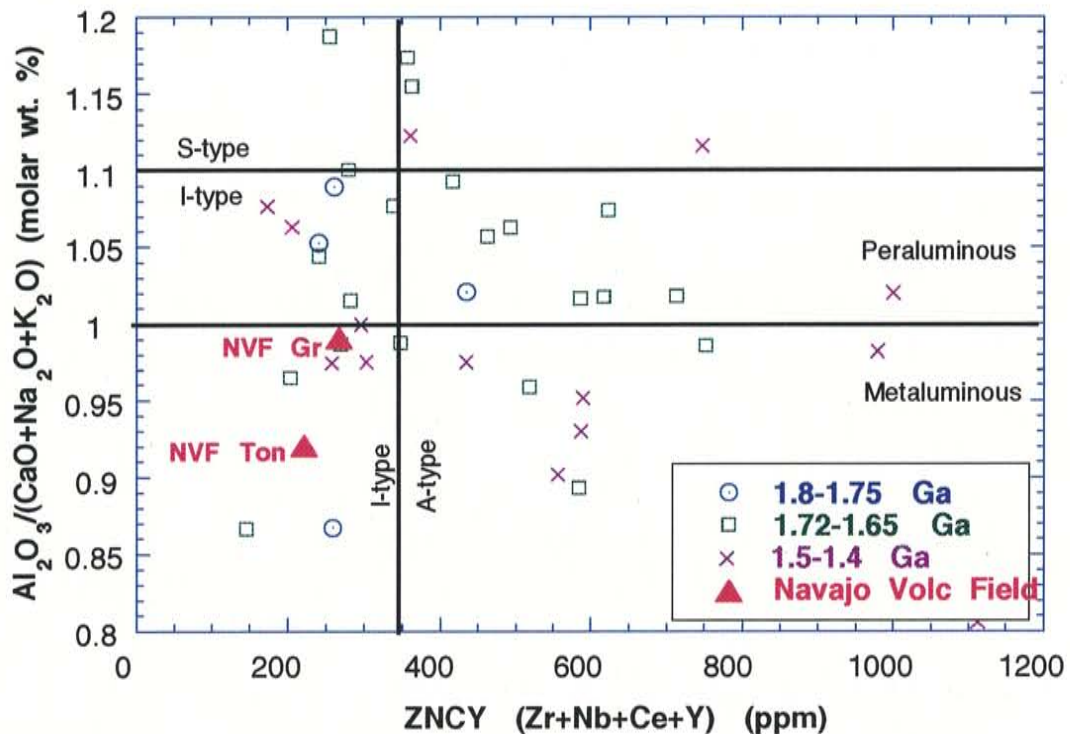
Figure 4.7. ASI versus the ZNCY index showing the average composition of Proterozoic granitoids from the Southwestern United States. NVF Gr is an average of all granitoids xenoliths.

Southwestern granitoids dominantly plot in the volcanic arc and within plate fields on the tectonic discriminant diagrams (Figure 4.8). Most of the 1.4-1.5 Ga granitoids fall in the within plate field. The NVF granitoids are unusual in that they all plot in the volcanic arc field, suggesting a juvenile Early Proterozoic source for these granitoids. The differences between the NVF granitoids and other Proterozoic granitoids from the Southwest may be attributed to generation from variable sources.
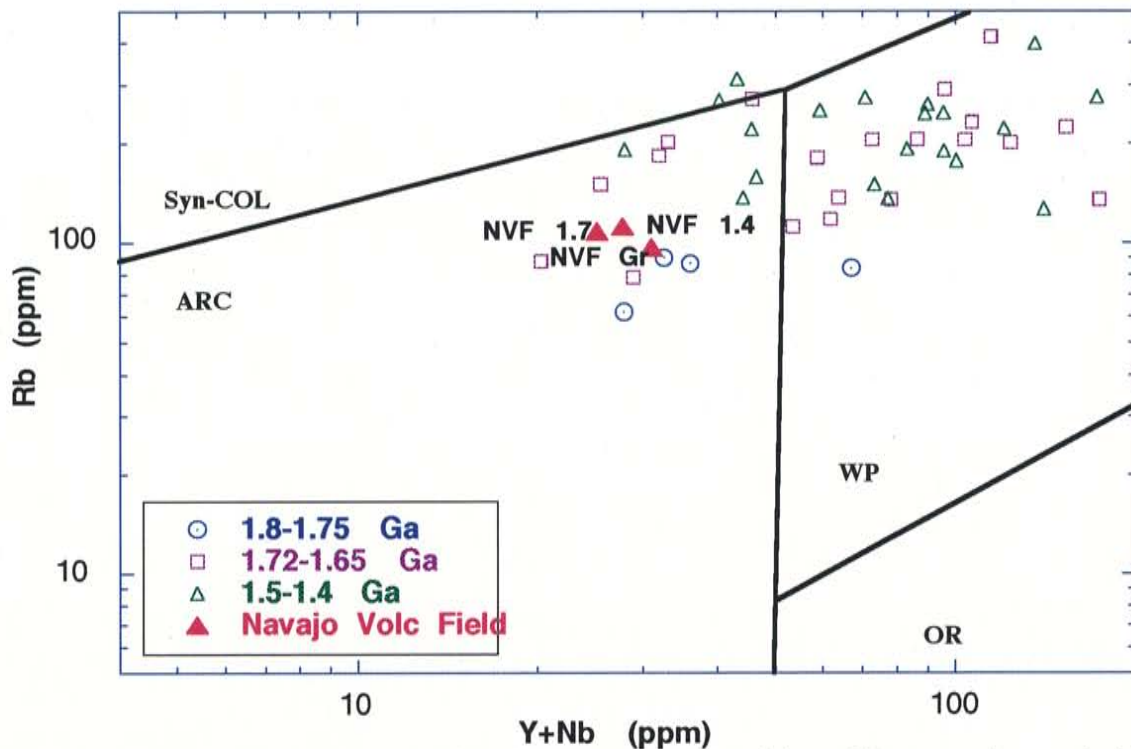
Figure 4.8. Rb versus Y+Nb showing the average composition of Proterozoic granitoids from the Southwest. NVF 1.7, 1.4, and Gr are averages of 1700 Ma, 1400 Ma, and all granitoid xenoliths, respectively.

4.7 Source Characteristics

Partial melting is an important process of differentiation within the continental crust and most granitoids are generated from crustal melts (Ebadi and Johannes, 1991). To characterize the source of the NVF granitoids, several models were tested using data from other NVF xenolith studies. The protolith and/or restite may be represented in the NVF

76

xenolith population. Models incorporating various possible source rocks (Condie and Selverstone, 1997; Mattie *et al.*, 1997) are considered to constrain the characteristics of granite sources and to gain a better insight into the evolutionary history of the NVF felsic magmas. Modifications may occur during ascent, fractional crystallization, crustal contamination and alteration by late- or post-magmatic fluids and hence, an unequivocal source cannot be determined for most granitoids (Harris and Inger, 1992).

4.8 Geochemical Models

Major Element Models

Major-element models require knowing the distribution of major elements between mineral phases and mineral proportions in the source and melt, by which the major element composition is calculated and compared with the observed granitoid element concentrations. The major-element model used for the NVF granitoids is a general mass balance model and is not specific to magmatic conditions. The major-element compositions are calculated using the following mass balance relationship for each major element (Rollinson, 1993):

$$Z=[C_{m1}x(FxX_{m1})/Fx(X_{m1}+X_{m2}+.....)]+[C_{m2}x(FxX_{m2})/Fx(X_{m1}+X_{m2}+.....)]+.....$$

where Z is the calculated bulk concentration of major-elements in the whole rock and is dependent on the concentration of major elements in minerals which constitute the rock (C), the modal concentration of the particular minerals (m1, m2, etc.) in the melt (X), and the weight fraction of melt produced in partial melting (F).

Average major element contents of the granitoids have been used in the models for the average magma composition (Table 4.2). Biotite tonalite and biotite-sillimanite-quartz schist sources are tested for the granitoids using a major-element mass balance model. Average modal compositions have been determined for the average biotite tonalite and average

77

Table 4.2. Average Major Element Concentrations of NVF Granitoids

Element	Observed Melt Composition
SiO_2	70.09
TiO_2	0.27
Al_2O_3	13.93
Fe_2O_3T	2.55
MgO	0.89
CaO	2.61
Na_2O	3.43
K_2O	3.65
P_2O_5	0.13
Total	97.55
A/CNK	0.97
A/NK	1.45

biotite-sillimanite-quartz schist xenoliths (Figures 4.9 and 4.10). Mineral compositions (C) are taken from Deer *et al.* (1992) for minerals which compose granites that are mineralogically similar to the NVF granitoids. The calculated major element compositions for tonalite and metasedimentary mineralogy are compared with the observed average chemical composition of the NVF granitoids in Figures 4.9 and 4.10 (values are listed in Appendix I).
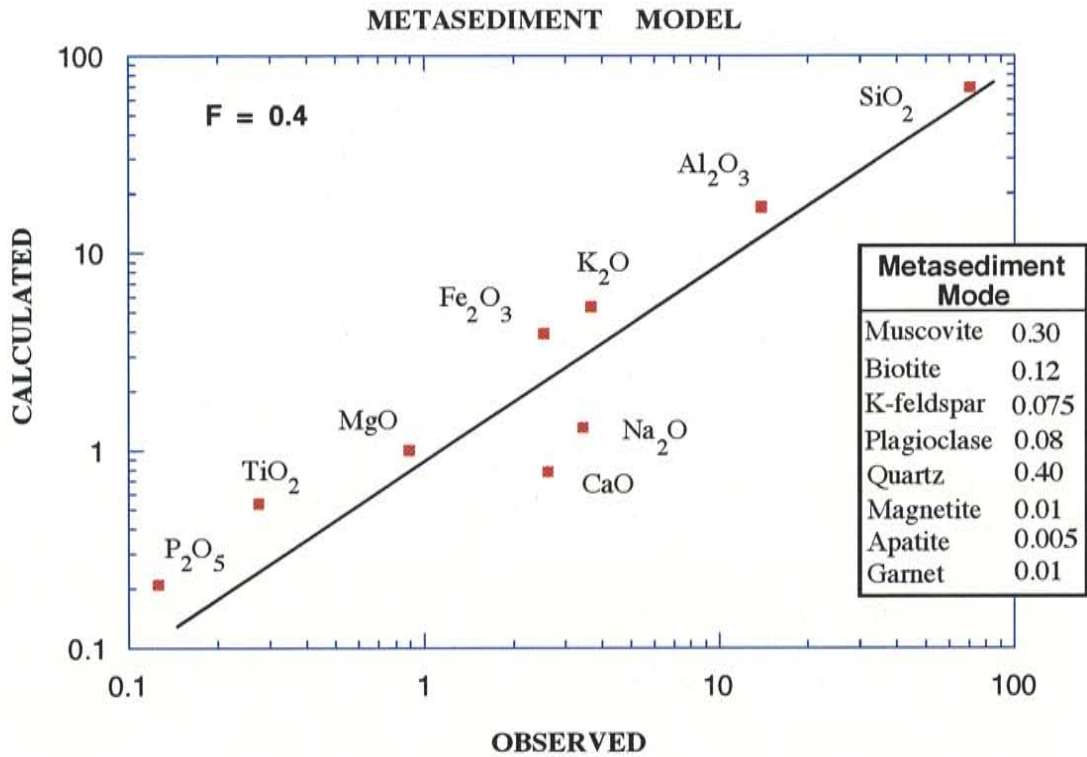
Figure 4.9. Major-element model of a NVF biotite-sillimanite-quartz schist source for the NVF granitoids. Observed values are average NVF granitoid major-element concentrations and calculated values are obtained by using the distribution of major-elements between mineral phases and modal mineral proportions of the metasediments (values listed in Appendix I).
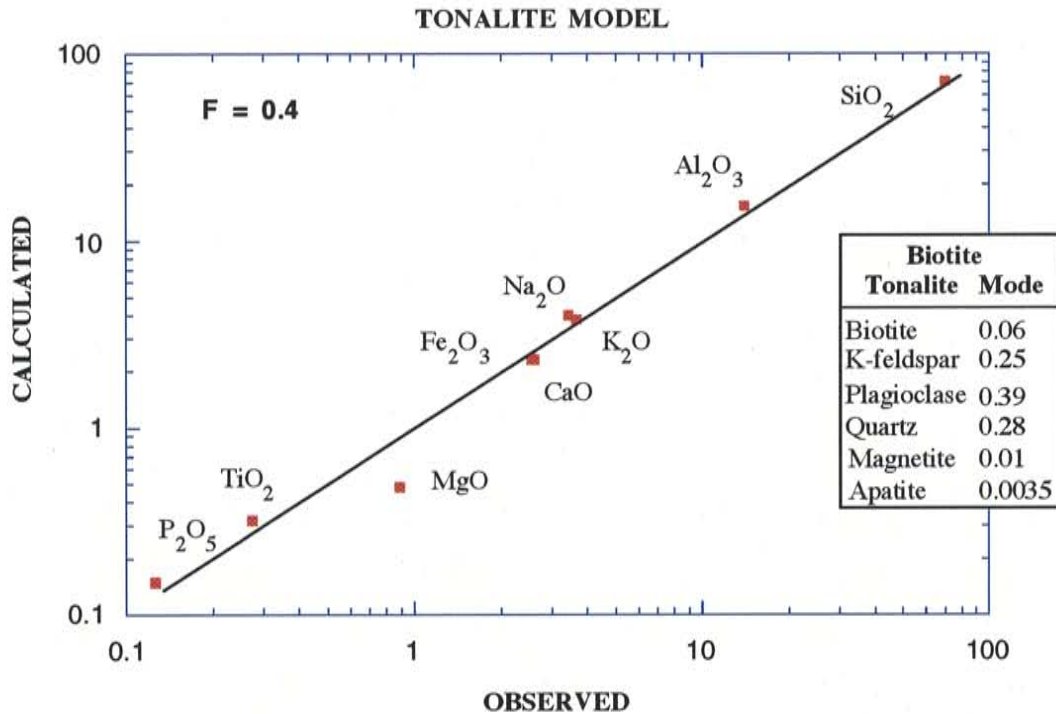
Figure 4.10. Major-element model of a NVF biotite tonalite source for the NVF granitoids. Observed values are average NVF granitoid major-element concentrations and calculated values are obtained by using the distribution of major-elements between mineral phases and modal mineral proportions of the tonalites (values listed in Appendix I).

Model values for the metasedimentary source do not agree with NVF granitoid concentrations. CaO and Na_2O concentrations in a melt produced by melting biotite-sillimanite-quartz schist are less than those in the NVF granitoids and the other major elements occur in greater concentrations in the metasediments. The modal melt composition for a tonalite source is in close agreement to the composition of the average NVF granitoid (Figure 4.10). Only MgO is lower than the observed value and this may be due to an error in the assumed MgO content of biotite, since biotite has a wide variety of compositions. Biotite in the NVF granitoids may be more Mg-rich than the composition used to calculate the distribution coefficient. Considering the fairly good agreement between the calculated and observed values for the tonalite source and the NVF granitoids, tonalite is considered a possible source for the granitic magmas.

Trace Element Models

Trace element abundances in a melt are controlled by composition of the source and the presence or absence of a vapor phase during incongruent melting reactions of muscovite and biotite (Harris and Inger, 1992). For the models described below, it is assumed that chemical equilibrium is established between melt and coexisting solid phases. In some cases, a unique source may be identified for a felsic system (Harris and Inger, 1992) due to the high viscosity and incomplete separation between melt and restite (Chappell *et al.*, 1987).

LILE distributions are important in constraining the petrogenetic history of granitoids (McDermott *et al.*, 1996). A rock's Rb, Ba, and Sr concentrations are useful in ascertaining magmatic conditions since they reside in the major phases (micas, feldspars) (Harris and Inger, 1992). Mineral/melt partition coefficients for relevant elements are listed in Table 4.3. In this study these elements are modeled to determine the composition of possible source material for the NVF granitoids. Both batch melting and incongruent melting models are tested.

Table 4.3. Mineral/Melt Partition Coefficients

Mineral	Rb	Sr	Ba
K-feldspar	0.40	9.00	7.00
Plagioclase	0.05	6.00	0.50
Biotite	3.40	0.50	7.50
Hornblende	0.02	0.02	0.05
Apatite	0.00	2.00	0.00
Garnet	0.01	0.02	0.01
AlSilicates	0.01	0.00	0.00
Orthopyroxene	0.02	0.02	0.01

Values modified after Henderson, 1982.

Ba has an affinity for K-feldspar, biotite and muscovite in which it is concentrated relative to the melt by factors of 3-13. Sr is incorporated in the feldspars relative to the melt by

factors of 3-4. Rb is concentrated in biotite, muscovite and somewhat in K-feldspar by 1-2 times than the melt concentration (Mittlefehldt and Miller, 1983).

Extended feldspar fractionation tends to deplete elements in residual liquids with a bulk partition coefficients greater than one in the melt, such as Ba and Sr, and concentrate elements with partition coefficients less than one, such as Rb (Rollinson, 1993). Therefore, fractional crystallization will decrease Ba and Sr and increase Rb concentrations in the evolving melt. In this study two types of trace element models were tested: batch melting and incongruent melting.

Batch   Melting

Batch melting involves a partial melt which is constantly re-equilibrating with the residue at the site of melting until the melt escapes as a 'batch' of magma (Rollinson, 1993). The general non-modal batch melting equation considers the initial mineralogy of the source and the proportions contributed from each phase to the melt (see Table 4.4 for explanation of abbreviations used):

$$C_l/C_o = 1/[(D_o - PF) + F]$$

This relationship does not consider new phases introduced during melting. Small degrees of melting can substantially enrich the melt and deplete the source in incompatible elements. Compatible elements are not as easily affected by partial melting and will remain close to their initial concentrations (Rollinson, 1993).

Incongruent   Melting

Incongruent melting involves transformation of a solid phase into a different one, giving the liquid a different composition than the original solid. Generation of anatectic granites includes the loss of some minerals (primarily hydrous) and addition of new anhydrous

phases in the residual material. Incongruent melting is represented by the following

relationship:

$$C_l/C_o=1/[D(1-F)+F]$$

This equation assumes that Kd remains constant during melting. This is valid since

granitoid compositions do not change significantly as long as major contributing phases are

not depleted (Inger and Harris, 1992). Vapor-absent conditions occur when there is an

absence of excess water and the breakdown of hydrous minerals such as biotite and

Table 4.4. Abbreviations Used in the Melting Equations

C_l=weight of trace element in the liquid
C_o=weight of trace element in the original unmelted solid
D_o=bulk distribution coefficient of a trace element of the original solids
P=weight contribution of a trace element to the melt at the time of separation of melt and residue
F=weight fraction of melt relative to original parent
Kd=mineral/melt distribution coefficient for a trace element for a particular mineral

Symbols after Harris and Inger (1992) and Rollinson (1993).

muscovite contribute water to the melt. However, small amounts of water are not usually

adequate to saturate the melt and form a vapor phase (Vielzeuf and Holloway, 1988).

Model   Results

The approach of Harris and Inger (1992) employing vapor-present and vapor-absent

melting models of pelites to generate granitic magma is used to test sedimentary and tonalite

source for NVF granitoids. C_o values to be tested were obtained from tonalite and biotite-

sillimanite-quartz xenolith data from the NVF (Condie and Selverstone, 1997). C_l values

are assumed to represent a range of Ba, Rb and Sr values of the NVF granitoids. There is

little geochemical between the two age populations (1400 Ma and 1700 Ma) therefore,

similar sources were involved in magma production at the different times. Observed C_l/C_o

ratios (Table 4.5) for the NVF granitoids are compared to calculated C_l/C_o values for

tonalites and metasediments (Table 4.6, 4.7) in Figures 4.11-4.14.

Table 4.5. Average Rb, Sr, Ba Composition of NVF Granitoids and Possible Source Material Used for Trace Element Modeling

	Metasedimentary Source				Tonalite Source		
	Rb	Sr	Ba		Rb	Sr	Ba
C_o- concentration in source (ppm)	127	247	817		45	569	768

	Metasedimentary Source				Tonalite Source		
C_1- concentration in melt (ppm)	40-145	70-600	365-2220		40-145	70-600	365-2220

	Metasedimentary Source				Tonalite Source		
C_1/C_o	0.3-1.1	0.3-2.4	0.5-2.7		0.9-3.2	0.1-1.1	0.5-2.9

Metasedimentary source represents the average composition of a biotite-sillimanite-quartz schist xenoliths (Condie and Selverstone, 1997). Tonalite source represents the average composition of NVF tonalite xenoliths with SiO_2 contents between 52-65%.

Table 4.6. Calculated Trace Element Values for Non-Modal Batch Melting and Incongruent (Vapor-Absent) of Biotite Tonalite

Incongruent Melting	
Mineral	**Restite Range**
biotite	0.04-0.13
plagioclase	0.32-0.67
quartz	0.17
garnet	0.00-0.15
zircon	0.00034
apatite	0.005-0.02
amphibole	0.00-0.10
sphene	0.00336
orthopyroxene	0.00-0.15

Non-Modal Batch Melting		
Mineral	**Mode**	**Melt**
biotite	0.10	0.05-0.10
plagioclase	0.55	0.30-0.37
K-feldspar	0.08	0.20-0.30
quartz	0.25	0.30-0.37
magnetite	0.01	0.01
zircon	0.0004	0.0005
apatite	0.005	0.005
sphene	0.002	0

Element	D	C_1/C_o Range
Ba	1.346	0.75-2.04
Sr	4.13	0.25-0.51
Rb	0.491	1.96-5.20

Element	D_o	P	C_1/C_o
Ba	1.58	1.96-3.00	0.79-1.20
Sr	4.08	4.05-4.56	2.66-2.86
Rb	0.40	0.269-0.475	0.61-0.69

Tonalite mineral modes were derived from average NVF tonalite data. D is the bulk distribution coefficient of fractionating products during fractional crystallization. D_o is the bulk distribution coefficient of the original minerals in the protolith. P is the bulk distribution coefficient of phases which compose the melt.

Table 4.7. Calculated Trace Element Values for Non-Modal Batch Melting and Incongruent(Vapor-Absent)Melting of Biotite-Sillimanite-Quartz Schist

Incongruent Melting		Non-Modal Batch Melting		
Mineral	**Restite Range**	**Mineral**	**Mode**	**Melt**
muscovite	0.00	muscovite	0.12	0.50-0.30
plagioclase	0.17-0.2	plagioclase	0.17	0.08-0.15
K-feldspar	0.03-0.1	K-feldspar	0.03	0.075-0.15
quartz	0.31-0.4	garnet	0.07	0.01
magnetite	0.00	quartz	0.40	0.20-0.40
zircon	0.00	magnetite	0.01	0.01
apatite	0.02	zircon	0.0004	0.0005
Alsilicate	0.13-0.15	apatite	0.004	0.005
biotite	0.05-0.10	Alsilicate	0.05	0-0.185
garnet	0.10-0.12	biotite	0.15	0.12-0.20
orthopyroxene	0.05			

Element	D	C_l/C_o Range	Element	D_o	P	C_l/C_o
Ba	1.381	0.66-1.43	Ba	2.021	2.965	1.13-1.23
Sr	1.464	0.51-0.66	Sr	1.434	1.375	0.70-1.28
Rb	0.587	2.41-4.41	Rb	0.892	1.342	0.75-0.92

Metasediment mineral modes were derived from average NVF biotite-sillimanite-quartz schists. D is the bulk distribution coefficient of fractionating products during fractional crystallization. D_o is the bulk distribution coefficient of the original minerals in the protolith. P is the bulk distribution coefficient of phases which compose the melt.
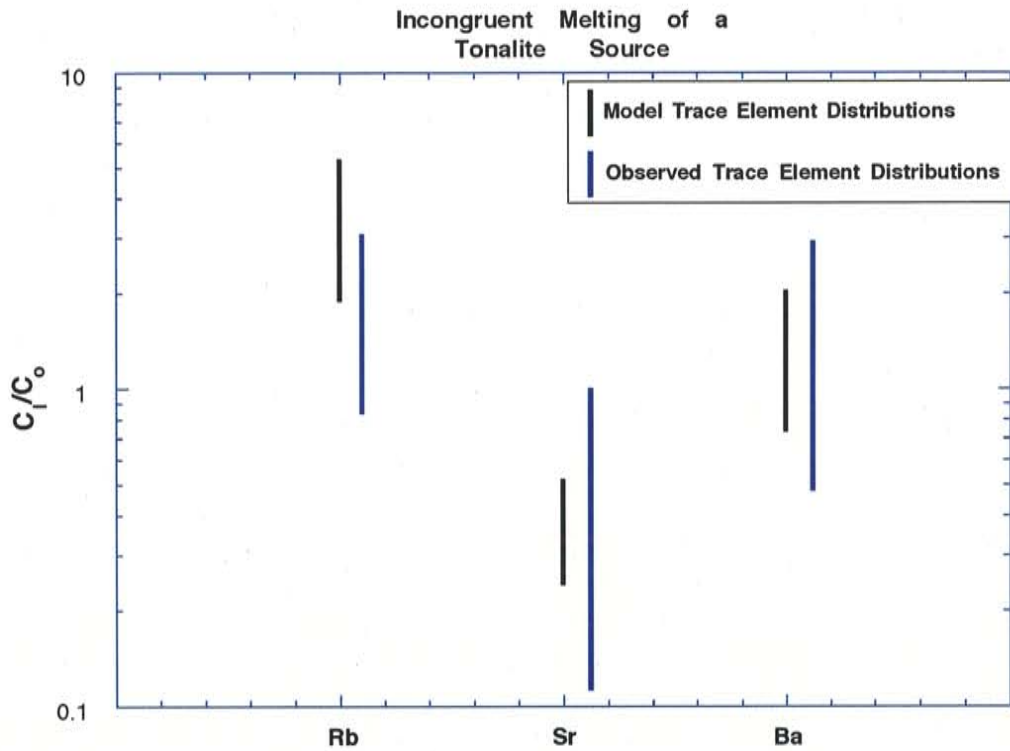
Figure 4.11. Model and observed trace-element distributions in derivative incongruent granite melts of NVF tonalites.
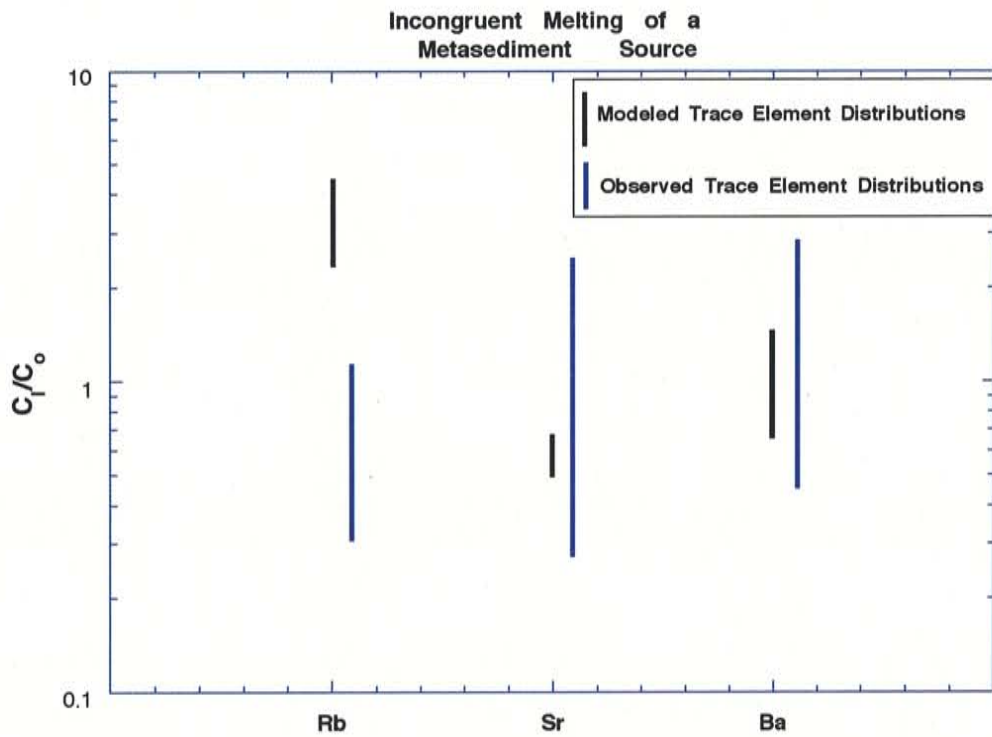
Figure 4.12. Model and observed trace-element distributions in derivative incongruent granite melts of NVF biotite-sillimanite-quartz schist.

The range of calculated C_l/C_o values for incongruent melting of tonalites overlaps the observed C_l/C_o values of NVF granitoids (Figure 4.11). A range of modal mineral concentrations in the restite following extraction of the melt are tested to acquire the full range of possible C_l/C_o values generated from tonalites of various compositions. However, Rb and Ba are extremely sensitive to abundance of biotite due to the mineral's high Kd values for the two elements. Crystallization of plagioclase also has a large effect on Sr concentration in the restite for the same reason. Therefore, a large range in C_l/C_o is observed for small changes in modal abundances of plagioclase and biotite in the restite.

Incongruent melting of a metasediments under vapor-absent conditions is not a feasible way of generating the NVF granitoids. The calculated C_l/C_o values for Rb acquired by melting NVF metasediments do not match C_l/C_o values of the NVF granitoids (Figure 4.12). The calculated metasediment C_l/C_o ratio is higher for Rb and falls in the observed range for Sr and Ba.

Non-modal batch melting is tested as a possible means of generating the NVF granitoids by partially melting tonalite and metasediments having the range of compositions found in the NVF xenoliths. The C_l/C_o values produced by melting tonalite do not match the C_l/C_o values of the NVF granitoids (Figure 4.13). The C_l/C_o values of Rb are lower, while Sr values are higher in the material derived from a tonalite source than the C_l/C_o ratio of the granitoid. However, the calculated C_l/C_o ratio is consistent with observed C_l/C_o values for Ba. C_l/C_o values for non-modal batch melting of metasediments for Rb, Sr and Ba are in close agreement with the C_l/C_o values of the NVF granitoids (Figure 4.14).
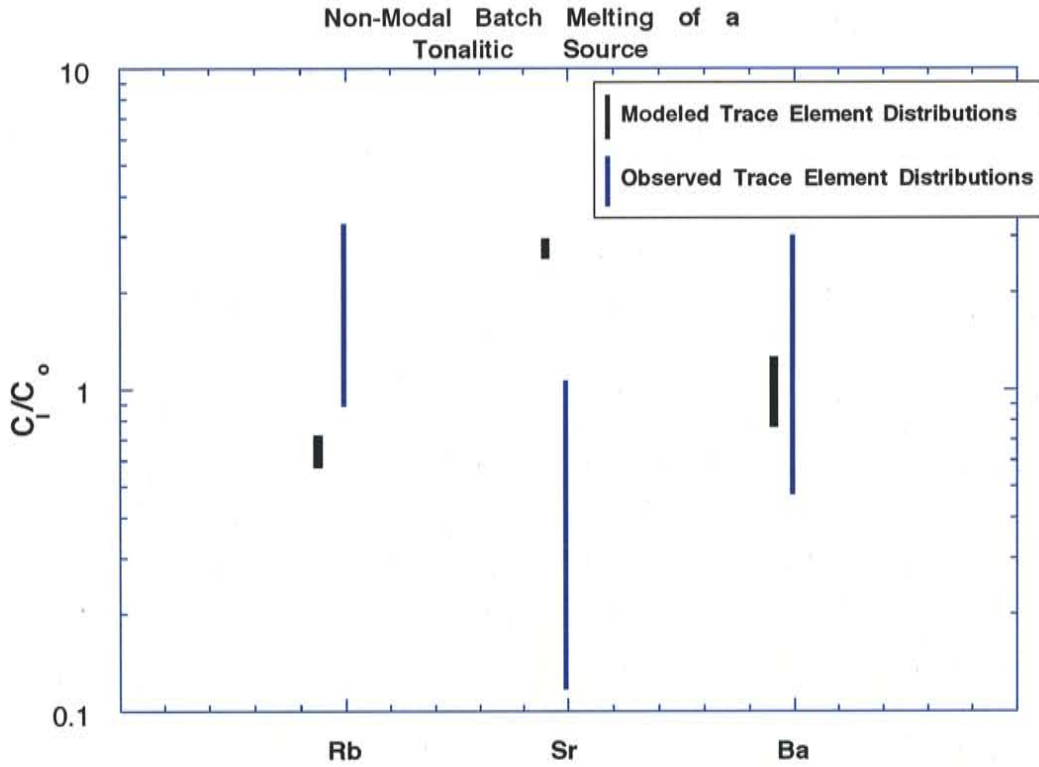
Figure 4.13. Model and observed trace-element distributions in derivative non-modal batch granite melts of NVF tonalites.
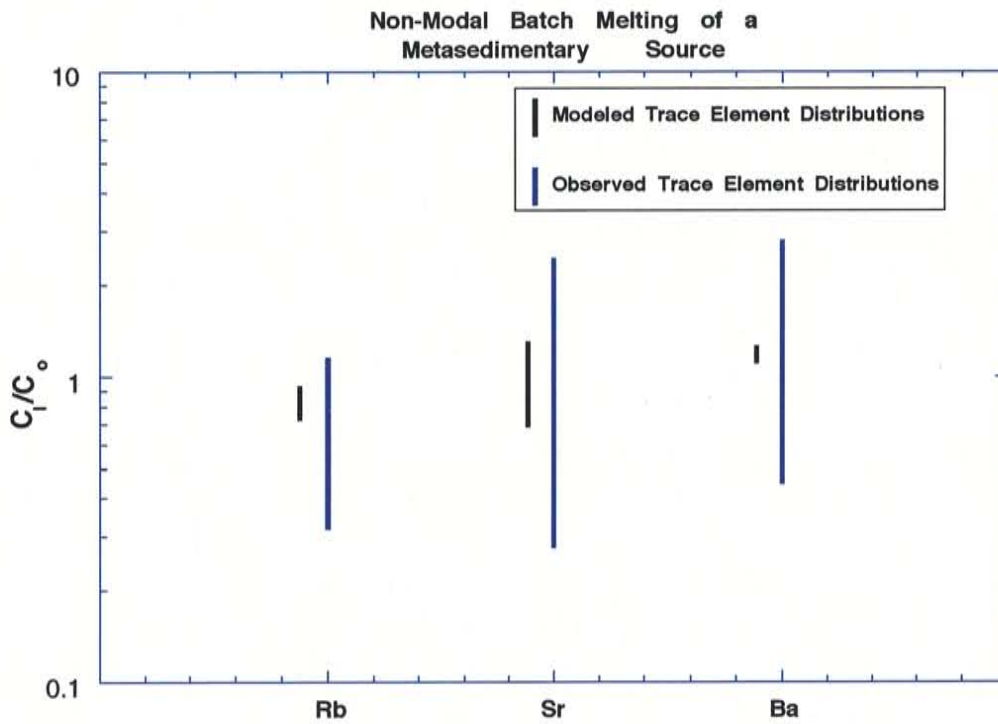
Figure 4.14. Model and observed trace-element distributions in derivative non-modal batch granite melts of NVF biotite-sillimanite-quartz schist.

Model results suggest that biotite-sillimanite-quartz schist metasediments may have contributed minor amounts to the source of NVF granitoid magmas (see Figure 4.2) and major element models support this conclusion. The NVF granitoids may have variable sources. Major element and trace-element values acquired through incongruent melting support a tonalite source from which the NVF granitoids were generated. However, non-modal batch melting of a sedimentary source may also be feasible for generation of the NVF granitoids.

CHAPTER 5: CONCLUSIONS

1. With the exception of two populations at Shiprock, there is no apparent correlation between geochemical characteristics, age, geographic location, alteration or degree of deformation among the NVF granitoid xenoliths.

2. The NVF granitoid xenoliths show variable modal abundances and are commonly altered. Mobilization of alkalis during alteration has resulted in loss of these elements.

3. Although NVF granitoid xenoliths come from different plutons, their evolution conforms to the calc-alkaline trend, and a majority of the granitoids are granites and granodiorites.

4. The NVF granitoid xenoliths are chiefly I-types, unlike many 1.4 Ga Proterozoic granitoids of the Southwest, which are chiefly A-types.

5. Ta and Nb are depleted in the NVF granitoids, which reflects a subduction component that was probably inherited from the volcanic arc source. Th depletion in the NVF granitoids may indicate granulite metamorphism of the source, and Sr depletion may be due to loss during alteration of plagioclase or by its retention in the restite component. Depletion in P and Ti may be due to fractionation of apatite and hornblende or sphene, respectively.

6. REE patterns are quite variable in the NVF granitoids. Although all samples show LREE enrichment and with the exception of one sample, HREE depletion, both positive and negative Eu anomalies are observed. Variable Eu abundances are controlled by plagioclasefractionation.

7. There are at least four 1700-Ma plutons represented in the NVF xenoliths. At least two 1700-Ma plutons occur at depth in the Shiprock vicinity, and at least three occur beneath the Thumb diatreme, two of which were generated during the 1700-Ma event. A 1400-Ma and a 1700-Ma pluton exist in the crust beneath Red Mesa. There are at least three plutons beneath Moses Rock, two of which were generated during the 1400 Ma event.

8. ε_{nd} data suggests that NVF metasediments are not protoliths for the NVF granitoids. Instead, the 1.4 Ga and 1.7 Ga granitoids appear to have been derived by melting the juvenile 1.75-1.8 Ga crust. The 1400-Ma granitoids may have experienced minor Archean crustal contamination. Metasediments may have made minor contributions to generation of the granitoid xenoliths.

9. NVF granitoids of all ages (1412-1440 Ma, 1691-1799 Ma) are variably deformed and were probably emplaced in collisional zones related to accretionary continental growth during the Proterozoic. However, the granitoids have volcanic arc signatures indicating that the nature of the host terrane has a greater influence on their geochemical trends than the tectonic setting in which they were emplaced. There is no correlation between degree of deformation and geochemical characteristics in the xenoliths.

10. Both major and trace element models support a tonalite source from which most of the NVF granitoids were generated. A sedimentary source may also be feasible for generating some of the NVF granitoids.

References

Anderson, J.L., 1983. Proterozoic anorogenic granite plutonism of North America. In Medaris, L.G., Jr., Byers, C.W., Mickelson, D.M., and Shanks, W.C. (Editors), Proterozoic geology: Selected papers from an international Proterozoic symposium: Geological Socitey of America Memoir 161, P. 133-154.

Anderson, J.L. and Bender, E.E., 1989. Nature and origin of Proterozoic A-type granitic magmatism in the southwestern United States of America. Lithos, 23: 19-52.

Barker, F. and Arth, J.G., 1976. Generation of trondhjemitic-tonalitic liquids and Archaean bimodal trondhjemite-basalt suites. Geology, 4: 596-600.

Bennett, V.C. and DePaolo, D., 1987. Proterozoic crustal history of the western United States as determined by neodymium isotopic mapping. Geol. Soc. Am. Bull., 99: 674-685.

Boily, M., Crooks, C., Ludden, J.N. and James, D.E., 1989. Chemical and isotopic evolution of the Coastal batholith of southern Peru. J. Geophys. Res., 89: 12483-498.

Brown, G.C., Thorpe, R.S. and Webb, P.C., 1984. The geochemical characteristics of granitoids in contrasting arcs and comments on magma sources. Geol. Soc. London, 141: 413-426.

Carr, M.J., 1994. Igpet2.1 for the Mac. Terra Softa Inc., New Jersey.

Chappell, B.W., 1984. Source rocks of I- and S-type granites in the Lachland Fold Belt, southeastern Australia. Trans. R. Soc. Lond., A310: 693-707.

Chappell, B.W. and Stephens, W.E., 1988. Origin of infracrustal (I-type) granite magmas. Trans. R. Soc. Edinburgh: Earth Sciences, 79: 71-86.

Chappell, B.W., White, A.J.R. and Wyborn, D., 1987. The importance of residual source material (restite) in granite petrogenesis. J. Petrol., 28: 1111-1138.

Chappell, B.W. and White, A.J.R., 1992. I- and S-type granites in the Lachlan Fold Belt. Trans. R. Soc. Edinburgh: 83: 1-26.

Condie, K.C., 1978. Geochemistry of Proterozoic grantitic plutons from New Mexico, U.S.A. Chem. Geol., 21: 131-149.

Condie, K. C., 1989. Plate Tectonics and Crustal Evolution. Pergamon, New York, pp. 112-113.

Condie, K.C., 1991. Precambrian granulites and anorogenic granites: are they related? Precambrian Res., 51: 161-172.

Condie, K.C., 1992. Chemical composition and evolution of the upper continental crust: Contrasting results from surface samples and shales. Chem. Geol., 104: 1-37.

Condie, K.C. and J. Selverstone, 1997. Metasedimentary xenoliths from the Navajo Volcanic Field, SW USA: Evidence for Silica and REE mobilization at midcrustal depths. (in prep.)

Creaser, R.A., Price, R.C., and Wormald, R.J., 1991. A-type granites revisited: Assessment of a residual-source model. Geology, 19: 163-166.

Deer, W.A., Howie, R.A., and Zussman, J., 1992. An Introduction to the Rock-Forming Minerals. Longman Scientific & Technical,England.

Delaney, P.R. and Pollard, D.D., 1981. Deformation of host rocks and flow of magma during growth of minette dikes and breccia-bearing intrusions near Ship Rock, New Mexico. U.S. Geol. Surv. Prof. Pap., 1202.

DePaolo, D.J., 1981. Neodymium isotopes in the Colorado Front Range and crust-mantle evolution in the Proterozoic. Nature, 291: 193-196.

DePaolo, D.J., 1988. Neodymium Isotope Geochemistry. Springer-Verlag, Germany.

DePaolo, D.J., Linn, A.M. and Schubert, G., 1991. The continental crustal age distribution: methods of determining mantle separation ages from Sm-Nd isotopic data and application to the southwestern United States. J. Geophys. Res., 96: 2071-2088.

Ebadi, A. and Johannes, W., 1991. Beginning of melting and composition of first melts in the system $Qz-Ab-Or-H_2O-CO_2$. Contrib. Mineral. Petrol., 106: 286-295.

Faure, G., 1986. Principles of Isotope Geology, John Wiley and Sons, New York.

Govindaraju, K., 1994. 1994 compilation of working values and sample description for 383 geostandards, Geostandards Newsletter, Special Issue: 18: 1-158.

Hall, A., 1971. The relationship between geothermal gradient and the composition of granitic magmas in orogenic belts. Contr. Mineral. Petrol., 32: 186-192.

Hallett, B., 1990. Geology and geochemistry of early Proterozoic granitoids from the northern Wet Mountains-southern Front Range, south-central Colorado. M.S. thesis, New Mexico Institute of Mining and Technology, Socorro, N.M.

Hallett, B.R., and Kyle, P.R., 1993. XRF and INAA determinations of major and trace elements in Geological Survey of Japan Igneous and sedimentary rock standards. Geostandards Newslett., 17: 127-133.

Harris, N.B.W., Pearce, J.A. and Tindle, A.G., 1986. Geochemical characteristics of collision-zone magmatism. In: Coward, M.P. and Ries, A.C. (Editors), Collision Tectonics, Geol. Soc. Am., Spec. Publ., 19, pp. 67-81.

Harris, N.B.W. and Inger, S., 1992. Trace element modelling of pelite-derived granites. Contrib. Mineral. Petrol., 110: 46-56.

Haskin, L.A., Haskin, M.A., Frey, F.A. and Wilderman, T.R., 1968. Relative and absolute terrestrial abundances of the rare earths. In: L.H. Ahrens (Editor), Origin and Distribution of the Elements. Pergamon, London, pp. 891-912.

Hassanen, M.A., 1997. Post-collision, A-type granites of Homrit Waggat Complex, Egypt: petroglogical and geochemical constraints on its origin. Precambrian Res., 82: 211-236.

Jacobsen, S.B. and Wasserburg, G.J., 1980. Sm-Nd isotopic evolution of chondrites. Earth. Planet. Sci. Lett., 50: 139-155.

Laughlin, A.W. and Aldrich, M.J., 1992. Mid-Tertiary stress patterns in the Four Corners region, Colorado Plateau. In S.C. Semken (Editor), Western Slope Geologic Field Conference. Navajo Community College.

Laughlin, A.W. and Charles, R.W., 1992. Lamprophyric dikes of the Navajo Volcanic Field. In: S.C. Semken (Editor), Western Slope Geologic Field Conference. Navajo Community College.

Leake, B.E., 1996. Geochemically unravelling the sedimentary components of Archaean metasediments from Western Australia. J. Geol. Soc. London, 153: 637-651.

Maniar, P.D. and Piccoli, P.M., 1989. Tectonic discrimination of granitoids, Geol. Soc. Am. Bull., 101: 635-643.

Mattie, P.D., 1996. Geochemical study of xenoliths from the Navajo Volcanic Field; Arizona, New Mexico, and Utah. M.S. thesis, New Mexico Institute of Mining and Technology, Socorro, N.M.

Mattie, P.D., Condie, K.C., Selverstone, J. and Kyle, P.R., 1997. Origin of the continental crust in the Colorado Plateau: geochemical evidence from mafic xenoliths from the Navajo Volcanic Field, southwestern USA. Geochim. Cosmochim. Acta, 61: 2007-2021.

McCulloch, M.T. and Bennett, V.C., 1994. Progressive growth of the Earth's continental crust and depleted mantle: Geochemical constraints. Geochim. Cosmochim. Acta, 58: 4717-4738.

McDermott, F., Harris, N.B.W. and Hawkesworth, C.J., 1996. Geochemical constraints on crustal anatexis: a case study from the Pan-African Damara granitoids of Namibia. Contrib. Mineral. Petrol., 123: 406-423.

McGetchin, T.R. and Silver, L.T., 1972. A crustal-upper-mantle model for the Colorado Plateau based on observations of crystalline rock fragments in the Moses Rock dike. J. Geophys. Res., 77: 7022-7037.

McGetchin, T.R., Smith, D., Ehrenberg, S.N., Roden, M. and Wilshire, H.G., 1977. Navajo kimberlites and minettes. In: Second International Kimberlite Conference, 1-38.

McGetchin, T.R., Nikhanj, Y.S. and Chodos, A.A., 1973. Carbonatite-Kimberlite relations in the Cane Valley diatreme, San Juan County, Utah. J. Geophys. Res., 78: 1854-1869.

Menzies, M.A., Arculus, R.J., Best, M.G., Bergman, S.C., Ehrenberg, S.N., Irving, A.J., Roden, M.F. and Schulze, D.J., 1987. A record of subduction process and within-plate volcanism in lithospheric xenoliths of the southwestern USA. In: P.H. Nixon (Editor), Mantle Xenoliths. John Wiley & Sons Ltd., New York, pp. 59-74.

Mittlefehldt, D.W. and Miller, C.F., 1983. Geochemistry of the Sweetwater Wash Pluton, California: Implications for "anomalous" trace element behavior during differentiation of felsic magmas. Geochim. Cosmochim. Acta., 47: 109-124.

Naeser, C.W., 1971. Geochronology of the Navajo-Hopi diatremes, Four Corners Area. J. Geophys. Res., 76: 4978-4985.

Nash, W.P. and Crecraft, H.R., 1985. Partition coefficients for trace elements in silicic magmas. Geochim. Cosmochim. Acta., 49: 2309-2322.

O'Connor, J.T., 1965. A classification for quartz-rich igneous rock based on feldspar ratios. U.S. Geol. Surv. Prof. Paper, 525B, B79-B84.

O'Sullivan, R.B., and Beikman, H.M., 1963. Geology, structure, and uranium deposits of the Shiprock Quardrangle new Mexico and Arizona. In: USGS Map I-345.

Pearce, J.A., Harris, N.B.W. and Tindle, A.G., 1984. Trace element discrimination diagrams for the tectonic interpretation of granitic rocks, J. Petrol., 25: 956-983.

Peccerillo, A. and Taylor, S.R., 1976. Geochemistry of Eocene calc-alkaline volcanic rocks from the Kastamonu area, Northern Turkey. Contr. Miner. Petrol., 58: 63-81.

Raymond, L. A., 1995. Petrology, The Study of Igneous, Sedimentary, Metamorphic Rocks. Wm. C. Brown Publishers, Chicago, pp. 32-53, 191-258.

Roden, M.F., 1981. Origin of coexisting minette and ultramafic breccia, Navajo Volcanic Field. Contrib. Mineral. Petrol., 77: 195-206.

Rollinson, H., 1993. Using geochemical data: evaluation, presentation, interpretation. Longman Scientific & Technical, New York.

Rudnick, R., 1992. Xenoliths-Samples of the lower continental crust. In: D.M. Fountain, R. Arculus and R.W. Kay (Editors), Continental Lower Crust. Elsevier, New York, pp. 269-316.

Semken, S.C., 1992. Field guide to a geologic excursion in the northeastern Navajo Nation. In: S.C. Semken (Editor), Western Slope Geologic Field Conference. Navajo Community College.

Semken, S.C., Slate, C. and Crank, L., 1992. Road Log, Shiprock (New Mexico) to Chinle (Arizona), Navajo Nation. In: S.C. Semken (Editor), Western Slope Geologic Field Conference. Navajo Community College.

Shand, S.J., 1951. Eruptive Rocks, Murby and Co., London.

Silver, L.T., Chappell, B.W. and Brown, P.E., 1988. The Peninsular Ranges Batholith; an insight into the evolution of the Cordilleran batholiths of southwestern North America; the origin of granites. Trans. R. Soc. Edinburgh, 79: 105-121.

Streckeisen, A., 1976. To each plutonic rock its proper name. Earth Sci. Rev., 12: 1-33.

Sun, S. and McDonough, W.F., 1989. Chemical and isotopic systematics of oceanic basalts: implications for mantle composition and processes. Geol. Soc. London, Spec. Public., 42: 313-345.

Vaniman, D., Laughlin, A.W. and Gladney, E.S., 1985. Navajo minettes in the Cerros de las Mujeres, New Mexico. Earth Planet. Sci. Lett., 74: 69-80.

Vielzeuf, D. and Holloway, J.R., 1988. Experimental determination of the fluid-absent melting relations in the pelitic system. Contrib. Mineral. Petrol., 98: 257-276.

Vielzeuf, D. and Montel, J.M., 1994. Partial melting of metagreywackes. Part I. Fluid-absent experiments and phase relationships. Contrib. Mineral. Petrol., 117: 375-393.

Wasserburg, G.J., Jacobsen, S.B., DePaolo D.J., McCulloch, M.T. and Wen, J., 1981. Precise determinations of Sm/Nd ratios, Sm and Nd isotopic abundances in standard solutions. Goechim. Cosmochim. Acta, 45: 2311-2323.

Wendlandt, E., DePaolo, D.J. and Baldridge, W.S., 1993. Nd and Sr isotope chronostratigraphy of Colorado Plateau lithosphere: implications for magmatic and tectonic underplating of the continental crust, Earth Planet. Sci. Lett., 116: 23-43.

Whalen, J.B., Currie, K.L. and Chappell, B.W, 1987. A-type granites: geochemical characteristics, discrimination and petrogenesis. Contrib. Mineral. Petrol., 95: 407-419.

Williams, H., 1936. Pliocene volcanoes of the Navajo-Hopi country. Geol. Soc. Am. Bull., 47: 111-172.

Zen, E-an and Hammarstrom, J.M., 1984. Magmatic epidote and its petrologic significance. Geology, 12: 515-518.

Zen, E-an, 1986. Aluminum enrichment in silicate melts by fractional crystallization: some mineralogic and petrographic constraints. J. Petrol., 27: 1095-117.

Thin Section Descriptions

GR-2

ModalMineralogy
Quartz-33%
Plagioclase-18%
K-feldspar-38%
Biotite-8%
Epidote-1%
Opaques-1%
Sericite-1%

SampleDescription

The sample is homogeneous with a lineated fabric. Approximately 60% of the sample has been recrystallized and is indicated by the anhedral character of all major minerals and similarity in size between most grains. K-feldspar are the dominant megacrysts and are scattered throughout the sample. However, most K-feldspar grains are small and have been recrystallized. Fractures dissect the sample at right angles to the foliation. Zones of extreme recrystallization parallel the foliation. In these zones the grains are extremely small. Distinct domains in quartz, tapered twins in plagioclase, and developed subgrains at edges of minerals indicate deformational stress. Little alteration has affected the sample. Myrmekitic and micrographic textures are present, at edges and corners of plagioclase and K-feldspar grains, respectively. Alteration of biotite to muscovite is widespread throughout sample.

MineralDescription

Quartz
-size range:<0.25 mm-2.0 mm; mean size: 0.5 mm
-distinct domains present in all grains
-grains are slightly elongate, paralleling deformational fabric
-grains are commonly dissected by fractures and subgrains have formed at edges
-hosts apatite, zircon, K-feldspar

Plagioclase
-size range: 0.5 mm-2.5 mm; mean size: 1.0 mm
-composition: An_{26}
-core-rim extinction present in few grains
-twins are commonly tapered
-myrmekitic texture is present in 10% of the grains
-alteration affects 30% of the grains, comprising <5% of most grains
    -alteration is composed of 50% sericite, 50% epidote
    -alteration commonly concentrated in cores of crystals
    -sericite appears to preferentially replace alternating twin lamellae
    -epidote exists haphazardly throughout crystals
    -accessory muscovite exists in small clumps, associated with sericite
-hosts apatite, sericite, epidote, quartz, individual plagioclase grains

K-feldspar
-microcline
-size range-0.25 mm-2.5 mm; mean size: 1.0 mm
-smaller K-feldspar grains are concentrated in interstices between other minerals
-all twins are blurry which may be indicative of deformational stress

-micrographic texture found in association with 15% of the K-feldspar grains

   -micrographic texture present in corners and at edges of grains in contact with other minerals

   -exsolution of albite occurs as small oval blebs scattered throughout a few grains

-hosts quartz (small blebs), biotite, apatite

Biotite

-size range: <0.25 mm-1.5 mm; mean size: 1.0 mm

-exists in elongated clumps, pronouncing the sample's lineated fabric

   -concentrated in interstices between other grains

-commonly associated with sphene

-epidote alteration affects 30% of grains, composing <50% of grains

   -biotite grades into epidote which may indicate replacement by epidote

   -1% of grains are completely altered to epidote

   -muscovite is concentrated at the borders of most grains, but is relatively minor

-oikocryst for apatite, zircon (around which pleichroic halos are observed)

AccessoryMinerals

Iron-Oxide-concentrated in small round patches, throughout the sample

Opaques-commonly associated with epidote, biotite and is scattered as individual grains throughout sample

Apatite-ubiquitous throughout sample, occurs as solitary grains, hosted by plagioclase, K-feldspar, biotite

Zircon-commonly resides in interstices, sometimes hosted by K-feldspar, plagioclase

GR-20
ModalMineralogy
Sericite-27%
Muscovite-46%
Hornblende-10%
Quartz-12%
Biotite-3%
Opaques-2%

SampleDescription

The sample is homogeneous with a lineated fabric. It is almost completely altered. Hornblende, sericite and muscovite have replaced most grains, except quartz, which is relatively pristine in places. Plagioclase twins can rarely be distinguished, due to sericite replacement. Muscovite and hornblende have completely replaced biotite. Opaques exist in clumps throughout the sample. Quartz grain sizes range from 0.1 to 0.5 mm and are elongate. Quartz has distinct domains and is concentrated in clusters which are heavily dissected by fractures. Altered biotite grains are locally aligned and display radiating patterns in some places. Muscovite is scattered throughout sericitized fields. Zircon grains are resistant to alteration and are pristine. Muscovite is concentrated in interstices between pseudomorphs, easing identification of relic mineral grains.

GR-44
ModalMineralogy
Quartz-25%
Plagioclase-12%
K-Feldspar-37%

Chlorite-16%
Garnet-5%
Calcite-3%
Opaques-0.5%
Iron-Oxide-1.5%

SampleDescription

The sample is heterogeneous with a slight fabric. Calcite fills fractures which dissect most grains. Chlorite alteration is extensive, abundant in pseudomorphs of remnant garnet grains. Garnet porphyroblasts are locally aligned and along with quartz, appear stretched out. Most minerals display preferred orientation. Little recrystallization has occurred (~10%), although subgrains have formed at most grain boundaries. Small recrystallized patches are elongate, paralleling the preferred orientation which other grains have adopted. The sample has been exposed to stress indicated by: recrystallization, foliated fabric, undulatory extinction domains in quartz and tapered twins in plagioclase. Despite the presence of alteration products, the individual grains are fairly pristine and are only affected by alteration where they are fractured and at the grain boundaries.

MineralDescription

Quartz
-size range-<0.5 mm-4.0 mm; mean size-2.0 mm
-oikocryst for rutile, apatite, opaques, K-feldspar
        -apatite and rutile display alignment within host quartz crystals

Plagioclase
-size range-0.5 mm-4.0 mm; mean size-0.75 mm
-composition-An_{27}
-alteration affects most plagioclase grains
        -sericite alteration appears in 90% of the crystals, accounts for 1% of most grains
        -muscovite alteration appears in 5% of the crystals, accounts for <0.5% of most grains
-apatite crystals appear aligned with twin planes in grains, although rutile is haphazardly scattered throughout the grains
-pericline twinning is common
-hosts rutile, apatite, muscovite, sericite, other plagioclase grains

K-feldspar
-orthoclase
-size range-0.5 mm-5.0 mm; mean size-1.5 mm
-core-rim zoning is present in 20% of the crystals
-sericite alteration exists in 80% of the grains, accounts for 1% of most grains
-veins of calcite and chlorite present in 50% of the grains
        -calcite exists in round concentrations (~0.25 mm in size) in K-feldspar grains
-exists as small, individual inclusions in garnet grains
-hosts opaques

Garnet
-size range of individual grains-0.2-1.0 mm; mean size-0.3 mm
        -size range of pseudomorphs-0.5-4.0 mm
-alteration is extensive, affects all garnet grains
        -80% of garnet grains are 75% altered
        -20% of garnet grains are 20% altered
        -larger sized porphyroblasts display a greater degree of alteration
-pseudomorphs are fractured

-pseudomorphs are dominantly filled with chlorite, although calcite and iron-oxide
are also present
-small garnet grains exist in center of pseudomorphs
-chadacrysts of quartz and K-feldspar reside in pseudomorphs and are not affected by
alteration

AccessoryMinerals
Iron-Oxide
-coexists with chlorite in heavily altered areas
-fills few interstices
-radiates from garnet pseudomorphs, where it is concentrated

Opaques-concentrated in interstices and is surrounded by chlorite, limonite

Zircon-hosted by quartz, K-feldspar

Apatite-hosted by plagioclase

Rutile-ubiquitous throughout sample, acicular, hosted by plagioclase, quartz, K-feldspar

MR-1A
ModalMineralogy
Quartz-2%
Biotite-2%
Opaques-2%
Hornblende-4%
K-Feldspar-1%
Plagioclase-1%
Muscovite-50%
Sericite-38%

SampleDescription
Sample is homogeneous. Approximately 98% of the sample has been recrystallized. The
sample is almost completely altered. Prior to alteration the sample was recrystallized, this is
indicated by ghost megacrysts of plagioclase, which are completely sericitized and
surrounded by muscovite. Small grains of quartz and K-feldspar are scattered throughout
sample. The groundmass is composed of equant grains, size=~0.3 mm, and consists of
muscovite, biotite, sericite, hornblende and opaques. Sericite displays a dendritic, skeletal
pattern. Biotite exists in elongated clusters, in close association with hornblende, which
may be replacing the biotite. Individual biotite grains are extremely small, <0.25 mm.
Opaques also occur in elongated clusters and may be alteration products of biotite. Biotite
and opaque clusters are locally aligned. Modal mineral percentages are difficult to assign
due to recrystallization and extensive alteration.

MR-1B
ModalMineralogy
Quartz-33%
Plagioclase-10%
K-Feldspar-30%
Biotite-17%
Sericite-5%
Muscovite-5%

<u>SampleDescription</u>

The sample is heterogeneous without an apparent fabric. Sample displays a porphyritic texture and alteration is extensive. Approximately 90% of the sample has been recrystallized. Megacrysts of quartz, K-feldspar and plagioclase are surrounded by recrystallized grains. Plagioclase is almost completely altered to sericite and the twins are difficult to distinguish. Quartz and K-feldspar megacrysts are fairly pristine in comparison. Megacrysts are dissected by fractures and have developed subgrains at the edges. Biotite clusters consist of small recrystallized grains. Alteration is ubiquitous. Muscovite and sericite replace plagioclase. Sericite and muscovite are scattered throughout the groundmass, preferentially altering plagioclase, but giving the entire sample an altered appearance. No trace minerals are observed.

<u>MineralDescription</u>

<u>Megacrysts</u>

Quartz
-megacryst size range-~2.5 mm
-distinct domains are evident
-hosts K-feldspar, apatite

Plagioclase
-megacryst size range: 2-4 mm
-alteration affects all plagioclase grains
      -extremely altered to sericite and epidote
      -alteration comprises: 30-60% of grain
            -alteration composed of 50% muscovite, 50% sericite
-hosts K-feldspar

K-Feldspar
-microcline
-megacryst size range: 2-8 mm
-prominent grid-iron twinning
-perthitic texture is common
-minor amounts of muscovite and sericite alteration is present
      -alteration is concentrated in cores of grains and albite exsolutions
-hosts quartz, plagioclase, other K-feldspar grains

Biotite
-size range of clusters-1.0-2.0 mm, individual grain size: <0.25 mm
-most grains are altered to muscovite and display little chloritization
-closely associated with epidote
-commonly exists in interstices

<u>Groundmass</u>
-grains are equigranular
-sericite and muscovite alter all plagioclase grains, comprising 10-60% of the grains
-small quartz grains are fairly pristine
-no twinning is apparent in K-feldspar grains, probably due to recrystallization

MR-2
<u>ModalMineralogy</u>
Quartz-20%
Plagioclase-31%
K-Feldspar-17%

101

Biotite-22%
Epidote-3%
Calcite-2%
Muscovite-3%
Sericite-1%
Opaques-1%

SampleDescription
The sample is homogeneous with a lineated fabric. Approximately 30% of sample has been recrystallized. Recrystallization products include quartz, K-feldspar, and plagioclase. Primary minerals have been affected by stress and exhibit subgrains at edges. Grains are slightly elongate, paralleling the dominant fabric. Grains in recrystallized patches do not host chadacrysts. Little alteration affects the sample. Calcite appears to replace a few crystals. Some recrystallization is apparent. Recrystallization, distinct domains in quartz and tapered twins in plagioclase indicate exposure to deformational stress.

MineralDescription
Quartz
-size range: <0.25-1.0 mm; mean size: 0.25 mm
-~5% crystals are stained by iron-oxide patches
-distinct domains are apparent

Plagioclase
-size range: 0.25-2.0 mm; mean size: 1.0 mm
-composition: An_{25}
-core-rim zoning is present in few crystals
-tapered twins exist in some grains
-~30% of grains display alteration to sericite and muscovite
       -alteration comprises 2-30% of the grains
-hosts apatite, biotite, epidote, quartz

K-Feldspar
-orthoclase
-size range: 0.25-1.0 mm; mean size: 0.75 mm
-core-rim zoning is common
-grains are relatively pristine, displaying little alteration
-hosts apatite, sphene, plagioclase

Biotite
-size range: 0.25-2.0 mm; mean size: 1.0 mm
-exists in aggregates, homogeneously scattered throughout sample
-few biotite books are bent and distorted
-grains are altered to calcite and muscovite
       -~5% of grains are replaced by calcite
       -~20% of grains are partially replaced by muscovite
         -2% are completely replaced by muscovite
-few grains are altering to epidote and perhaps sphene
       -epidote displays a 'moth-eaten' appearance and surrounds biotite grains
-exists in close association with epidote, muscovite, sphene, calcite

AccessoryMinerals
Opaques-some grains are disaggregated and are always associated with biotite

Zircon-hosted by plagioclase, muscovite

Apatite-commonly exists in clusters, plagioclase is the dominant host, also found in K-feldspar, biotite

MR-5
<u>ModalMineralogy</u>
Quartz-15%
Plagioclase-10%
K-feldspar-65%
Biotite-4%
Sphene-1%
Epidote-1%
Muscovite-1.5%
Hornblende-1%
Opaques-0.5%
Sericite-1.0%

<u>SampleDescription</u>
The sample is heterogeneous with no apparent fabric. K-feldspar grains are the dominant megacrysts and are extremely large compared to other minerals. The sample has experienced little recrystallization. However, deformational stress is indicated by the presence of subgrains at the edges of most minerals, dissecting fractures and distinct domains in quartz. Alteration is minor, of which sericite is the main constituent, mostly affecting plagioclase. Minor replacement of biotite by muscovite is concentrated at the edges of the grains. Perthitic texture is common in K-feldspar grains.

<u>MineralDescription</u>
Quartz
-size range-1.5 mm-8.0 mm; mean size-3.0 mm
-fractures dissect most grains
-oikocryst for biotite, opaques, apatite, plagioclase, K-feldspar

Plagioclase
-size range-0.75 mm-4.0 mm; mean size-1.5 mm
-composition: An_{25}
-growth bands experience a higher degree of alteration and are observed in few grains
-pericline twinning is common
-twins are pristine, no tapering is observed
-sericite alteration affects all grains, comprising 5-20% of grains
      -alteration is concentrated in core of most grains and along growth zones
      -individual muscovite grains coexist with sericite and comprise 20% of alteration
      -epidote chadacrysts are observed in plagioclase sericite fields and may be alteration products
-myrmekitic texture present in some grains
-small fractures dissect the grains
-hosts epidote, sericite, muscovite

K-feldspar
-microcline
-size range-1.0 mm-9.0 mm; mean size: 4.0 mm
-distinct grid-iron twinning
-perthite texture is present in 40% of grains
      -perthitic lamellae are altered to sericite, making them easy to distinguish within the grains
-growth bands present in some grains

-alteration is extremely minor and is comprised of epidote, sericite
   -40% of grains display alteration, accounts for <1% of total grain
   -concentrated in fractures
-hosts plagioclase, biotite, zircon, opaques

Biotite
-size range-0.5 mm-4.0 mm; mean size: 1.5 mm
-grains commonly exist as clumps, in interstices of other minerals
   -commonly occurs adjacent to muscovite, epidote, opaques, sphene
-biotite is altering to epidote and muscovite
   -80% of grains are altering to muscovite, which accounts for 10-60% of crystals
   -3% of biotite grains are completely replaced by epidote, whose size is <0.5 mm
-hosts zircon, apatite, opaques

Hornblende
-size range: <0.25-1.0 mm; mean size: 1.0 mm
-concentrated in interstices
-exists in close association with muscovite, epidote, opaques

Accessory Minerals

Sphene
-size range: <0.25-2.0 mm; mean size: 1.0 mm
-may be alteration an product of hornblende and biotite with which it is found in close
   association
-commonly exists in grains interstices

Iron-Oxide-occurs in close proximity to opaques and biotite
Opaques-concentrated around biotite grains and solitary grains are scattered throughout
   sample

Zircon-commonly hosted by biotite, K-feldspar

Apatite-hosted by plagioclase

MR-9
Modal Mineralogy
Quartz-18%
Plagioclase-31%
K-Feldspar-35%
Biotite-15%
Epidote-1%

Sample Description
The sample is homogeneous. A slight lineation is present and is displayed by most grains
which have a preferred orientation. Approximately 50% of the sample has been
recrystallized. Megacrysts of plagioclase and quartz are surrounded by recrystallized zones,
whose dominant constituent is K-feldspar. Zones of recrystallization are elongate and
parallel the preferred orientation of megacrysts. Sample has undergone extreme stress,
indicated by ubiquitous fractures which affect most grains, formation of subgrains at edges
of minerals, distinct domains in quartz and tapered twins in plagioclase. Myrmekitic and
micrographic textures are present. Alteration is minor, constituting less than 1% of total
sample. Biotite is altered to epidote and muscovite. Alteration patches of sericite and
muscovite partially replace plagioclase grains. Patches of iron-oxide affect all minerals and
stain portions of the sample.

<u>Mineral Description</u>

Quartz
-size range-<0.25 mm-4.0 mm diameter; mean size-0.75 mm
-small quartz grains (<0.4 mm in size) commonly reside in interiors of plagioclase and K-
        feldspar crystals
-grains serve as oikocrysts for small K-feldspar crystals (<0.5 mm in size)

Plagioclase
-size range-0.5 mm-5.0 mm; mean size-1.25 mm
-composition-An_{26}
-core-rim extinction present in 1/3 of the grains
-sericite alteration affects 90% of the grains, accounting for <1% of most plagioclase grains
        -alteration exists preferentially along alternating twins in some grains, contributing
        a linear fabric to the crystal
        -alteration is concentrated along fractures which dissect most of the grains
        -acicular muscovite grains are scattered throughout sericitized patches
-mymekitic texture is present at edges of plagioclase crystals, especially where the grains
        are in contact with different minerals
- hosts zircon, quartz, sericite, muscovite

K-Feldspar
-microcline
-size range-<0.25 mm-5.0 mm; mean size-0.5 mm
-prominent grid-iron twinning is blurred and prominent in all crystals
-small recrystallized grains are concentrated in interstices between larger sized minerals
-granophyric texture is present at contacts with other K-feldspar crystals
-sericite alteration is minor
        -alteration occurs in 90% of grains
                -accounts for <0.25% of the individual K-feldspar crystals
        -alteration is concentrated at the edges of fractures which dissect grains
        -few muscovite crystals coexist with sericite
-hosts quartz, sericite, muscovite, plagioclase and other K-feldspar crystals

Biotite
-size range-0.5 mm-2.0 mm; mean size-1.0 mm
-biotite grains are scattered throughout sample as single solitary grains, but dominantly
        exist in aggregates
        -reside in interstices between other minerals
        -chadacrysts in plagioclase and K-feldspar grains
-biotite is altered to chlorite, which mantles grains
-alteration to muscovite affects 40% of the crystals and is concentrated at edges of crystals
        -alteration accounts for 2%-10% of the crystals
                -<1% of the grains are completely replaced
-epidote is found at edges of biotite grains, in close association with muscovite and may
        also be an alteration product
-sphene is extremely rare in sample, but is always found in close association with biotite of
        which it may also be an alteration product

<u>Accessory Minerals</u>
Zircon-hosted by plagioclase, K-feldspar

Apatite-hosted by plagioclase, K-feldspar and quartz

105

MT-6

ModalMineralogy
Quartz-31%
Plagioclase-30%
K-Feldspar-25%
Sericite-7%
Epidote-1%
Biotite-5%
Opaques-1%

SampleDescription
Sample is heterogeneous with a lineated fabric. Approximately 95% of the sample has been recrystallized. Megacrysts are elongate, paralleling the dominant fabric. Megacrysts have been partially recrystallized and have developed subgrains at the edges. Megacrysts are surrounded by recrystallized, glassy material, composed of all major minerals. Sample is extremely altered by sericite and stained by iron-oxide. Quartz grains are unaffected by alteration. Accessory minerals are not easily observed due to recrystallization and alteration of sample.

MineralDescription

Quartz
-size range: <0.5-2.0 mm; mean size: 1.0 mm
-grains are extremely fractured
-distinct domains are present

Plagioclase
-size range: 0.5-3.0 mm; mean size: 2.0 mm
-grains are extremely sericitized
    -twins are difficult to distinguish due to alteration
    -alteration is homogeneously distributed and gives grains a notched appearance
-myrmekitic texture is present

Biotite
-grains are extremely small, size range: ~0.25 mm
-exists in interstices and is concentrated in clusters
-commonly altering to muscovite which is concentrated at edges of grains

K-Feldspar
-orthoclase
-size range; 0.5-4.0 mm; mean size: 2.0 mm
-exsolution blebs of albite are present in a few grains
-micrographic texture is present in few grains
-little sericitization occurs at edges of grains

MT-7

ModalMineralogy
Quartz-30%
Plagioclase-25%
K-Feldspar-30%
Sericite-8%
Epidote-1%
Biotite-5%
Opaques-1%

Sample is heterogeneous with a lineated fabric. Approximately 95% of sample has been recrystallized. Megacrysts composed of quartz and K-feldspar are elongate, paralleling the dominant fabric. Megacrysts have been partially recrystallized, and have developed subgrains at the edges. Megacrysts are surrounded by recrystallized, glassy material, composed of all major minerals. Sample is extremely altered by sericite and stained by iron-oxide, giving the sample a notched, dirty appearance. Quartz grains are left relatively undisturbed and are relatively pristine. Accessory minerals are not easily observed due to recrystallization and alteration of the sample.

MineralDescription

Quartz
-size range: <0.5-2.0 mm; mean size: 1.0 mm
-grains are extremely fractured
-distinct domains are present

Plagioclase
-size range: 0.5-3.0 mm; mean size: 2.0 mm
-grains are extremely sericitized
-myrmekitic texture is present

Biotite
-grains are extremely small, size range: ~0.25 mm
- concentrated in clusters of biotite grains are common in interstices
-commonly altering to muscovite, which is concentrated at edges of grains

K-Feldspar
-orthoclase
-size range; 0.5-4.0 mm; mean size: 2.0 mm
-exsolution blebs of albite are present in a few grains
-micrographic texture is present in few grains
-little sericitization occurs at edges of grains

RM-2
ModalMineralogy
Quartz-23%
Plagioclase-26%
K-Feldspar-32%
Biotite-15%
Sphene-1%
Muscovite-1%
Sericite-1%
Epidote-1%

SampleDescription
The sample is homogeneous and has a lineated fabric. Approximately 60% of sample has been recrystallized. Megacrysts of plagioclase are surrounded by much finer grains and are probably the only pristine grains left from the original texture. Plagioclase grains are aligned and recrystallized patches are elongate, paralleling the dominant fabric. Fractures are ubiquitous and dissect all grains. Most of the plagioclase is altering to sericite. Tapered twins in the plagioclase and distinct domains in quartz indicate deformational stress has affected the sample. Most of the biotite is altering to muscovite.

Quartz
-size range: <0.25-2.5 mm; mean: 0.75 mm
-most grains are highly fractured
-hosts apatite, K-feldspar

Plagioclase
-size range: <0.25-2.5 mm; mean: 1.25 mm
-composition: An_{24}
-pericline twinning is present in few grains
-core-rim zoning common
-sericite alteration affects ~85% of the grains
    -commonly comprises ~5% of grains
        -alteration concentrated in centers of most grains and commonly parallels twins
        -small muscovite and epidote grains are scattered throughout sericitized areas
-fractures dissect some grains which are filled and surrounded by recrystallized grains
-hosts biotite, apatite, epidote

K-Feldspar
-microcline
-size range: 0.25-2.5 mm; mean: 1.5 mm
-prominent grid-iron twinning
-grains are relatively pristine and unaffected by alteration
-micrographic texture is present in ~1% of grains
-core-rim zoning observed in a few grains
-hosts quartz (extremely small), plagioclase, zircon, sphene and other K-feldspar grains

Biotite
-size range: 0.25-2 mm; mean: 1 mm
-grains commonly exist in interstices between grains of other lithologies
    -occurs in clusters
-~98% of grains display some alteration to muscovite
    -4% of the grains are completely altered to muscovite
-epidote is found in close association with biotite of which it may be an alteration product
    -epidote intrudes biotite grains and has a disaggregated appearance
-opaques are commonly found in close association with biotite
-grains are chloritized and display a greenish hue
-hosts zircon, epidote

AccessoryMinerals

Sphene
-size range: ~0.75 mm
-commonly found in association with biotite
-hosted by K-feldspar

Apatite-hosted by K-feldspar, plagioclase, quartz

Zircon-exists as chadacrysts and in grain interstices and is hosted by biotite, K-feldspar, plagioclase

RM-3
ModalMineralogy
Quartz-25%
Plagioclase-22%

108

K-Feldspar-38%
Biotite-7%
Sericite-3%
Muscovite-4%
Opaques-1%

SampleDescription

The sample is heterogeneous with no distinct fabric. Approximately 5% of the sample has been recrystallized. Recrystallized products are composed of plagioclase, quartz, K-feldspar and occupy interstices and small pockets. Grains are inequigranular. Plagioclase grains display the greatest alteration and are replaced by sericite. Other grains are relatively pristine. The sample has experienced little deformation compared to other NVF granitoids. Besides recrystallization, indications of stress exist in quartz, which displays distinct domains and twins are tapered in plagioclase.

MineralDescription

Quartz
-size range: 0.5-5.0 mm; mean size: 3.0 mm
-hosts plagioclase, K-feldspar

Plagioclase
-size range: 1.0-5.0 mm; mean size: 2.0 mm
-composition: An_{23}
-sericite comprises ~20-50% of the grains
      -concentrated along alternating twin lamellae
      -muscovite grains are scattered throughout sericitized fields and often display radiating patterns
-myrmekitic texture is present
-tapered twins and microfaults which offset twins are common

K-Feldspar
-microcline
-size range: 0.5-5.0 mm; mean size: 4.0 mm
-perthitic texture is common
-albite exsolutions in K-feldspar are sericitized
-hosts quartz, plagioclase, muscovite, apatite

Biotite
-size range: 1.0-4.0 mm, mean size: 2.5 mm
-commonly occurs in clumps, although few solitary grains exist
-minor muscovite replacement affects some biotite grains
-grains are chloritized
-commonly associated with opaques, epidote, sphene

AccessoryMinerals

Hornblende
-size range: <0.5-1.0 mm; mean size: 0.5 mm
-associated with biotite and epidote

Opaques
-subhedral grains are all of relatively equant size: ~0.3 mm
-always associated with biotite and epidote

Sphene
-grains are small: <0.5 mm
-clusters in close proximity to biotite, of which it may be an alteration product

Apatite-ubiquitous, hosted by all major minerals

Zircon-extremely minor in sample, hosted by plagioclase

RM-4
ModalMineralogy
Quartz-25%
Plagioclase-27%
K-Feldspar-34%
Biotite-8%
Muscovite-2%
Sericite-2%
Opaques-1%
Epidote-1%

SampleDescription
The sample is homogeneous displaying a slightly lineated fabric. The sample has been completely recrystallized, evident by equant grain sizes which are aligned providing fabric to the rock. Minor alteration affects the sample. K-feldspar grains are relatively large compared to the rest of the minerals. Distinct domains are present in quartz and tapered twins are present in plagioclase. Plagioclase is partially replaced by sericite, which is concentrated in cores of most of the grains. Biotite grains are partially replaced by muscovite. Many grains have developed subgrains at the edges.

MineralDescription
Quartz
-size range: <0.5-2.0 mm; mean size: 0.5 mm
-hosts biotite, plagioclase

Plagioclase
-size range: <0.25-1.25 mm; mean size: 0.75 mm
-most twins are tapered
-sericite alteration is concentrated in grain cores, or in patches which are haphazardly
        dispersed throughout the grains
        -sericite comprises ~5-15% of grains
        -muscovite grains coexist with sericite and exist as radiating aggregates
-myrmekitic texture present
-hosts sericite, epidote, apatite

K-Feldspar
-microcline
-size range: <0.5-4.0 mm; mean size: 1.5 mm
-occurs in clusters, concentrated in interstices between other grains
-micrographic and perthitic textures are common
-hosts quartz, muscovite, biotite, plagioclase, other K-feldspar grains

Biotite
-size range: <0.5-1.0 mm; mean size: 0.75 mm
-commonly occurs in clusters, concentrated in interstices
-few grains are altered to muscovite, which comprises ~2% of the grains

-few biotite grains are completely replaced by muscovite
-few grains are chloritized
-epidote borders most biotite grains
-hosts zircon, K-feldspar, epidote, apatite

Accessory Minerals

Epidote
-exists as small aggregates, size: ~0.5 mm
-associated with biotite, borders biotite in most cases
-aggregates surround inclusions of K-feldspar, quartz
-ubiquitous throughout sample

Opaques-concentrated around biotite

Apatite-ubiquitous throughout sample, concentrated in clusters, especially around biotite
and in K-feldspar

Rutile-acicular habit, hosted by quartz

Zircon-hosted by plagioclase

RM-12
Modal Mineralogy
Quartz-30%
Plagioclase-22%
K-Feldspar-33%
Biotite-3%
Muscovite-5%
Sericite-5%
Epidote-1%
Sphene-1%

Sample Description
The sample is relatively homogeneous with a slightly foliated fabric. Approximately 50% of the sample has been recrystallized. Primary megacrysts of plagioclase are surrounded by smaller recrystallized products of quartz, plagioclase, K-feldspar (dominant recrystallization product). Few original K-feldspar megacrysts are present since most have been recrystallized. Quartz grains have been dissected and are elongate, paralleling the dominant fabric direction. Micrographic and myrmekitic texture is present in the feldspars. Presence of recrystallization products, distinct domain in quartz and tapered twins in plagioclase indicate exposure to deformational stress. Fractures are ubiquitous in the sample, dissecting most grains. Alteration is extensive. Plagioclase is largely altered to sericite and muscovite. Growth zones in plagioclase are apparent. Iron-oxide stain has affected a few grains in the sample and fills interstices.

Mineral Description
Quartz
-size range: <0.25-5.0 mm; mean size: 2.5 mm
-distinct domains are present in grains
-fractures dissect the grains
-subgrains are common at edges of grains
-grains are elongate, paralleling dominant fabric
-hosts K-feldspar

111

Plagioclase
-size range: 0.5-3.5 mm; mean size: 2.5 mm
-composition: An_{25}
-all grains are altering to sericite and muscovite
       -alteration is concentrated in cores of grains
       -most grains are ~30% altered
       -~2% of the grains are ~80% altered
       -sericite comprises ~15-50% of the alteration
       -muscovite comprises ~15-50% of the alteration
       -small grains of epidote are present in altered fields
-tapered twins indicate exposure to deformational stress
-core-rim zoning is common
-hosts K-feldspar

K-Feldspar
-microcline
-size range: <0.25-3.5 mm; mean size: 2.0 mm
-most grains have been recrystallized and surround larger quartz and plagioclase
       megacrysts

Biotite
-size range: 0.5-1.5 mm; mean size: 1.0 mm
-grains aggregate in clusters and are locally aligned commonly occurring in interstices
-commonly associated with epidote, which displays a 'moth-eaten' appearance
       -epidote alteration marginally affects ~28% of grains, comprising <20% of grain
       -epidote aggregates surround and penetrate biotite grains
-30% of biotite is altering to muscovite
       -2% of biotite grains are completely altered to muscovite
-biotite sheets are misshapen, contorted and are wavy, perhaps in response to stress
-grains display are chloritized and exhibit a green hue

Accessory Minerals
Opaques-mostly associated with epidote and biotite

Zircon-hosted by plagioclase, K-feldspar, biotite

Apatite-hosted by plagioclase

RM-23
Modal Mineralogy
Quartz-32%
Plagioclase-30%
K-Feldspar-21%
Biotite-15%
Garnet-2%

Sample Description
The sample is homogeneous and has been entirely recrystallized. The sample exhibits an interlocking texture. Grains are of relatively similar size and do not display their usual habits. Grains have a notched appearance. Quartz is elongate and has distinct domains indicating deformational stress. Plagioclase and K-feldspar display contorted shapes. Subgrains are common at edges of most grains. No apparent fabric is present and the sample is relatively pristine with little alteration. Sericite and muscovite alteration of plagioclase and biotite, respectively, is minor and comprises most of the alteration.

<u>Mineral Description</u>

Quartz
-size range: 0.25-4.0 mm; mean size: 1.0 mm
-hosts K-feldspar, biotite

Plagioclase
-size range: 0.5-2.0 mm; mean size: 1.5 mm
-composition-An_{26}
-pericline twinning is present in few grains
-minor sericite alteration is present in ~40% of the grains
    -sericite comprises ~0.5% of the grains
    -sericite appears to preferentially affect alternating twins
    -larger flakes of muscovite (accounting for 25% of alteration) and small epidote
    grains are present in the sericitized fields
-myrmekite texture is present in ~5% of the grains
-~10% of the grains display tapered twins
-oikocryst for zircon, biotite, quartz (small round grains)

K-Feldspar
-microcline
-size range: 0.25-2.0 mm; mean size: 1.0 mm
-twins are always blurred and distorted, perhaps indicative of deformational stress
-commonly exists in interstices between plagioclase and quartz grains

Biotite
-size range: 0.25-2.0 mm; mean size: 1.0 mm
-most grains are solitary and do not occur in clusters
-grains commonly reside in interstices between other grains
-muscovite alteration occurs at edges of 20% of grains
    -alteration accounts for ~1% of the total grains
-grains are chloritized and have a green hue
-hosts opaques

Garnet
-size range: 0.25-1.5 mm; mean size: 1.0 mm
-although the grains are relatively pristine
    -~1% of the grains are chloritized and pseudomorphs remain
-hosts biotite, quartz

<u>Accessory Minerals</u>
Sphene-always associated with biotite, which it may be altering

Iron-Oxide-surrounds opaques

Apatite-occurs as solitary grains, hosted by plagioclase

Zircon-commonly occurs at grain interstices, hosted by biotite, quartz

Opaques-concentrated around biotite grains, associated with iron-oxide stain

SR-1
<u>Modal Mineralogy</u>
Quartz-31%
Plagioclase-10%

113

K-Feldspar-48%
Biotite-8%
Calcite-1%
Sericite-1%
Opaques-1%

SampleDescription

The sample is homogeneous with a slightly apparent fabric. Approximately 15% of the sample has been recrystallized. Quartz grains are elongate in the direction of the dominant fabric. Recrystallization products include quartz, plagioclase, K-feldspar. Recrystallized areas exist as thin veinlets, filling interstices and surrounding megacrysts. These areas have calcite patches and sericite is scattered throughout the sample, giving the sample a 'dirty' appearance. Biotite grains are locally aligned. Granophyric and myrmekitic texture is common. Calcite is ubiquitous throughout sample, penetrating and surrounding grains. Recrystallization, tapered twins in plagioclase and distinct domains in quartz indicate the sample has experienced deformational stress. Sericite commonly replaces plagioclase.

MineralDescription

Quartz
-size range: 1.0-4.0 mm; mean size: 2.5 mm
-core-rim zoning appears in some grains
-hosts biotite, K-feldspar, plagioclase, opaques

Plagioclase
-size range: 0.5-2.0 mm; mean size: 1.0 mm
-composition: An_{26}
-tapered twins are common
-sericite alteration fills in dissecting fractures in every grain
        -sericite alteration accounts for ~2% of the grains
        -generally alteration is scattered haphazardly throughout grains, although it is
        sometimes concentrated at edges and cores of grains
-myrmekite texture occurs in ~30% of the grains
-chlorite penetrates and surrounds some grains
-pericline twinning is common
-calcite blebs commonly found in plagioclase grains, providing a wormy appearance
-hosts opaques, biotite

K-Feldspar
-microcline
-size range: 0.75-4.25 mm; mean size: 1.5 mm
-lamellae are often blurred and distorted
-granophyric texture occurs in ~80% of the grains
        -recrystallization at edges, near granophyric domains, is common
-sericite alteration at edges of grains occurs in few grains

Biotite
-size range: 0.25-1.5 mm; mean size: 1.0 mm
-most grains commonly reside in interstices
-often occurs in clusters, although solitary grains exist
-~10% of grains are altering to muscovite, which is concentrated at edges
-epidote is concentrated at edges of few biotite grains which it may be replacing
-hosts opaques

114

Opaques-euhedral grains, concentrated around biotite grains and exist as solitary grains

Zircon-hosted by K-feldspar

Apatite-commonly found in recrystallized areas, hosted by quartz, K-feldspar

SR-3
ModalMineralogy
Quartz-25%
Plagioclase-29%
K-feldspar-35%
Biotite-7%
Hornblende-1%
Sericite-3%

SampleDescription
Sample is heterogeneous with no apparent fabric. K-feldspar megacrysts display a pinkish hue in hand sample. Approximately 15% of sample has been recrystallized. Veinlets and clusters of recrystallized material are scattered throughout sample and are concentrated in interstices. K-feldspar and quartz megacrysts are especially large compared to plagioclase and biotite grains. Perthitic and myrmekitic textures are common in the feldspars. Extensive sericitization engulf most plagioclase grains, especially ones which are chadacrysts in K-feldspar grains or ones surrounded by K-feldspar. Quartz displays distinct domains.

MineralDescription
Quartz
-size range: 1.0-5.0 mm; mean size: 3.0 mm
-core-rim extinction common
-hosts plagioclase, K-feldspar

Plagioclase
-size range: 1.0-4.0 mm; mean size: 2.0 mm
-composition: An_{24}
-sericite replaces all grains
      -80% of grains display ~30% replacement by sericite
      -20% of grains display ~10% replacement by sericite
      -plagioclase grain chadacrysts in K-feldspar are ~80% replaced by sericite
      -sericite is often concentrated in growth bands, or among alternating twin lamellae
      -epidote grains are present in sericitized areas
-hosts epidote, K-feldspar, apatite

K-Feldspar
-microcline
-size range: 0.5-6.0 mm; mean size: 3.0 mm
-exsolution blebs of albite occur in ~70% of grains
-perthitic texture present in ~60% of grains
-few grains occur as small aggregates in interstices between plagioclase and quartz grains
-hosts plagioclase, quartz, apatite, biotite, hornblende, other K-feldspar crystals

Biotite
-size range: 0.5-1.5 mm; mean size: 1.0 mm
-commonly occur in clumps, although few solitary grains exist
-occur in interstices and as chadacrysts in other grains

-opaques and epidote are commonly found in close association
-grains are chloritized and display a greenish hue

Hornblende
-size range: <0.5 mm
-exist as small individual clumps
-commonly associated with biotite and epidote

AccessoryMinerals
Opaques-found in and around biotite clumps

Zircon-ubiquitous throughout sample, dominantly hosted by plagioclase

Apatite-ubiquitous, concentrated around biotite grains

SR-4
ModalMineralogy
Quartz-27%
Plagioclase-23%
K-Feldspar-36%
Biotite-7%
Calcite-4%
Sericite-1%
Iron-Oxide-<1%
Opaques-<1%

SampleDescription
The sample is homogeneous with no apparent fabric. Approximately 40% of the rock has been recrystallized. Small veinlets of recrystallized products fill interstices between larger, less stress affected grains. Recrystallized products mostly consist of plagioclase and K-feldspar. Larger grains have not been completely recrystallized, however they display subgrains. Fractures are ubiquitous throughout sample. Calcite surrounds most grains, fills interstices and replaces a few grains. Iron-oxide heterogeneously stains most minerals. Recrystallized textures, distinct domains in quartz and tapered twins in plagioclase indicate exposure to deformational stress.

MineralDescription
Quartz
-size range: 0.5-4.0 mm; mean size: 2.0 mm
-many grains display core-rim zoning
-hosts apatite, zircon

Plagioclase
-size range: 0.5-2.5 mm; mean size: 1.0 mm
-composition: An_{23}
-most grains are extremely fractured
-edges of grains are recrystallized
-pericline twinning is present in few grains
-twins are extremely tapered in some grains
-sericite alteration affects ~15% of the grains
        -alteration comprises ~3% of grains
        -alteration commonly concentrated in cores of grains, or along alternating lamellae
-myrmekitic texture is present
-hosts biotite, sericite

116

K-Feldspar
-microcline
-size range: 0.5-3.0 mm; mean size: 1.5 mm
-distinct grid-iron twinning
-perthitic texture is present in some grains
-edges of grains are recrystallized
-micrographic texture is present
-hosts apatite, biotite

Biotite
-size range: <0.25-1.0 mm; mean size: 0.5 mm
-grains are concentrated in aggregates
-mostly exist in interstices
-grains commonly coexist with opaques

<u>Accessory Minerals</u>
Opaques-commonly associated with biotite

Apatite-found in most grains

Zircon-extremely minor, compared to other samples in this study, hosted by quartz

SR-5
<u>Modal Mineralogy</u>
Quartz-28%
Plagioclase-23%
K-Feldspar-30%
Biotite-15%
Calcite-2%
Sericite-1%
Iron Oxide-1%

<u>Sample Description</u>
The sample is heterogeneous with a lineated fabric. Approximately 30% of the sample has been recrystallized. Recrystallized veins are ubiquitous throughout sample. They surround megacrysts, filling interstices and consist of quartz, plagioclase and K-feldspar. Megacrysts and recrystallized veins are aligned providing fabric to the rock. Fractures are ubiquitous throughout the sample. Fractures contain recrystallized material, which appears finer than the products in the recrystallized veins. Megacrysts are mostly comprised of quartz and K-feldspar. Calcite and iron-oxide are ubiquitous throughout sample, filling interstices and fractures which penetrate most grains. Iron-oxide is heterogeneously scattered throughout sample as small patches.

<u>Mineral Description</u>
Quartz
-size range: 0.75-5.0 mm; mean size: 3.0 mm
-distinct domains are present

Plagioclase
-size range: 0.25-5.0 mm; mean size: 1.5 mm
-composition: An_{24}
-pericline twinning is present in some grains
-twins are sometimes tapered
-sericite alteration affects ~75% of grains

117

-generally sericite comprises ~3% of a grain
        -alteration is concentrated in grain cores, alternating twins and along fractures
-myrmekitic texture is present
-hosts biotite, epidote, zircon, apatite, other plagioclase grains

K-Feldspar
-microcline
-size range: 0.2-5.0 mm; mean size: 1.0 mm
-grains display prominent grid-iron twinning
-alteration affects ~40% of the grains
        -alteration consists of sericite and muscovite
        -generally alteration comprises ~1% of a grain
-micrographic and perthitic textures are present

Biotite
-size range: 0.25-3.0 mm; mean size: 1.5 mm
-exist in clusters, although smaller grains are scattered throughout sample
-few grains display little alteration to muscovite, however most grains are fairly pristine
-grains commonly occur in interstices and as chadacrysts in other minerals

AccessoryMinerals

Apatite-hosted by plagioclase

Zircon-hosted by quartz and plagioclase

Sphene-primary, occurs along grain interstices

SR-7
ModalMineralogy
Quartz-27%
Plagioclase-24%
K-Feldspar-25%
Biotite-14%
Epidote-5%
Sericite-3%
Hornblende-1%
Calcite-1%

SampleDescription
The sample is heterogeneous with no apparent fabric. Approximately 10% of the sample
has been recrystallized. Small veinlets, composed of plagioclase, quartz, and K-feldspar fill
interstices and are scattered throughout sample. Megacrysts are fairly large (in comparison
with other samples from this study). The K-feldspar is extremely pink in hand sample.
Alteration is extensive. Plagioclase displays a high degree of sericite alteration. Evidence of
recrystallization, distinct domain in quartz and tapered twins in plagioclase indicate
exposure to deformational stress.

MineralDescription
Quartz
-size range: 1.0-7.0 mm; mean size: 3.0 mm
-core-rim zoning is common
-recrystallized products surround quartz grains and are concentrated in fractures
-hosts apatite, biotite

Plagioclase
-size range: 0.25-4.0 mm; mean size: 2.0 mm
-composition: An_{25}
-95% of grains display sericite alteration which composes 10-30% of most grains
     -3% of grains are replaced by sericite almost completely (95%)
     -alteration is concentrated in center of grains, along twin lamellae and along growth zones
     -epidote grains are often present in sericite fields
-myrmekite texture is present
-hosts sericite, apatite

K-Feldspar
-microcline
-size range: 0.5-7.0 mm; mean size: 4.0 mm
-grid-iron twinning is prominent
-exsolved albite patches are preferentially replaced by sericite
-perthitic texture is common
-hosts biotite, epidote, plagioclase, apatite

Biotite
-size range: 0.5-4.0 mm; mean size: 2.0 mm
-grains commonly exist in interstices between other minerals and lie across contacts
-grains exist in aggregates in close association with epidote and opaques
     -epidote ranges in size: <0.1-1.0 mm; mean size: 0.75 mm
     -has a 'moth-eaten' appearance
     -exists at edges and interiors of biotite grains
-few grains display rounded cleavage planes
-grains are chloritized and display a greenish hue
-hosts K-feldspar, plagioclase, epidote

Hornblende
-size range: 0.25-0.75 mm; mean size: 0.5 mm
-exists in close association with biotite
-has a vibrant aqua and blue color
-hosts biotite, epidote, opaques

<u>Accessory Minerals</u>
Opaques-occur in close association with biotite, have a 'moth-eaten' appearance

Apatite-commonly exists in clusters, hosted by plagioclase and biotite

Zircon-hosted by K-feldspar, biotite

TH-6
<u>Modal Mineralogy</u>
Quartz-30%
Plagioclase-17%
K-Feldspar-45%
Chlorite-2%
Calcite-3%
Opaques-2%
Sericite-1%

119

<u>SampleDescription</u>
The sample is homogenous with a foliated fabric. Approximately 70% of sample has been recrystallized. The foliation is exhibited by parallel veins, scattered throughout sample. Foliated regions display a much greater degree of crystallization, where grains are ten times smaller than grains outside of the banded regions. Recrystallization veins consisting of quartz, K-feldspar and plagioclase grains are surrounded by sericite and patches of iron-oxide. All grains are distorted. They are elongate and display a 'jigsaw puzzle' appearance. Minerals do not display their usual habits. Some of the minerals may not have been completely recrystallized, but all have been affected by deformational stress. Grains are similar in size. Most grains have developed subgrains at edges and are dissected by fractures. Alteration is prominent. Heavily recrystallized regions have experienced a greater degree of alteration to calcite, sericite and stained by iron-oxide and chlorite, than the less disturbed regions. Calcite veins are ubiquitous, dissecting and surrounding grains. Sericite alteration is present in plagioclase grains. Recrystallization, distinct domains in quartz and tapered twins in plagioclase indicate exposure to deformational stress.

<u>MineralDescription</u>
Quartz
-size range: <0.25-4.0 mm; mean size: 1.0 mm

Plagioclase
-size range: 0.25-2.0 mm; mean size: 1.0 mm
-composition: An_{25}
-95% grains are altered
    -alteration comprises 20-85% of grains
    -average alteration comprises ~25% of the grains
    -alteration is comprised of 50% muscovite and 50% sericite
    -sericite alteration is concentrated around fractures
-serves as oikocryst for quartz, K-feldspar, zircon

K-Feldspar
-size range: 0.5-3.0 mm; mean size: 1.0 mm
-perthitic texture is present
-micrographic texture is present
    -texture is irregular
        -some blebs are rectangular, some are extremely long, others are oval
-hosts zircon, plagioclase, quartz, apatite

<u>AccessoryMinerals</u>
Biotite
-average size: 0.25 mm
-altered and surrounded by chlorite
-commonly resides adjacent to opaques

Opaques
-evenly distributed throughout sample
-exists in close association with biotite
-commonly surrounded by chlorite and iron-oxide

Zircon-scattered throughout sample, hosted by plagioclase and K-feldspar

Apatite-largely hosted by K-feldspar

TH-8
<u>ModalMineralogy</u>
Quartz-30%
Plagioclase-25%
K-Feldspar-33%
Calcite-7%
Opaques-1%
Chlorite-2%
Sericite-1%
Iron-Oxide-1%

<u>SampleDescription</u>
The sample is homogeneous and displays a pinkish hue. The sample is foliated.
Approximately 40% of sample has been recrystallized. Veins of recrystallized products
surround larger, elongate megacrysts. All grains are elongate. Minor recrystallization has
affected all grains since many grains are bordered by subgrains. Iron-oxide stain is
homogeneously distributed throughout sample, but mostly affects plagioclase and K-
feldspar. The sample is highly altered, calcite being the main alteration constituent. Veins
filled with calcite are ubiquitous throughout the sample. Chlorite also fills interstices and
commonly surrounds opaques. Presence of recrystallized products, distinct domains in
quartz and tapered twins in plagioclase indicate exposure to deformational stress.

<u>MineralDescription</u>
Quartz
-size range: 0.25-4.0 mm; mean size: 1.0 mm
-core to rim extinction occurs in a few grains
-hosts plagioclase, zircon

Plagioclase
-size range: 0.3-3.0 mm; mean size: 0.75 mm
-composition: An_{25}
-pericline twinning is present in a few grains
-calcite surrounds and intrudes grains via fractures and preferentially replaces alternating
        twins
-twins are bent and taper in some grains
-microfaults dissect grains, indicated by offset lamellae
-minor sericite alteration affects most grains, accounts for <0.5% of a grain
        -small muscovite grains coexist with sericite
-hosts muscovite, sericite, calcite

K-Feldspar
-orthoclase
-size range: 0.5-3.0 mm; mean size: 1.5 mm
-micrographic texture is present at edges of some crystals
-perthitic texture occurs in few grains
-hosts plagioclase, zircon

<u>AccessoryMinerals</u>
Opaques
-size range: 0.3-3.0 mm; mean size: 0.75 mm
-some grains are altered, displaying a moth eaten appearance
-iron-oxide stain and calcite surround many grains

Apatite-hosted by plagioclase

Zircon-hosted by K-feldspar, quartz

Rutile-acicular, hosted by quartz

TH-10A
ModalMineralogy
Quartz-25%
Plagioclase-22%
K-Feldspar-32%
Biotite-15%
Sericite-2%
Epidote-2%
Sphene-1%
Opaques-1%

SampleDescription

The sample is relatively homogeneous, with a distinct fabric. Approximately 95% of the sample has recrystallized. Primary remnant plagioclase and K-feldspar grains are scattered throughout the finer grained recrystallized material. Most grains, including the megacrysts, are elongate, paralleling direction of dominant fabric. Fractures are ubiquitous in sample. Recrystallization, apparent fabric, prominent domains in quartz and tapered twins in plagioclase indicate sample's exposure to deformational stress. Micrographic and myrmekitic textures are present in the feldspars. Most of the biotite is being replaced by muscovite.

MineralDescription

Quartz
-size range: <0.25-4.0 mm; mean size: 1.0 mm
-hosts apatite, opaques

Plagioclase
-size range: 1.0-4.0 mm; mean size: 2.5 mm
-composition: An_{25}
-core-rim zoning is present in some crystals
-pericline twinning occurs in few grains
-sericite alteration occurs in ~95% of the grains
        -alteration commonly accounts for ~1% of the grain
        -sericite is concentrated in cores of grains or preferentially alters alternating lamellae
        -sericite concentrated at contacts between two separate plagioclase grains
        -acicular sericite grains display preferred orientation parallel to contact
-fairly large muscovite grains occur in the sericite fields
        -accounts for ~3% of the total grain
-hosts biotite, apatite

K-Feldspar
-microcline
-size range: <0.25-4.0 mm; mean size: 1.5 mm
-prominent grid-iron twinning
-micrographic texture is present at edges of grains
-perthitic texture apparent in a few crystals
-hosts quartz, apatite, plagioclase and individual K-feldspar grains

Biotite
-size range: <0.25-1.5 mm; mean size: 0.75 mm

-commonly occurs in congregations with other grains
-alteration occurs at edges of grains
        -~85% of grains are altering to epidote and muscovite
-opaques and sphene commonly found in close association with biotite
-hosts apatite, zircon, quartz

<div align="center">AccessoryMinerals</div>

Sphene
-size range: 1-3 mm
-grains are elongate and disaggregated
-coexists with sericite in plagioclase grains

Opaques-associated with biotite, epidote, sometimes included in biotite grains

Zircon-mostly occurs in grain interstices

Apatite-hosted by K-feldspar, quartz, plagioclase

<div align="center">

TH-10B
ModalMineralogy
Quartz-35%
Plagioclase-13%
K-Feldspar-38%
Chlorite-10%
Calcite-2%
Opaques-1%
Garnet-1%

</div>

<div align="center">SampleDescription</div>

The rock is heterogeneous. Approximately 65% of the sample has been recrystallized and a lineated fabric is apparent. The rock is highly altered. Some grains are completely replaced by calcite and sericite. Quartz grains are elongated and parallel the lineated fabric. Large porphyroblasts of garnet are surrounded by chlorite and are concentrated in the more intensely deformed zones. Domains in quartz, tapered twins in plagioclase and recrystallization indicate deformation stress has affected the sample. Calcite is ubiquitous throughout the sample. It fills fractures, interstices and replaces a few minerals.

<div align="center">MineralDescription</div>

Quartz
-size range: <0.5-10 mm; mean: 3 mm
-distinct domains observed in all grains
-hosts rutile, plagioclase, apatite, zircon

Plagioclase
-size range: 0.25-2.5 mm; mean size: 1 mm
-composition: An_{26}
-fractures filled with calcite and chlorite dissect grains
-antiperthite texture is observed in few grains
-sericite alteration occurs in ~25% of grains
        -alteration comprises <2% of most grains
        -alteration comprises ~50-100% of <2% grains
        -chlorite, calcite occur in close association with sericitized grains
        -sericite alteration give grains a notched appearance
-twins are tapered and bent in many grains

<div align="center">123</div>

-microfractures offset twins
-pericline twinning present in some grains
-hosts K-feldspar, apatite, zircon

K-Feldspar
-orthoclase
-size range: 0.5-4 mm; mean: 1.5 mm
-perthitic texture is present in ~5% of grains
       -exsolved albite is preferentially altered to sericite
-grains are pristine and unaltered
-most grains are fractured
-hosts apatite, rutile, plagioclase

Garnet
-size range: <0.25-0.5 mm; mean: 0.25 mm
- disaggregated garnet grains are concentrated in cores of garnet pseudomorphs
       -pseudomorphs range in size: 0.5-10 mm
       -chlorite and iron-oxide surround and penetrate pseudomorphs and radiate to other minerals in sample
       -garnet fields are concentrated in recrystallized areas and may be secondary
-quartz grains, which have developed subgrains and distinct domains, are scattered throughout pseudomorphs

Accessory Minerals

Iron-Oxide
-exists in interstices between grains
-dissects, surrounds chlorite fields and opaques
-radiates from chlorite garnet porphyroblasts and surrounds adjacent grains
-occasionally exists in small patches, scattered throughout the sample

Opaques
-size range: <0.25-3 mm; mean: 1 mm
-commonly exists at grain contacts, concentrated in chlorite garnet fields, in close association with iron-oxides

Rutile-acicular, hosted by K-feldspar, quartz (in which it is concentrated)

Zircon-not commonly found in grain interstices, hosted by K-feldspar

Apatite-ubiquitous and concentrated in plagioclase

TH-12
Modal Mineralogy
Quartz-32%
Plagioclase-10%
K-Feldspar-29%
Calcite-20%
Sericite-2%
Biotite-5%
Opaques-1%
Iron-Oxide-1%

124

<div align="center"><u>SampleDescription</u></div>

The sample is relatively homogeneous, lacking a fabric. Sample is extremely altered. Calcite fills most fractures which dissect most grains, concentrated in triple junctions and replaces few minerals. Sericite alters plagioclase and K-feldspar. Iron-oxide is ubiquitous throughout the sample. It fills interstices, fractures and surrounds other grains. Quartz grains are relatively pristine, compared to the other grains. Biotite occurs in large clusters and is locally aligned. Subgrains have formed at edges of most minerals.

<div align="center"><u>MineralDescription</u></div>

Quartz
-size range: <0.5-5.0 mm; mean size: 3.0 mm
-distinct domains are present

Plagioclase
-size range: 0.5-4.0 mm; mean size: 2.0 mm
-worm like fractures, filled with calcite, dissect all grains
-calcite comprises ~10-20% of grains
-minor sericite alteration affects plagioclase grains
         -sericite comprises ~5-20% of grains
-grains are heavily altered and distinct twins cannot be distinguished for compositional
         analysis

K-Feldspar
-orthoclase
-size range: 1.0-5.0 mm; mean size: 3.0 mm
-fractures filled with calcite dissect most grains
         -calcite comprises ~5-20% of grains
-minor sericite alteration affects K-feldspar, comprising ~3% of the grain
-albite exsolution blebs are sericitized and are present in few grains
Biotite
-size range: <0.5-3.0 mm; mean size: 2.0 mm
-occurs in aggregates
-hosts tiny opaque grains which give crystals a notched, dirty appearance

<div align="center"><u>AccessoryMinerals</u></div>

Opaques-grains are extremely small and are mostly hosted by biotite

Zircon-ubiquitous throughout sample

Rutile-acicular, ubiquitous

Apatite-relatively minor in comparison to other NVF granitoids

<div align="center">

TH-27
<u>ModalMineralogy</u>
Quartz-37%
Plagioclase-22%
K-Feldspar-24%
Garnet-10%
Chlorite-5%
Calcite-1%
Opaques-0.5%
Iron-Oxide-0.5%

</div>

<u>SampleDescription</u>
The sample is heterogeneous, displaying a partially recrystallized texture. Approximately 60% of sample has been recrystallized. Zones of intense recrystallization parallel the lineated fabric of the rock. Quartz is extremely elongated, not displaying the typical spherical habit. Fractures are ubiquitous throughout sample and dissect every grain. Garnet megacrysts are concentrated in recrystallized zones and may be secondary. Most of the garnet grains are replaced by chlorite and calcite. Recrystallized minerals are dissected, fractured and stained by iron-oxide and chlorite. Sericite is scattered throughout sample and is concentrated in plagioclase. Prominent domains in quartz, tapered twins in plagioclase, presence of subgrains in the larger crystals, and recrystallization are indicative of deformational stress. Calcite alteration is ubiquitous, filling fractures and interstices.

<u>MineralDescription</u>
Quartz
-size range: 0.5-10 mm; mean size: 4 mm
-grains are irregularly shaped, indicative of deformational stress
-calcite filled veins dissect ~60% of the grains
-hosts apatite, rutile, plagioclase, K-feldspar, zircon

Plagioclase
-size range: 0.5-3.0 mm; mean size: 1.0 mm
-composition: An_{26}
-microfaults offset twins in few grains
-fractures filled with calcite and sericite dissect most grains
-few grains have been completely recrystallized and altered
        -often surrounded by chlorite and smaller recrystallized plagioclase grains
-sericite alteration is extremely minor
        -occurs in ~10% of grains and comprises ~0.5% of most grains
        -sericite often parallels twins
- tapered and curved twins are indicative of deformational stress
-hosts epidote, sericite, zircon, apatite, rutile

K-Feldspar
-orthoclase
-size range: 0.5-4 mm; mean: 1 mm
-veins filled with calcite and chlorite dissect most grains
-grains display blurred and muddled twins, which may be indicative of stress
-formation of subgrains at edges of crystals common
-hosts apatite, rutile, zircon

Garnet
-size range: <0.25-2.5 mm; mean: 0.75 mm
- small remnant garnet grains typically reside in middle of pseudomorphs
        -all pseudomorphs are altered by chlorite, calcite and surrounded by iron-oxide
        -chlorite radiates from garnet grains and penetrates adjacent crystals
        -fractures give pseudomorphs a shattered appearance
-opaques reside in close association with garnet grains
-garnet grains occur in clusters, few solitary grains are present
-hosts zircon, K-feldspar, quartz

<u>AccessoryMinerals</u>
Apatite- occurs in clusters and is commonly hosted by plagioclase and K-feldspar grains, found in a few recrystallized and chloritized areas

126

Rutile-acicular, found in all major minerals, except garnet

Zircon-found in most major minerals, mostly exists as chadacrysts

Appendix B

Major and Trace Chemical Analyses

Table B.1: Major Element Analyses in Wt. % (XRF)

Sample	Group	SiO_2	TiO_2	Fe_2O_3	MnO	Al_2O_3	MgO	CaO	Na_2O	K_2O	P_2O_5	LOI	Total
GR-2	GR	61.21	0.15	1.46	0.02	11.91	0.38	1.82	3.72	3.34	0.04	0.32	84.37
GR-20	GR	64.23	0.42	3.69	0.04	16.94	1.94	4.29	4.63	0.92	0.12	1.80	99.02
GR-22	GR	66.49	0.37	3.02	0.03	17.25	1.56	3.49	5.00	1.94	0.11	0.76	100.03
GR-27	GR	70.29	0.23	4.44	0.10	13.67	1.28	1.78	3.46	3.10	0.06	0.50	98.90
GR-44	GR	70.39	0.28	2.03	0.03	13.31	0.84	4.06	2.77	3.33	0.06	2.29	99.39
MR-1A	MR	70.46	0.25	2.24	0.03	14.48	0.73	2.35	4.25	2.31	0.08	2.90	100.06
MR-1B	MR	71.87	0.20	2.62	0.04	14.04	0.92	0.92	3.83	4.04	0.05	1.30	99.80
MR-2	MR	58.96	0.63	5.22	0.08	18.21	2.89	4.79	3.39	2.52	0.35	1.46	98.50
MR-5	MR	73.18	0.20	1.41	0.04	14.25	0.62	1.17	3.90	5.03	0.04	0.47	100.31
MR-7	MR	58.21	1.25	7.94	0.18	15.84	2.78	4.41	4.46	2.32	0.51	1.50	99.40
MR-9	MR	70.28	0.27	2.44	0.04	14.77	0.93	2.85	4.29	2.46	0.08	0.56	98.98
MR-10	MR	69.53	0.28	2.24	0.03	15.54	1.15	3.14	5.15	1.13	0.08	0.52	98.79
MR-25	MR	81.40	0.12	1.22	0.01	9.28	1.03	0.87	3.04	1.19	0.01	0.57	98.74
MT-6	MT	73.41	0.11	1.52	0.02	13.13	0.32	0.99	3.19	5.57	0.03	0.51	98.79
MT-7	MT	74.42	0.10	1.49	0.01	12.56	0.50	0.76	2.78	6.05	0.03	0.51	99.20
RM-1	RM	71.02	0.27	2.28	0.02	13.68	0.85	0.80	2.61	5.74	0.08	1.05	98.40
RM-2	RM	70.09	0.26	2.53	0.06	14.77	1.23	2.49	2.50	2.70	0.08	0.72	97.44
RM-3	RM	71.64	0.33	1.96	0.04	14.03	0.62	0.87	3.64	5.67	0.07	0.63	99.49
RM-4	RM	71.65	0.21	1.68	0.02	14.56	0.61	1.87	3.94	4.19	0.06	0.46	99.24
RM-7	RM	70.26	0.32	6.05	0.10	13.08	0.76	3.11	4.00	1.13	0.08	0.50	99.37
RM-8	RM	63.36	0.36	2.82	0.04	15.80	1.29	3.15	4.55	2.26	0.11	0.65	94.39
RM-9	RM	72.41	0.19	3.23	0.05	13.12	0.81	3.18	3.26	1.23	0.04	1.41	98.93
RM-10	RM	73.65	0.15	1.25	0.02	14.06	0.38	1.39	3.97	4.28	0.04	0.63	99.82
RM-11	RM	64.47	0.67	7.79	0.10	15.74	2.01	2.06	2.87	2.56	0.14	0.86	99.26
RM-12	RM	74.96	0.11	1.17	0.02	13.57	0.43	1.53	3.58	4.05	0.03	0.57	100.00
RM-16	RM	72.03	0.22	1.94	0.03	14.18	0.90	2.09	3.70	3.65	0.07	0.68	99.48
RM-17	RM	64.74	0.43	3.45	0.04	17.76	1.46	4.26	4.84	2.13	0.13	0.68	99.92
RM-23	RM	73.91	0.19	3.67	0.11	12.56	0.41	1.82	4.22	1.91	0.03	0.54	99.36
SR-1	SR-A	74.49	0.11	1.35	0.05	13.18	0.21	1.72	3.52	4.55	0.04	0.82	100.03
SR-3	SR-A	72.37	0.16	1.83	0.04	14.32	0.45	1.21	3.74	4.83	0.05	0.57	99.55
SR-4	SR-A	70.21	0.12	1.33	0.06	13.13	0.28	2.87	3.14	5.20	0.04	1.92	98.29
SR-5	SR-B	66.90	0.62	4.28	0.11	14.22	1.05	4.49	3.31	3.31	0.22	1.61	100.11
SR-6	SR-B	67.39	0.51	3.97	0.06	14.98	1.07	2.89	3.72	3.84	0.13	0.96	99.51
SR-7	SR-B	66.26	0.58	4.66	0.07	15.08	1.33	3.06	3.64	3.87	0.15	0.93	99.62
SR-8	SR-A	72.75	0.14	1.56	0.03	13.22	0.31	1.17	3.27	5.18	0.05	0.41	98.09
TH-2	TH	67.47	0.35	2.03	0.01	13.41	0.16	2.09	1.86	6.58	2.27	3.38	99.60
TH-3	TH	74.76	0.02	0.56	0.07	13.04	0.32	0.51	2.52	7.09	0.01	0.43	99.32
TH-4	TH	76.02	0.05	1.01	0.02	12.07	0.39	0.82	2.49	6.06	0.04	0.64	99.60
TH-6	TH	71.05	0.16	1.19	0.02	14.32	0.65	2.82	2.50	4.93	0.05	2.38	100.06
TH-7	TH	70.86	0.11	0.79	0.02	14.31	0.55	2.50	2.53	5.32	0.04	2.00	99.03
TH-8	TH	66.25	0.41	4.00	0.03	13.18	0.78	5.15	2.78	3.58	0.12	3.37	99.63
TH-9	TH	72.30	0.14	1.62	0.01	14.35	0.96	2.77	3.60	2.85	0.04	1.06	99.70
TH-10A	TH	69.48	0.24	2.20	0.04	14.80	0.87	2.70	4.40	2.46	0.08	0.50	97.77
TH-10B	TH	71.25	0.22	2.21	0.03	13.02	0.80	4.11	2.97	2.70	0.04	2.16	99.52
TH-11	TH	72.78	0.29	1.77	0.02	12.07	0.95	4.41	3.17	1.28	0.05	2.84	99.64
TH-12	TH	71.48	0.15	1.10	0.02	11.90	0.93	2.84	1.85	5.91	0.05	2.84	99.08
TH-22	TH	63.34	0.01	0.58	0.10	12.11	0.36	7.93	2.16	6.25	0.06	6.31	99.21
TH-24	TH	74.95	0.13	1.76	0.04	11.73	0.34	1.72	2.46	5.47	0.04	1.26	99.90
TH-27	TH	73.75	0.31	2.15	0.04	12.24	1.29	3.69	2.96	0.75	0.02	1.32	98.52

128

Table B.2: Trace Element Analyses in ppm (XRF)

Sample	Group	V (4)	Cr (3)	Ni (2)	Cu (4)	Zn (4)	Ga (1)	As (4)	Rb (1)	Sr (1)	Y (2)	Zr (2)
GR-2	GR	15.90	9.40	ND	7.80	39.40	15.10	ND	92.60	280.8	4.7	96.1
GR-20	GR	48.80	20.20	17.60	22.20	44.40	18.60	ND	1.70	627.4	4.2	110.9
GR-22	GR	38.20	16.60	10.10	28.00	56.30	20.40	ND	84.20	665.3	5	126.6
GR-27	GR	41.40	ND	31.70	ND	ND	13.90	ND	50.00	213	27.5	131
GR-44	GR	34.90	20.90	13.30	9.70	15.10	11.40	ND	22.80	363.5	11.8	88.7
MR-1A	MR	29.70	14.50	9.20	7.10	48.10	16.90	4.00	61.90	398.5	4.3	92.6
MR-1B	MR	6.00	9.60	13.70	5.40	38.40	16.70	4.00	103.40	153.8	41.6	190.8
MR-2	MR	93.10	10.10	31.20	44.60	109.40	19.80	ND	85.30	1592.9	23.4	145.1
MR-5	MR	10.60	9.50	10.40	5.00	34.00	17.90	4.00	152.00	229.6	16	128.7
MR-7	MR	59.50	6.00	19.40	22.60	99.40	19.20	ND	44.50	626.6	54.7	178.1
MR-9	MR	27.70	16.80	16.60	6.70	51.10	17.90	ND	64.60	431.6	8.7	116.9
MR-10	MR	22.70	12.50	12.40	12.40	46.60	18.60	ND	54.20	542.8	5.5	116.1
MR-25	MR	ND	8.80	13.20	4.40	62.30	19.10	ND	13.00	89.2	77.2	284.7
MT-6	MT	ND	8.20	2.20	8.20	19.40	13.90	ND	130.40	127.3	15.7	168.9
MT-7	MT	5.90	13.60	3.20	11.00	39.80	13.10	10.80	142.90	155.8	20.3	131.4
RM-1	RM	17.50	8.30	12.30	5.90	52.50	15.40	ND	109.70	222	18.3	279.9
RM-2	RM	26.30	19.70	14.40	ND	63.90	19.40	ND	112.30	314.4	14.7	109.6
RM-3	RM	14.90	9.70	15.90	15.10	43.40	15.30	ND	108.40	206.4	45.4	262.7
RM-4	RM	14.80	13.50	13.20	6.50	39.60	18.00	ND	122.80	342.8	3.7	138.3
RM-7	RM	ND	12.50	6.20	ND	50.50	17.50	ND	24.60	214.3	53.6	147.8
RM-8	RM	31.80	17.30	9.20	15.40	57.10	20.50	ND	83.50	644.5	14.6	145.1
RM-9	RM	34.60	14.50	10.90	9.10	26.40	10.40	ND	24.70	263.2	14.2	98.5
RM-10	RM	10.70	10.40	5.10	ND	27.00	18.20	ND	143.60	235.7	9	115
RM-11	RM	104.00	101.70	37.10	ND	102.00	17.90	ND	78.30	307.2	26.2	148
RM-12	RM	10.70	9.30	10.30	4.60	17.30	15.10	ND	92.60	332.9	6.9	74.7
RM-16	RM	14.20	8.00	7.50	9.60	43.70	15.80	ND	104.40	374.4	5.8	160.4
RM-17	RM	46.30	20.00	15.00	25.00	64.30	20.80	ND	57.20	745.8	6.2	154.3
RM-23	RM	2.50	5.20	5.90	27.40	49.10	14.20	ND	44.00	80.5	49	171.3
SR-1	SR-A	9.60	11.00	3.00	4.40	34.00	18.00	ND	265.20	133	30.7	101.7
SR-3	SR-A	7.80	16.10	4.00	30.20	24.10	17.50	ND	131.10	145.9	16.4	127
SR-4	SR-A	9.80	9.20	2.80	6.60	37.40	17.00	ND	236.00	404.8	26.4	116.5
SR-5	SR-B	47.70	20.00	9.40	8.90	74.00	16.40	ND	93.00	594	26.1	284.1
SR-6	SR-B	38.10	10.90	6.40	10.00	60.00	19.10	ND	123.10	231.6	24.8	188.4
SR-7	SR-B	57.70	14.90	8.20	12.10	70.30	19.40	ND	124.00	249	25.6	197.4
SR-8	SR-A	10.20	10.30	2.70	6.00	40.30	15.50	ND	223.10	155.7	23.2	135.1
TH-2	TH	25.00	8.90	36.80	20.30	22.50	10.40	15.20	86.40	326.2	6.3	521.4
TH-3	TH	4.60	7.90	3.50	6.20	5.50	13.60	ND	138.80	51.4	49	82.4
TH-4	TH	ND	7.30	6.60	5.00	17.10	13.80	ND	132.80	83.6	3.5	100.2
TH-6	TH	20.50	12.30	11.40	26.90	22.80	14.10	ND	69.60	481	2.8	130.2
TH-7	TH	20.40	9.60	12.10	61.30	15.10	14.40	ND	73.30	467.9	2.7	108.6
TH-8	TH	50.10	15.80	38.10	17.40	34.70	13.70	15.30	34.50	540.1	5.2	191.7
TH-9	TH	12.30	12.20	5.30	6.30	21.10	15.30	ND	32.80	403.4	ND	64
TH-10A	TH	22.10	15.10	16.30	4.90	48.00	17.70	ND	61.80	435.8	6.4	113.6
TH-10B	TH	34.40	10.00	13.30	11.10	19.00	12.60	ND	20.20	391.3	5.2	59.8
TH-11	TH	34.00	10.30	10.90	6.30	16.90	13.10	ND	11.30	303.5	2	111
TH-12	TH	17.80	8.50	17.40	11.40	37.60	12.10	ND	126.40	211.3	7.9	196.6
TH-22	TH	9.70	9.50	8.90	9.50	5.10	13.10	ND	91.60	125.5	37.6	57.4
TH-24	TH	ND	9.70	6.80	5.20	39.00	12.90	ND	94.50	122.2	43.9	142.8
TH-27	TH	32.80	19.20	24.60	13.70	13.50	12.40	ND	6.80	299.2	33.7	120.6

(#)-Lower Limits of Detection (ppm); ND-Not Detected

129

Table B.2: Trace Element Analyses in ppm (XRF) (continued)

Sample	Group	Nb (2)	Mo (2)	Ba (10)	Pb (2)	Th (3)	U (2)
GR-2	GR	5.6	2.1	1078.8	13.7	4.1	ND
GR-20	GR	ND	ND	634.6	4.9	ND	ND
GR-22	GR	2.5	ND	1080.2	10	ND	ND
GR-27	GR	6.4	ND	1080	16.3	ND	ND
GR-44	GR	ND	2.4	2224.6	7.8	ND	ND
MR-1A	MR	4	2	1124.5	12.1	3	3.4
MR-1B	MR	12.5	2	1000.8	13.2	7.8	5.6
MR-2	MR	7.8	ND	1694.4	18.3	7.1	5.5
MR-5	MR	10.9	2	1017.7	30.3	9.3	4.4
MR-7	MR	8.6	ND	989.8	6	3.6	2.8
MR-9	MR	5.1	2.5	998.8	11.3	3.6	ND
MR-10	MR	4.3	3	364.8	11.4	5.6	ND
MR-25	MR	18.9	ND	627.1	8	ND	ND
MT-6	MT	7.3	3.3	881.9	11.5	7.4	ND
MT-7	MT	8.2	2	1239	68.4	5.3	2.6
RM-1	RM	6.1	4.7	1753.3	48	31.9	4
RM-2	RM	12.2	3.6	757.2	16.4	8	3.4
RM-3	RM	15.3	3.2	1024.3	29.3	5.8	ND
RM-4	RM	5.6	2.5	1656.4	22.6	6.2	3
RM-7	RM	6.3	ND	371.2	6	3.4	ND
RM-8	RM	10.8	2.9	903.9	11.4	3.5	2.1
RM-9	RM	4	3.5	554.4	7.7	3	2.3
RM-10	RM	9.5	3.4	1010.6	25.3	4.5	7.3
RM-11	RM	10.3	ND	735.6	17.1	8.9	3.3
RM-12	RM	4.5	3.8	1771.9	11.1	ND	ND
RM-16	RM	5.8	3.8	1484.2	15.6	3.1	ND
RM-17	RM	4.3	2.2	1036.1	10.1	3.5	ND
RM-23	RM	8.6	2.7	670.2	9.3	4	ND
SR-1	SR-A	26.7	2.7	519.9	31.6	26.3	ND
SR-3	SR-A	11.3	3.4	869.9	15.7	8.1	ND
SR-4	SR-A	23.7	3.2	898.4	32.7	24.7	4.4
SR-5	SR-B	15.4	ND	1742	18.6	ND	ND
SR-6	SR-B	16.1	2.9	808.7	24.5	16.4	3.3
SR-7	SR-B	15.4	ND	897.3	23.8	11.6	5.2
SR-8	SR-A	26.5	2.9	798.5	30	32.4	12
TH-2	TH	ND	4.1	2460.6	13.1	28.7	ND
TH-3	TH	3.4	ND	412.6	48.1	9.7	10.5
TH-4	TH	3.9	2.7	534.3	32	ND	ND
TH-6	TH	ND	2.9	1899.1	11.3	ND	ND
TH-7	TH	ND	3.3	2227.4	11	ND	ND
TH-8	TH	2.4	2	3298.9	6.2	3	2
TH-9	TH	ND	2.8	1376.5	6.9	ND	ND
TH-10A	TH	4.8	2.7	1078.5	10.7	3	ND
TH-10B	TH	ND	3.1	1545.8	7.1	ND	ND
TH-11	TH	2.4	3	477.8	4.3	ND	ND
TH-12	TH	7	3.5	1954	18.1	ND	ND
TH-22	TH	ND	ND	812.7	23.8	ND	2.8
TH-24	TH	3	2.7	776	17.7	ND	ND
TH-27	TH	2	3	365.6	4.5	ND	ND

(#)-Lower Limits of Detection (ppm); ND-Not Detected

Table B.3. Trace Element Analyses in ppm (INAA)

Element	GR-20	RM-3	RM-4	RM-11	RM-23	SR-3	SR-7	TH-10A	TH-12
Na_2O (Wt. %)	5.04	3.77	3.91	2.98	4.29	3.87	3.7	4.4	1.93
FeO (T) (Wt. %)	3.05	2.12	1.3	7.23	3.26	1.73	4.15	1.91	1
Cr	8	2.8	1.78	85.4	1.8	2.7	5.9	7	3.1
Zn	39.1	46.2	36.1	94	45	24	73.5	42.1	37.6
As	ND	NR	0.42	ND	3.8	0.86	1.2	NA	2.99
Rb	ND	113	120	70.2	46.9	125	125	57.2	125
Ba	575	1003	1701	649	673	822	862	1046	2053
Th	ND	8.3	6.78	8.41	4.92	8.78	13.65	5.19	2.25
U	ND	2.47	2.48	2.34	1.12	1.92	5.1	1.09	0.62
Sb	0.04	ND	0.04	ND	0.06	0.01	0.24	ND	0.11
Sc	5.85	3.15	1.994	15.83	4.24	3.43	9.23	3.55	1.841
Co	7.66	2.44	2.497	16.99	1.266	2.329	10.5	6.64	3.64
Se	NA	ND	NA	ND	0.73	NA	ND	ND	NA
Br	ND	ND	ND	ND	ND	0.17	0.59	ND	ND
Cs	0.06	2.38	1.675	0.94	0.197	1.73	4	0.97	0.704
La	10.19	82.10	17.50	30.90	30.50	28.51	38.60	8.33	11.64
Ce	19.27	187.20	32.30	66.50	61.80	55.20	81.00	18.40	22.60
Nd	8.50	85.00	11.10	35.30	28.80	19.60	36.50	8.50	7.30
Sm	1.49	13.93	1.73	6.23	5.56	3.31	6.86	1.51	1.78
Eu	0.79	1.72	0.46	1.35	0.88	0.54	1.17	0.47	1.02
Tb	0.17	1.43	0.16	0.80	0.97	0.33	0.83	0.21	0.21
Yb	0.43	4.28	0.27	2.09	7.90	1.29	2.15	0.57	0.67
Lu	0.06	0.58	0.05	0.32	1.22	0.21	0.33	0.09	0.11
Hf	3.33	9.12	3.58	5.05	4.77	4.17	5.89	3.31	6.57
Ta	0.03	1.17	0.55	0.65	0.24	0.52	1.12	0.29	0.26
W	ND	ND	ND	ND	ND	ND	ND	ND	0.51

Wt. %=Weight Percent; NA=Not Analyzed; ND=Not Detected

131

Table B.4. CIPW Norms

Sample	%AN	Q	or	ab	an	C	di	hy	wo	mt	il	hem	tl	ap	ru
GR-2	15.87	27.42	23.48	37.45	7.06	0	2.21	0.10	0	0	0.05	1.74	0.37	0.11	0
GR-20	34.36	22.40	5.59	40.34	21.12	0.85	0	5.71	0	2.87	0.83	0	0	0.29	0
GR-22	28.18	20.65	11.58	42.66	16.74	0.85	0	3.93	0	2.36	0.72	0.27	0	0.26	0
GR-27	22.43	32.03	18.67	29.84	8.63	1.55	0	6.16	0	2.55	0.44	0	0	0.13	0
GR-44	37.48	33.98	20.24	24.16	14.48	0	4.53	0.06	0	0	0.54	1.84	0.02	0.15	0
MR-1A	23.66	31.96	14.06	36.99	11.47	0.94	0	1.86	0	0.81	0.49	1.24	0	0.19	0
MR-1B	11.61	31.44	24.24	32.92	4.32	1.84	0	2.32	0	2.27	0.38	0.16	0	0.11	0
MR-2	42.80	15.35	15.42	29.69	22.22	2.09	0	9.98	0	3.19	1.23	0	0	0.84	0
MR-5	14.30	27.99	29.78	33.04	5.51	0.38	0	1.54	0	0	0.09	1.41	0	0.10	0.15
MR-7	30.19	9.88	14.09	38.77	16.77	0	1.87	10.87	0	4.10	2.44	0	0	1.22	0
MR-9	27.27	29.12	14.78	36.93	13.85	0.06	0	2.35	0	1.26	0.53	0.93	0	0.20	0
MR-10	25.64	27.57	6.78	44.35	15.29	0.36	0	2.91	0	0.63	0.54	1.38	0	0.19	0
MR-25	14.03	56.83	7.16	26.24	4.28	1.47	0	2.60	0	0	0.02	1.25	0	0.03	0.11
MT-6	14.88	31.57	33.46	27.48	4.80	0.13	0	0.82	0	0	0.03	1.55	0	0.06	0.09
MT-7	13.26	33.24	36.23	23.83	3.64	0.12	0	1.25	0	0	0.02	1.50	0	0.07	0.09
RM-1	13.58	31.94	34.87	22.71	3.57	1.95	0	2.17	0	0.78	0.53	1.29	0	0.18	0
RM-2	35.94	39.60	16.49	21.89	12.28	3.51	0	3.16	0	1.74	0.51	0.62	0	0.18	0
RM-3	11.28	26.48	33.89	31.13	3.96	0.48	0	1.56	0	0	0.35	1.85	0	0.15	0.15
RM-4	21.05	28.31	25.06	33.72	8.99	0.30	0	1.54	0	0	0.05	1.70	0	0.14	0.19
RM-7	29.91	33.40	6.77	34.34	14.65	0	0.45	6.91	0	2.68	0.61	0	0	0.18	0
RM-8	27.93	21.25	14.27	41.09	15.92	0.44	0	3.42	0	2.01	0.73	0.60	0	0.27	0
RM-9	35.96	41.51	7.47	28.33	15.91	0.76	0	3.03	0	2.51	0.37	0	0	0.10	0
RM-10	16.53	31.01	25.48	33.85	6.71	0.47	0	0.95	0	0	0.04	1.26	0	0.09	0.13
RM-11	27.65	28.60	15.44	24.86	9.50	4.94	0	11.81	0	3.22	1.31	0	0	0.33	0
RM-12	19.59	35.03	24.04	30.46	7.42	0.60	0	1.07	0	0	0.03	1.18	0	0.07	0.09
RM-16	24.03	31.28	21.84	31.71	10.03	0.52	0	2.27	0	0.11	0.42	1.66	0	0.16	0
RM-17	33.12	17.57	12.72	41.30	20.45	0.07	0	3.93	0	2.83	0.83	0	0	0.31	0
RM-23	19.88	37.37	11.42	36.17	8.98	0.33	0	2.85	0	2.48	0.36	0	0	0.06	0
SR-1	18.37	33.31	27.07	30.06	6.76	0	1.05	0.04	0	0	0.10	1.36	0.15	0.09	0
SR-3	15.23	29.30	28.83	32.00	5.75	0.86	0	1.12	0	0.17	0.30	1.56	0	0.11	0
SR-4	19.38	28.28	31.87	27.55	6.62	0	1.56	0	2.37	0	0.12	1.38	0.14	0.09	0
SR-5	33.57	25.82	19.91	28.51	14.41	0	5.45	1.06	0	3.13	1.20	0	0	0.52	0
SR-6	28.92	23.77	23.04	32.04	13.04	0	0.54	3.31	0	2.96	0.98	0	0	0.31	0
SR-7	30.36	21.92	23.23	31.25	13.62	0	0.63	4.81	0	3.06	1.12	0	0	0.36	0
SR-8	16.64	31.80	31.36	28.30	5.65	0.21	0	0.80	0	0	0.06	1.60	0	0.11	0.12
TH-2	39.13	34.45	40.43	16.37	4.60	5.04	0	0.40	0	0	0.39	1.92	0	5.45	0.15
TH-3	10.25	31.82	42.38	21.53	2.46	0.33	0	0.79	0	0.19	0.03	0.43	0	0.03	0
TH-4	15.42	36.50	36.21	21.25	3.87	0.01	0	0.98	0	0	0.04	1.02	0	0.08	0.03
TH-6	38.66	31.62	29.80	21.62	13.63	0	0	1.66	0	0	0.04	1.22	0.24	0.12	0.04
TH-7	35.85	30.67	32.39	22.07	12.34	0	0	1.42	0	0	0.03	0.82	0.11	0.10	0.05
TH-8	35.45	27.61	22.01	24.48	13.44	0	6.83	0	1.65	2.88	0.80	0	0	0.30	0
TH-9	30.69	33.63	17.07	30.92	13.69	0.39	0	2.42	0	0	0.01	1.64	0	0.09	0.14
TH-10A	25.69	28.40	14.95	38.30	13.24	0.19	0	2.23	0	0.79	0.47	1.24	0	0.19	0
TH-10B	36.19	36.00	16.40	25.80	14.64	0	4.42	0	0.17	0.92	0.43	1.13	0	0.09	0
TH-11	35.70	41.46	7.80	27.74	15.40	0	4.63	0.31	0	0	0.05	1.83	0.67	0.12	0
TH-12	29.85	33.53	36.32	16.30	6.94	0	5.19	0	0.08	0	0.05	1.15	0.32	0.13	0
TH-22	21.17	18.13	39.78	19.64	5.27	0	2.09	0	14.20	0.33	0.02	0.39	0	0.14	0
TH-24	18.84	36.89	32.77	21.09	4.89	0	1.87	0	0.46	0.13	0.25	1.57	0	0.08	0
TH-27	41.63	45.22	4.56	25.80	18.40	0	0.23	3.20	0	0.26	0.60	1.68	0	0.04	0

Values expressed in weight %. CIPW Norms calculated using IGPET computer program.

Appendix C

Sample Preparation Methods

Approximately 55 samples were collected during the summer of 1995. Only samples resembling granitoids were selected for this study. Care was taken to collect samples without well weathered surfaces. Samples were dissected and one piece was retained for hand reference, another for thin section analysis and the rest for geochemical analysis. Of those selected, 49 samples were retained for geochemical analysis and of those, 26 were chosen for thin section analysis.

Each sample was shaved to trim the surrounding rind of weathered and host material. Samples chosen for analysis were at least 4 inches in diameter. The trimmed material was crushed in an electric steel jaw crusher to pieces of 1 cm or less, depending on durability of the sample. The samples were then pulverized in a Bico pulverizer, employing ceramic plates. During the crushing and pulverizing procedures the first few grams of sample were discarded to avoid the possibility of contamination from previous samples. The produced powder was divided between INAA and XRF analysis. Sample powders to be analyzed by INAA were ground in an agate grinder. Samples analyzed by XRF were ground in a steel swing (TEMA) mill. Contamination was minimized by running quartz sand through the mill between runs.

Appendix D

Analytical Methods

D.1. X-Ray Fluorescence

Major elements investigated include: Si, Ti, Al, Fe, Mn, Mg, Ca, Na, K, P, Ba, following the basic methods of Hallett and Kyle (1993). For major element analysis each of the samples were fused into glass disks. Roughly one gram of sample was fused with; six grams of lithium borate flux (12:22)-batch 846, .05 grams of LiBr (used as a nonwetting agent) and .05 grams of NH_4NO_3 (a strong oxidizer). The sample was heated at 1100 degrees Celsius for approximately 15 minutes, or until everything dissolved. The mixture was housed in 95% Pt, 5% Au crucibles. Subsequent to fusion, the liquid was poured into a mold, comprised of the same composition, and allowed to cool. The platinum crucibles were cleaned in a 10% nitric acid solution between samples.

Trace elements assessed in this study include: As, V, Cr, Ni, Cu, Zn, Ga, Rb, Sr, Y, Zr, Nb, Mo, Ba, Pb, Th, U. Whole rock pressed pellets were generated to determine trace element abundances. Five to seven grams (more for samples with higher silica content) of each sample were mixed with the same number of drops of 2% polyvinyl alcohol solution (which serves as a binding agent). Boric acid was added to serve as casing for the mixture, which was subjected to 10 tons of pressure for approximately a minute.

Initially samples were heated for three hours at 110 degrees Celsius, to dispel adsorbed adhesive water. Loss on ignition (LOI) values were determined by heating the samples at 1000 degrees Celsius for two hours.

Table D.1 a. Lower Limits of Detection for XRF analysis, determined using standard BIR-1.

Trace Element	Lower Limit of Detection (ppm)
As	4
Ba	10
Cr	3
Cu	4
Ga	1
Mo	2
Nb	2
Ni	2
Pb	2
Rb	1
Sr	1
Th	3
U	2
V	6
Y	2
Zn	4
Zr	2

Table D.1 b. Results for NMR Standard analyzed with the NVF granitoids by X-ray Fluorescence.

Major Elements	Mean n=5	Standard Deviation	C.V.	Trace Elements	Mean n=5	Standard Deviation	C.V.
SiO_2	69.74	0.24	0.35	Sr	293.4	0.62	0.21
TiO_2	0.44	0.004	0.95	Rb	153.6	0.38	0.25
Al_2O_3	13.85	0.07	0.52	Th	16.1	0.15	0.93
Fe_2O_3	2.50	0.02	0.67	Pb	20.5	0.07	0.332
MnO	0.06	0.00	0.00	Ga	16.7	0.30	1.80
MgO	0.43	0.002	0.48	Zn	47.2	0.02	0.03
CaO	1.58	0.002	0.13	Cu	9.4	0.19	2.04
Na_2O	3.68	0.01	0.20	Ni	6.9	0.07	1.03
K_2O	4.77	0.02	0.35	Ba	1149.1	6.67	0.58
P_2O_5	0.13	0.001	0.46	V	23.8	0.51	2.15
SO_3	0.02	0.001	3.94	Cr	14.4	1.10	7.63
BaO	0.12	0.001	0.50	As	3.3	0.18	5.58
LOI	0.97	0.01	1.1	U	3.5	0.08	2.32
Total	98.28			Y	28.2	0.10	0.36
				Zr	182.0	6.56	3.61
				Nb	21.4	0.09	0.40

C.V.=Coefficient of Variation; Coefficient of Variation=(Standard Deviation/Mean Concentration)x100

The samples were analyzed by a Philips PW2400 spectrometer at the New Mexico Institute of Mining and Technology. A Rhodium tube served as the primary X-ray source to generate the fluorescence X rays, which were examined by different analyzing crystals. Well characterized international standards were employed for major and trace element calibration.

D.2. Instrumental Neutron Activation Analysis

INAA was employed to analyze trace element concentrations: Na, Ca, Sc, Cr, Fe, Co, Zn, As, Br, Rb, Sb, Cs, Ba, La, Ce, Nd, Sm, Tb, Yb, Lu, Hf, Ta, W, Th, U at New Mexico Institute of Mining and Technology. Roughly 80 mg of sample powder were enclosed in clean suprasil glass vials. Samples were irradiated at the University of Missouri research reactor for thirty hours at a neutron flux of 2.4 x 10^{13} n cm^{-2} sec^{-1}.

Analytical procedure was derived from Hallett and Kyle (1993). The vials were enclosed in aluminum foil and placed inside a wall of a 3.35 inch irradiation vessel. The samples were rotated to maximize equal neutron flux among the samples. Several measurements were conducted. The first count occurred six to twelve days after irradiation, the second transpired 35-45 days after irradiation. Counting was performed on two coaxial p-type, high-purity Ge detectors with resolutions of: 1.8 keV at 1332 keV and 0.6 KeV at 122 keV. Nuclear Data 9900 system was used to collect the spectra, which was reduced by TEABAGS (Trace Element Analysis By Automated Gamma-ray Spectrometry) using a Digital VAXstation 3100 computer.

Table D.2 a. Results for BCR Standard analyzed with the NVF granitoids by Neutron Activation Analysis and compared to accepted values.

Element	This Run (ppm)	Mean (ppm) n=26	Standard Deviation	Accepted Values (ppm)
Na2O	3.27	3.30	0.02	3.27
FeO	12.03	12.08	0.11	12.08
Sc	32.05	32.03	0.2	32.6
Cr	10.9	11.0	0.46	16.0
Co	36.95	37.23	0.21	37.0
Zn	134	132	4.83	130.0
As	ND	0.32	0.42	0.7
Br	ND	0.05	0.08	0.072
Rb	48.8	48.5	0.8	47.0
Sb	0.56	0.58	0.03	0.62
Os	0.95	0.96	0.02	0.96
Ba	656	674	18	681.0
La	24.69	25.35	0.32	24.90
Ce	52.85	53.27	0.45	53.70
Nd	28.7	26.64	0.94	28.8
Sm	6.675	6.77	0.08	6.59
Eu	1.94	1.94	0.02	1.95
Tb	1.03	1.05	0.02	1.05
Yb	3.3	3.33	0.03	3.38
Lu	0.487	0.48	0.01	0.510
Hf	5.29	5.16	0.07	4.95
Ta	0.747	0.748	0.01	0.81
W	ND	0.31	0.5	0.40
Th	5.68	5.69	0.05	5.98
U	1.6	1.66	0.08	1.75

ND=Not Detected. Accepted values from Govindaraju (1994). Mean represents previous runs done by the INAA lab at New Mexico Institute of Mining and Technology. Standard Deviation is calculated for these runs to demonstrate precision.

Table D.2 b. Results for G-2 Standard analyzed with the NVF granitoids by Neutron Activation Analysis and compared to accepted values.

Sample	This Run (ppm)	Mean (ppm) n=26	Standard Deviation	Accepted Values (ppm)
FeO	2.35	2.37	0.03	2.4
Sc	3.33	3.32	0.03	3.5
Cr	7.79	7.67	0.39	8.7
Co	4.36	4.40	0.06	4.6
Zn	81.0	80.56	4.85	86
As	ND	ND	ND	ND
Rb	168.5	168.11	2.19	170
Sb	0.05	0.05	0.01	0.07
Os	1.32	1.34	0.02	1.34
Ba	1832.5	1861.58	34.75	1882
La	88.56	88.56	1.21	89.0
Ce	163.3	163.77	1.82	160.0
Nd	55.35	54.2	2.0	55.0
Sm	7.29	7.33	0.09	7.20
Eu	1.308	1.33	0.02	1.4
Tb	0.466	0.46	0.01	0.48
Yb	0.711	0.74	0.02	0.8
Lu	0.101	0.1	0.00	0.110
Hf	8.795	8.5	0.22	7.90
Ta	0.788	0.78	0.01	0.88
Th	23.680	23.73	0.29	24.70
U	1.925	2.09	0.19	2.07

ND=Not Detected. Accepted values from Govindaraju (1994). Mean represents previous runs done by the INAA lab at New Mexico Institute of Mining and Technology. Standard Deviation is calculated for these runs to demonstrate precision.

Appendix E

Normalization Values

Table E.1. Chondrite-normalizing REE values from Haskin *et al.* (1968).	
Element	**Values**
La	0.33
Ce	0.88
Nd	0.60
Sm	0.181
Eu	0.069
Gd	0.249
Tb	0.047
Yb	0.20
Lu	0.034

Table E.2. Primitive Mantle values from Sun and McDonough (1989).	
Element	**Values**
Rb	0.64
Ba	6.99
Th	0.09
K	0.03
Ta	0.04
Nb	0.71
La	0.69
Ce	1.78
Sr	21.2
P	0.02
Hf	0.31
Zr	11.20
Eu	0.17
Ti	0.22
Yb	0.49
Y	4.55

Appendix F

NVF Granitoid Ages

Table F.1. U-Pb Zircon Data for Seventeen Granitoid Xenoliths from the Navajo Volcanic Field.

Sample	Age (Ma)	Error (+/-Ma)
GR-2	1704	13
MR-1A	1412	20
MR-1B	1728	50
MR-5	1440	3
MR-9	1710	4
MT-6	1748	25
MT-7	1745	12
RM-3	1435	15
RM-4	1720	40
RM-17	1701	2
SR-1	1691	61
SR-3	1694	39
SR-5	1720	71
TH-6	1733	40
TH-7	1799	38
TH-8	1701	27
TH-12	1440	2

Data from W.R. Van Schmus and M. Kozuch at the University of Kansas.

Appendix G

Sm-Nd Isotopic Data

Table G.1. Sm-Nd Isotopic Results for the NVF Granitoid and Metasedimentary Xenoliths.

Sample	Age (Ga)	Nd (ppm)	Sm (ppm)	Sm^{147}/Nd^{144}	Nd^{143}/Nd^{144}	$\varepsilon_{nd}(0)$	$\varepsilon_{nd}(T)$	T_{DM} (Ga)
Metasediments								
GR-33	1.75	52.33	9.19	0.10622	0.51162	-19.8	0.5	2.02
GR-34	1.75	54.50	9.33	0.10347	0.51163	-19.6	1.4	1.95
MR-24	1.75	61.03	9.70	0.09607	0.51169	-18.4	4.2	1.75
RM-32	1.75	68.85	12.15	0.10666	0.51170	-18.2	2.0	1.91
RM-35	1.75	94.28	15.19		0.51170	-18.4	4.0	1.76
Granitoids								
GR-2	1.704	13.44	2.234	0.10051	0.51178	-16.7	4.3	1.70
RM-3	1.435	91.73	15.440	0.10175	0.51184	-15.6	1.9	1.64
SR-1	1.691	14.61	3.066	0.12690	0.51205	-11.5	3.6	1.74

Data from W.R. Van Schmus and M. Kozuch at the University of Kansas. Ages are U-Pb zircon ages from Appendix F. $\varepsilon_{nd}(0)$ represents the ε_{nd} value today. $\varepsilon_{nd}(T)$ represents the ε_{nd} value at time of crystallization. Data were reduced using a decay constant of 6.54×10^{-12} yr^{-1}. Nd data were normalized using ^{146}Nd/^{144}Nd= 0.72190 and adjusted for instrumental bias using ^{143}Nd/^{144}Nd for La Jolla Nd = 0.511860. Calculations are based on ε_{Nd} values were calculated assuming ^{146}Nd/^{144}Nd=0.512638, Sm^{147}/Nd^{144}=0.1967 for present-day CHUR (W.R. Van Schmus, personnal communication, 1997).

Appendix H

Primitive Mantle Plot Comparison Data

Table H.1. Peninsular Batholith (Silver and Chappell, 1988), Peru Coastal Batholith (Boily *et al.*, 1989) and Average Granodiorite data (Condie, 1992).

Element	Peninsular Batholith	Peru Coastal Batholith	Average Granodiorite
Rb	94.5	134	246
Ba	91.7	81.1	107
Th	84.7	106	212
K	64.8	86.4	160
Ta	0.75	34.2	36.6
Nb	9.40	12.6	28.1
La	23.3	30.6	69.9
Ce	19.7	23.1	64.8
Sr	17.7	20.5	5.66
P	6.00	9.22	3.69
Hf	0.31	11.7	22.7
Zr	12.4	11.6	21.4
Eu		5.36	5.95
Ti	3.00	3.00	1.29
Yb	0.42	3.70	7.10
Y	4.18	4.80	9.89

Table H.2. A-type Granites of Southwestern USA. A-type Granite Data From Anderson and Bender (1989).

Element	Gold Butte Granite	Hualapai Granite	Lawler Peak Granite	Dells Granite
Rb	387	326	533	463
Ba	262	172	40.1	3.58
Th	186	338	355	419
K	183	224	143	150
Ta	66.2	55.8	71.2	150
Nb	47.6	40.1	51.2	108
La	162	270	56.8	11.6
Ce				
Sr	11.3	30.0	4.86	0.52
P				
Hf	34.3	54.4	10.4	8.66
Zr	32.5	48.1	11.4	9.55
Eu				
Ti	3.46	1.89	1.02	0.14
Yb	11.1	8.82	10.3	22.5
Y	12.0	9.56	11.2	24.4

Table H.3. Early Proterozoic Granitoids From the Northern Wet Mountains of South-central Colorado (Hallett, 1990).

Element	Twin Mountain	Phantom Canyon	Garell Peak	Crampton Mountain
Rb	285	322	316	185
Ba	117	311	107	132
Th	221	146	402	135
K	155	175	173	116
Ta	37.3	42.7	74.8	21.7
Nb	22.4	35.8	53.8	24.0
La	128	98.7	135	61.0
Ce	64.6	81.0	107	45.6
Sr	7.08	13.0	5.55	8.02
P				
Hf	24.6	35.6	48.0	32.0
Zr	21.7	31.9	36.0	28.5
Eu	12.9	15.5	10.7	12.3
Ti	2.86	3.42	2.18	4.52
Yb	6.84	11.1	21.7	7.10
Y	9.39	13.4	21.2	9.81

142

Appendix I

Major-Element Modeling

I.1. Compositions Derived from Melting a Metasedimentary Source

Melt Fraction=0.40

Table I.1. Comparison Between the Observed Melt Composition of the NVF Granitoids and Calculated Melt Composition of Granitoids Produced by Melting a Metasedimentary Source.

Element	Observed Melt Composition	Calculated Melt Composition	Calculated Source Composition	Calculated Restite Composition
SiO_2	70.09	68.97	68.20	67.24
TiO_2	0.27	0.54	0.66	0.72
Al_2O_3	13.93	17.11	16.46	15.92
Fe_2O_3T	2.55	3.92	6.76	8.60
MgO	0.89	1.00	1.48	1.79
CaO	2.61	0.78	1.14	1.37
Na_2O	3.43	1.31	1.84	2.18
K_2O	3.65	5.33	3.13	1.66
P_2O_5	0.13	0.21	0.17	0.14
Total	97.55	99.17	99.84	99.62
A/CNK	0.97	1.83	1.94	2.02
A/NK	1.45	2.16	2.56	2.96

Table I.2. Modal Composition of Source and Melt.

Mineral	Melt Mode	Source Mode
Muscovite	30.00	12.00
Biotite	12.00	15.00
Kfeldspar	7.50	3.00
An20	8.00	17.00
Quartz	40.00	40.00
Magnetite	1.00	1.00
Fe Garnet	1.00	7.00
Apatite	0.50	0.40
Al Silicate	0.00	5.00
Total	100.00	100.40

Table I.3. Element Distributions in Minerals Comprising the Metasedimentary Source.

Element	Muscovite	Biotite	K-Feldspar	An_{20}	Al Silicate
SiO_2	48.00	36.00	65.00	62.50	37.00
TiO_2	0.00	3.70	0.00	0.00	0.00
Al_2O_3	38.00	18.00	19.50	23.50	63.00
Fe_2O_3T	0.00	22.00	0.10	0.10	0.00
MgO	0.00	8.00	0.00	0.00	0.00
CaO	0.20	0.30	0.40	4.50	0.00
Na_2O	1.00	1.00	2.50	8.80	0.00
K_2O	11.00	9.00	12.00	0.60	0.00
P_2O_5	0.00	0.00	0.00	0.00	0.00
Total	98.20	98.00	99.50	100.00	100.00

Element	Quartz	Magnetite	Fe-Garnet	Apatite
SiO_2	100.00	0.00	37.40	0.00
TiO_2	0.00	10.00	0.00	0.00
Al_2O_3	0.00	0.00	21.00	0.00
Fe_2O_3T	0.00	90.00	36.30	0.00
MgO	0.00	0.00	4.00	0.00
CaO	0.00	0.00	1.00	56.00
Na_2O	0.00	0.00	0.00	0.00
K_2O	0.00	0.00	0.00	0.00
P_2O_5	0.00	0.00	0.00	42.00
Total	100.00	100.00	99.70	98.00

I.2. Compositions Derived from Melting a Tonalite Source

Melt Fraction=0.40

Table I.4. Comparison Between the Observed Melt Composition of the NVF Granitoids
and Calculated Melt Composition of Granitoids Produced by Melting
a Tonalite Source.

Element	Observed Melt Composition	Calculated Melt Composition	Calculated Source Composition	Calculated Restite Composition
SiO_2	70.85	71.02	68.79	66.76
TiO_2	0.24	0.32	0.32	0.32
Al_2O_3	14.02	15.35	17.36	18.52
Fe_2O_3T	2.19	2.33	2.34	2.32
MgO	0.76	0.48	0.48	0.47
CaO	2.33	2.31	3.41	4.11
Na_2O	3.41	3.98	5.32	6.15
K_2O	4.07	3.78	2.07	0.93
P_2O_5	0.13	0.15	0.21	0.25
Total	97.98	99.73	100.29	99.83
A/CNK	0.98	1.03	1.01	1.00
A/NK	1.40	1.44	1.58	1.66

Table I.5. Modal Composition of
Source and Melt.

Mineral	Melt Mode	Source Mode
Biotite	6.00	6.00
Kfeldspar	25.00	10.00
An_{20}	30.00	45.00
An_{35}	9.00	15.00
Quartz	28.00	23.00
Magnetite	1.00	1.00
Apatite	0.35	0.50
Total	99.35	100.50

145

Table I.6. Element Distributions in Minerals Comprising the Tonalite Source.

Element	Biotite	K-Feldspar	An_{20}	An_{35}	Quartz	Magnetite	Apatite
SiO_2	36.00	65.00	62.50	60.00	100.00	0.00	0.00
TiO_2	3.70	0.00	0.00	0.00	0.00	10.00	0.00
Al_2O_3	18.00	19.50	23.50	25.00	0.00	0.00	0.00
Fe_2O_3T	22.00	0.10	0.10	0.40	0.00	90.00	0.00
MgO	8.00	0.00	0.00	0.00	0.00	0.00	0.00
CaO	0.30	0.40	4.50	7.00	0.00	0.00	56.00
Na_2O	1.00	2.50	8.80	7.00	0.00	0.00	0.00
K_2O	9.00	12.00	0.60	0.40	0.00	0.00	0.00
P_2O_5	0.00	0.00	0.00	0.00	0.00	0.00	42.00
Total	98.00	99.50	100.00	99.80	100.00	100.00	98.00

I.3. Explanation of Model Components

Observed Melt Composition is the average major-element concentrations of the NVF granitoids. The Calculated Melt Composition concentrations are calculated using the following equation for each element:

$$E_R = E_{M1} x[FxM1_m/F(M1_m + M2_m + ...)] + E_{M2} x[FxM2_m/F(M1_m + M2_m + ...)] + ...$$

E_R=Major-element concentration in whole rock
E_M=Major-element concentration in a particular mineral (M1, M2,.....)
F=Melt fraction (0.40)
M_m=Mineral concentration in melt
$M1_m + M2_m$=Total concentrations of all minerals in melt

The Calculated Source Composition is derived from the following equation:

$$E_S = E_{M1} x[M1_s/100] + E_{M2} x[M2_s/100] + ...$$

E_S=Major-element concentration in source
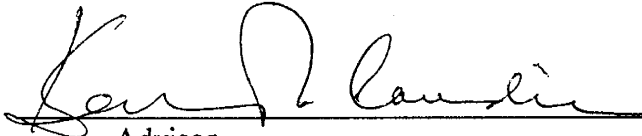E_M=Major-element concentration in a particular mineral (M1, M2,.....)
M_s=Mineral concentration in source
F=Melt fraction (0.40)

Calculated Restite Composition is derived using the following formula:

$$E_R = E_{M1} x[(M_S - [FxM1_m])/F[(M1_S - (FxM1_m)] + [(M2_S - (FxM2_m)] + ...$$

E_R=Major-element concentration in restite
E_M=Major-element concentration in a particular mineral (M1, M2,.....)
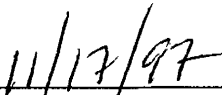M_s=Mineral concentration in source
F=Melt fraction (0.40)
M_m=Mineral concentration in melt

146

This thesis is accepted on behalf of the faculty

of the institute by the following committee:

_____
                 Advisor

_____

Nelia W. Dunbar
_____

_____

11/17/97
_____
     Date